Université Fédérale

Toulouse Midi-Pyrénées

THÈSE

En vue de l'obtention du

DOCTORAT DE L'UNIVERSITÉ DE TOULOUSE

Délivré par :

Université Toulouse 3 Paul Sabatier (UT3 Paul Sabatier)

Cotutelle internationale avec "Università della Calabria" et "Universiteit Twente"

Présentée et soutenue par :
Alessio FUOCO

le lundi 26 janvier 2015

Titre :

Computational and experimental studies on membrane-solute interactions in desalination systems using ion-exchange membranes

---

École doctorale et discipline ou spécialité :
ED MEGEP : Génie des procédés et de l'Environnement

Unité de recherche :
Laboratoire de Génie Chimique UMR 5503, CNRS, Université de Toulouse

Directeur/trice(s) de Thèse :
Hélène ROUX-de BALMANN, Directrice de Recherches, LGC - CNRS, Toulouse
Giorgio DE LUCA, Chercheur, ITM - CNR, Rende
Harmen ZWIJNENBERG, Chercheur, MST - EMI - UT, Enschede

Jury :
Giacomo SAIELLI, Professeur, CNR-Unipd, Padova (Rapporteur)
Anthony SZYMCZYK, Professeur, ISCR, Rennes (Rapporteur)
Laurent MARON, Professeur, LPCNO UPS, Toulouse (Examinateur)
Raffaele MOLINARI, Professeur, Diatic - Unical, Rende (Examinateur)
Stéphane DESOBRY, Professeur, LIBio - ENSAIA, Vandoeuvre (Examinateur)
Sylvain GALIER, Maitre de Conférences, LGC-UPS, Toulouse (Invité)
Kitty NIJMEIJER, Professeur, MST - UT, Enschede (Invité)

Université Fédérale

Toulouse Midi-Pyrénées

THÈSE

En vue de l'obtention du

DOCTORAT DE L'UNIVERSITÉ DE TOULOUSE

Délivré par :

Université Toulouse 3 Paul Sabatier (UT3 Paul Sabatier)

Cotutelle internationale avec "Università della Calabria" et "Universiteit Twente"

Présentée et soutenue par :
Alessio FUOCO

le lundi 26 janvier 2015

Titre :

Computational and experimental studies on membrane-solute interactions in desalination systems using ion-exchange membranes

---

École doctorale et discipline ou spécialité :

ED MEGEP : Génie des procédés et de l'Environnement

Unité de recherche :

Laboratoire de Génie Chimique UMR 5503, CNRS, Université de Toulouse

Directeur/trice(s) de Thèse :

Hélène ROUX-de BALMANN, Directrice de Recherches, LGC - CNRS, Toulouse
Giorgio DE LUCA, Chercheur, ITM - CNR, Rende
Harmen ZWIJNENBERG, Chercheur, MST - EMI - UT, Enschede

Jury :

Giacomo SAIELLI, Professeur, CNR-Unipd, Padova (Rapporteur)
Anthony SZYMCZYK, Professeur, ISCR, Rennes (Rapporteur)
Laurent MARON, Professeur, LPCNO UPS, Toulouse (Examinateur)
Raffaele MOLINARI, Professeur, Diatic - Unical, Rende (Examinateur)
Stéphane DESOBRY, Professeur, LIBio - ENSAIA, Vandoeuvre (Examinateur)
Sylvain GALIER, Maitre de Conférences, LGC-UPS, Toulouse (Invité)
Kitty NIJMEIJER, Professeur, MST - UT, Enschede (Invité)

Table of content

Table of content

Chapter I

Introduction

The expansion of worldwide population comes with a rising of natural resources demand while the Earth capabilities remain the same. Nowadays, in agreement with the Global Footprint Network analysis, human demand exceeds the regenerative capacity of our natural ecosystem and 1.5 Earths are needed to support the current human activities. [1] [2].

The impact of human activities on environment is visible in desertification, deforestation, climate changes, loss of biodiversity, water shortages and many other global issues. A possible way to contrast the increasing human demand and to support a sustainable industrial growth is process intensification. This concept was introduced in the chemical industrial world in the beginning of our century. In 2000, Stankiewicz and Moulin have defined it as: *"Process intensification consists of the development of novel apparatuses and techniques that, compared to those commonly used today, are expected to bring dramatic improvements in manufacturing and processing, substantially decreasing equipment-size/production-capacity ratio, energy consumption, or waste production, and ultimately resulting in cheaper, sustainable technologies. Or, to put this in a shorter form: any chemical engineering development that leads to a substantially smaller, cleaner, and more energy-efficient technology is process intensification!"[3].*

Membrane technology can play a primary role in this frame considering the match of the membranes intrinsic characteristic and the challenges of process intensification. In fact, membrane systems present lower energy consumption (in comparison with traditional methods), exceptional capability to transport in an efficient and selective way specific compounds (recycling of water, chemicals and/or raw material, possibility of 0 waste discharge), high potential to boost the reaction processes and good versatility to be built in modules (plants size reduction) [4] [5] [6]. Over the last decades, membrane engineering has already provided interesting solutions to increase the process performances in food, chemical, drugs and textile industry and beyond.

An example of process intensification by membrane processes is the desalination of water. The request of fresh water is increasing while its sources are decreasing, thus desalination systems are more and more growing. Even if water covers almost 71% of the total surface of the globe, about 97% of this water is in salty form thus not directly employable [7]. In this context, membrane processes can play an important role due to the smaller size of desalination plants and the lower energy consumption compared to traditional systems, like evaporation for instance. Indeed the energy required to desalinate seawater by evaporation is approximately 18

- 37 KW h m^{-3}, while that required using a membrane technology is lesser than 4KW h m^{-3}. So this explains why, nowadays, membrane technology is used to produce more than 50% of desalinated seawater [8] [9].

However, many are the industrial applications in which membrane technology has led improvements covering a very broad spectrum. Just to give an idea, membranes have improved the performances of processes in wine production (in replacement of cold stabilization), deacidifications of fruit juice, whey demineralization, treatment of brines, lixiviates, liquid radioactive wastes treatment, production of green chemicals building blocks (organic acids), purification of saccharides, textile industry waste treatment, tissue regeneration, gas separation, heavy and/or precious metal recovery, etc [4] [10] [11].

I.1 Impact of the ionic composition on the membrane process performances

The development of membrane processes is still limited since it is hardly possible to predict the process performances, especially when the composition of the fluid treated changes or when new uses, more constraining, are considered.

Membrane processes, and specially nanofiltration and electrodialysis, can help to solve such problems and they are growing since the last ten years. Applications extend to fluids of increasing complexity, containing both mineral and organic compounds sometimes at high concentrations. For instance, the applications move to the production and the treatment of food liquids, like organic acids fermentation broths, sugar juices or whey, with the objective to recover all the valuable components present in the solution with a high purity while minimizing the consumption of water and energy.

Membranes processes are also used to treat other complex fluids such as solution containing amino acids deriving from biochemical processes, as well as carboxylic solution produced in biorefinery industries. Another important application is the treatment of waste waters, like brines, lixiviates or other kind of waste waters (e. g. civil, pharmaceutical industries, radioactive) [10] [11] [12] [13] [14]. Again, the objective is to separate and recycle any valuable component present in the water. These liquids have a common key-factor, the presence, also at high concentration, of salts in solution. Different studies in the last ten - fifteen years, have pointed out that the presence of salts can change significantly the process performances because of the strong influence of the ionic composition on the transfer of organic solutes through the

membranes [15] [16] [17] [18] [19]. Most of the results, found in literature, concern the case of nanofiltration and only few of them the case of ion exchange membranes used in electrodialysis. The influence of the ionic composition on the transfer of a neutral solute through nanofiltration membranes was first reported by Wang et al. [15] in the case of sugar (glucose or sucrose) / NaCl solutions. It was shown that the transfer of sucrose is weakly affected by the presence of the electrolyte. On the contrary, the transfer of glucose was found to increase for increasing NaCl concentrations. Following this research, other studies were published in subsequent years, always in the framework of nanofiltration. In 2005, Bouchoux et al. [16] have also reported that the neutral mass transfer increase depends on the nature of the electrolyte. More precisely, they established a relationship between the hydration of the ions and the mass transfer increase of glucose in presence of salt. Increasingly hydrated ions were found to give increasing transfer of glucose. At the same time, Bargeman et al. [20] have drawn a correlation among the electrolyte concentration in the permeate and the transfer of glucose. This correlation was later confirmed by Umpush et al. [21] who have shown that the addition of ions completely retained by the membrane has no effect on the glucose transfer.

Other evidences of the salts effect on the transfer of organic molecules through NF membranes have been also observed with PEG (poly ethylene glycol). The transfer of this molecule was investigated by Bouranene et al. [17] for inorganic NF membrane, as well as by Escoda et al. [18] with an organic NF membrane. Both works have demonstrated that the presence of salts (KCl, LiCl, $MgCl_2$) increases the transfer of PEG trough the membrane and that the salt effect depends on its concentration as well as on its hydration.

As previously mentioned, studies related to the influence of the ionic composition on the mass transfer of neutral solute through ion-exchange membranes are rather scarce. Nevertheless, in the case of the demineralization of a synthetic liquid waste, containing acetic acid and different kinds of salts, it was reported that the diffusion of acetic acid through the ion-exchange membranes changed according to the salt composition. It was more important in presence of sodium sulfate or calcium chloride than with sodium chloride [19].

For uncharged molecules, sieving or size exclusion is the main mechanism governing the transfer through a membrane. Then, the transfer depends on the relative size of the solute and free fraction volume/pore dimension [22]. Consequently, the mass transfer increase can be ascribed to an increase of the free fraction volume of the membrane, to a decrease of the solute size or more probably to a combination of both.

Consequently, different assumptions were suggested to explain the experimental evidences previously discussed.

On one hand, for nanofiltration membranes, the addition of electrolyte can lead to an increase of the membrane charge density and to a higher concentration of counter-ions in the electrical double layer at the pore surface. Wang et al. [15] thus assumed that these electrostatic interactions result in a lower hydration shell at the pore surface. According to Bargeman et al. [20] the stronger repulsion forces between the pore walls can lead to an increase of the pore radius, commonly called "pore swelling", assuming a certain elasticity of the membrane. For polymeric ion-exchange membranes, like those used in electrodialysis, the electrolyte composition can change the membrane structural characteristics because of more complex interactions at the molecular scale between the membrane polymeric network and the solutes [23].

On the other hand, the influence of electrolyte on the overall transfer of neutral solutes can be explained by a change in the solute properties, more particularly by a modification of the solute hydration, since it is expected to vary with the ionic composition [24]. This latter explanation has been firstly proposed by Bouchoux et al. [16], who established a link between the hydration of ions and the increase of the transfer of organic solutes through NF membranes. These results were found to be in agreement with the dehydration of neutral solutes in presence of electrolyte since more hydrated electrolytes or higher concentrations inducing a higher dehydration, tend to increase the solute transfer.

As explained previously, the influence of the ionic composition on the transfer of neutral solute through a membrane results from the combination of two contributions, i.e. the modification of the membrane properties and/or the solute dehydration induced by the electrolyte. In the case of NF membranes, Escoda et al. [18] have dissociated these two contributions investigating, in the same conditions, the mass transfer of PEG through both types of membranes, an organic NF membrane and a ceramic one which is not expected to swell [17]. The Stokes radii of PEG in electrolyte solutions were evaluated from the experimental values of the retention of PEG in various electrolyte solutions obtained with the ceramic membrane, considering a fixed value of the pore radius [17]. Then the average pore radius of the organic membrane was computed from the value of the PEG retention obtained with the same electrolyte solution. In this manner, different apparent pore sizes were obtained depending on the electrolyte. For an increasing electrolyte concentration, increasing pore sizes were obtained, suggesting that the membrane can effectively swell. Moreover, it was shown that this “pore swelling” assumption can be

explained by an increase of the membrane surface charges.

The main difficulty to investigate the mass transfer mechanisms in such situations is that the two contributions and thus their combination can change with respect to the electrolyte composition and to the structural membrane properties. An original experimental approach has been recently developed in order to distinguish the contribution of each phenomenon. On one hand, the impact of the electrolyte on the membrane properties is estimated from the sugar flux in water measured through the membrane soaked in a given electrolyte. On the other hand, the impact of the electrolyte on the solute properties is evaluated from the difference between the sugar flux obtained in presence of electrolyte and that measured in water. Using this specific procedure, Boy et al. [22] have pointed out that the diffusion flux of sugars (xylose, glucose and sucrose) through a NF membrane, in presence of various electrolytes (NaCl, Na_2SO_4,$CaCl_2$, $MgCl_2$), is mainly fixed according to the influence of the electrolyte on the solute properties. That's to say that in the conditions investigated, the modification of the membrane properties according to the electrolyte composition is negligible. This study also confirmed that more hydrated electrolytes or higher concentrations induce a higher increase of the solute transfer (Table I.1)

	J_s ($x10^{-7}$ mol m^{-2} s^{-1})		
Electrolyte	**Xylose**	**Glucose**	**Sucrose**
Na_2SO_4	15.3	12.1	6.3
NaCl	7.5	4.6	0.7
$CaCl_2$	11.6	12.1	22.8
$MgCl_2$	13.2	14.4	18.3

Table I.1: Sugar diffusion fluxes through NF membrane in different electrolytes. [Sugar] =1 mol L^{-1} [electrolyte]= 1equiv. L^{-1}[22].

This effect was quantified by the determination of the apparent molar volume (AMV) and more precisely its variation, ΔV, a macroscopic parameter which characterizes the hydration state of the species in solute/electrolyte systems. A relationship was thus drawn between the apparent molar volume of saccharides and their transfer through a nanofiltration membrane in a diffusion regime for various electrolyte compositions. In such conditions, where the membrane properties do not change according to the electrolyte composition, it was confirmed that the increase of the saccharide transfer in presence of electrolyte is mainly due to its resulting dehydration [22].

The specific procedure developed to dissociate the contribution of each phenomenon has been also used by Savignac et al. [25] [26] to investigate the transfer of sugars through ion-exchange membranes. The mass transfer of various saccharides (xylose, glucose and sucrose) in different electrolytic solutions (NaCl, NH_4Cl, $CaCl_2$ and $MgCl_2$) was studied in a diffusion regime.

It was thus demonstrated that the influence of the electrolyte composition on the sugar transfer is mainly due to the following modifications of the membrane properties, which are fixed by the membrane soaking. A quantitative correlation has been established between the solute transfer and the hydration number of the membrane counter-ion. Indeed, the transfer of sugar through an ion-exchange membrane was found to decrease when the membrane is equilibrated with a more hydrated counter-ion, like calcium with respect to sodium in the case of CMX membrane (Table I-2).

	J_S ($x10^{-6}$ mol m^{-2} s^{-1})		
Electrolyte	**Xylose**	**Glucose**	**Sucrose**
NH_4Cl	23.31	16.65	2.63
NaCl	13.32	8.88	1.46
$CaCl_2$	9.99	6.11	0.88
$MgCl_2$	5.99	3.88	0.55

Table I.2: Sugar fluxes through CMX membrane soaked in different electrolytes in diffusion regime [Sugar] =1 mol L^{-1} [electrolyte]= 1equiv. L^{-1} [25].

Physical modification of anion/cation exchange membranes induced by the ionic composition of the surrounding solution was already reported in the literature. For example, several studies on Nafion membranes have shown a correlation among the counter-ion characteristic and the water content of the membrane [27] [28] [29]. A decrease of the free water content according to the counter-ion hydration properties is one possible interpretation of these data. Interesting results were also obtained by Tuan et al. [23] revealing a change in the swelling degree of the membrane due to the electrolyte solution. The swelling of the membrane can be associated to a modification in its free fraction volume, a property directly correlated with the membrane permeability to the water as well as to a solute. This is in agreement with other works dealing with a Nafion membrane soaked in NaCl solutions at different concentrations, which have also shown an increase of the wet membrane density with the electrolyte concentration [30]. Other

physical characteristics of IEM membranes can be influenced the presence of ions. For instance, Długołęcki et al. [31] have observed that the solution concentration can significantly affect the resistance of IEM. More precisely, a strong increase of the membrane electrical resistance was obtained for decreasing electrolyte concentrations.

Following the experimental evidences highlighted in the Savignac et al. [26] studies, some experimental methods were tested in order to check whether a change of the membrane properties, like its thickness, water content or "free volume" for instance, could be pointed out according to the solute/electrolyte composition. The thickness measurements have shown no change related to the kind of electrolyte solution used for the membrane conditioning. Concerning the water content, some variations were observed but they were too small to draw any clear conclusion regarding the mechanisms involved. For instance, the water content of the CMX membrane was 18.4% and 20% for a membrane soaked in $MgCl_2$ and NH_4Cl respectively. Some promising preliminary results were obtained from the determination of the electrical membrane conductivity which gives an image of the free volume. However, not enough experimental conditions (electrolyte, concentration range) have been investigated to draw any clear conclusion.

To summarize, different studies carried out this last years pointed out that the performances of the membrane process can be significantly affected when applied to solutions containing significant amount of salts. Indeed, it was reported, with NF membranes as well as with ion-exchange ones used in electrodialysis, that the transfer of an organic solute changes according to the electrolyte nature and concentration. In any case, the mass transfer modification has been correlated to the hydration state of the ions.

Recently, it was shown that the mass transfer modification through NF membranes is mainly fixed by the influence of the electrolyte on the solute properties. More precisely, the mass transfer increases with the hydration number of the ions in solution. On the contrary, for ion-exchange membranes, it was reported that the mass transfer variation is mainly governed by the modification of the membrane properties which are fixed by the ionic composition. In this case, the mass transfer decreases when the membrane is equilibrated with increasing hydrated counter-ion.

The effects observed at the macroscopic scale, i.e. the modification of the organic solute transfer in presence of salts, result from mechanisms taking place at the molecular scale. Indeed, these results confirm that the knowledge of the multiple interactions, taking place at the nano-scale,

between the polymer, the water and the solutes (ions, organic compounds) are a bottleneck regarding the improvement of the membrane processes. Thus, it is necessary to develop new complementary approaches to characterize these systems at the microscopic scale.

At this scale, weak non-covalent interactions are good candidates to explain the observed phenomena. For this reason, the investigation of non-covalent interactions involved in these systems will be the object of this Thesis.

I.2 Noncovalent interactions in Membrane Science

Noncovalent interactions are the base of supramolecular chemistry, which can be defined as "chemistry beyond the molecules". This means that, as atoms are connected by covalent bonds in order to form a molecule, molecules can be aggregated together by noncovalent interactions to construct supramolecular structures (e. g. membrane polymeric network) [32]. It is important to remark that the noncovalent character is not only additive but also cooperative during the formation of supramolecular structures. Thus, the whole interaction energy of a system is higher than the sum of the single interactions [33].

Noncovalent interactions can be divided in two categories: isotropic and anisotropic. The isotropic noncovalent bonds usually involve partially charged atoms and are short-medium range forces with weak interaction energy. Van der Waals interactions are included in this category and usually their influence is more on steric properties such as molecular packaging, size and shape. Among the anisotropic, the key noncovalent interaction is the hydrogen bond [34]. Hydrogen bond, with its average interaction energy of about 10 Kcal/mol but with peaks up to 30 Kcal/mol, is the stronger noncovalent interaction (excluding the ion-ion interactions among solid salts). Due to the strength and the directionality of its effect, it is also usually involved in the eventual functions on the molecules. The shape of a hydrogen bond is X-H...Y, where X and Y are two electronegative atoms (e. g. O, N). The electronegativity of the involved atoms gives the strength of the H-bond and at higher electronegativity for both atoms corresponds a stronger interaction. Furthermore, at higher interaction energy corresponds an elongation of X-H bonds causing a modification in the X-H stretching frequency [36].

From a molecular point of view, membranes can be seen as physical catalysts affecting the migration of species. This physical catalyst acts with a four step cycle process (adsorption, front and back diffusion in the bulk, desorption) [32]. However, since the role of supramolecular chemistry in nature was mainly perceived in the last three decades, and considering that also

the researchers effort on process intensification by membrane technology is relatively young, the use of supramolecular chemistry in the membrane related field (e. g. membrane preparation and characterization, transport mechanisms at molecular scale, fouling deposition), is still in a pioneering time. At this point, it is worth noting that supramolecular studies require the use of computational chemistry, and particularly the use of Quantum Mechanics. More information about the computational theories used in this Manuscript, are reported in chapter 2.

The investigation of noncovalent interactions from Quantum Mechanics approaches have been already used to explained experimental results obtained in the frame of membrane processes.

Experimentally, changes in the hydrophilic properties of the membrane were observed in Pebax membrane when N-ethyl-o,p-toluensulfonamide, KET, modifier was dissolved in the polymer matrix. Thus, De Luca et al [37] have analyzed, by mean of Quantum Mechanics, the hydrogen-bonding interactions involved in the adducts present in the membrane. This computational work has demonstrated that Pebax-KET and KET-KET interactions compete and that the competition is KET concentration dependent. In fact, for lower concentration of KET, there is an increase of the availability of polar moieties present in the membrane, and thus an increase of the membrane hydrophilicity. For higher concentrations of KET there is a saturation of the polar moieties, resulting in a decrease of the water sorption in the membrane.

Membrane degradation mechanisms are also other possible targets of Quantum Mechanics investigations. For example, different hypothesis were done on the Nafion membrane degradation in Fuel Cell [38]. On one hand, some research groups assumed that the membrane degradation was caused by the presence of more vulnerable defects in the polymer matrix. On the other hand, there was the suggestion of undesired Fenton's reagents in solution as side effect of the catalyst. Yu and colleagues, by mean of QM calculations, have demonstrated that radicals species (OH* and H*) formed on the catalyst surface have three different mechanisms by which they can cause degradation of defect free Nafion Membrane [38].

Computational investigation at molecular level is also used to understand the influence of noncovalent interactions on the solvent flux in ceramic nanofiltration and ultrafiltration membranes [39]. In this case, solvent- parameters such as minimal or effective diameter of the solvent molecule were evaluated by the study of the van der Waals surface and volume of the molecules of this solvent that are function of isotropic noncovalent interactions. The computed data, studied by ab initio approaches, thus free of adjustable parameters, were compared with the measured fluxes. A robust correlation among the square of solvent diameter and the total Hansen solubility parameters was found.

I.3 Aim and outline of the Thesis.

As previously mentioned, the knowledge of the multiple interactions, taking place at the nanoscale, in solute/electrolyte/polymer systems are one bottleneck regarding the improvement of the membrane processes like nanofiltration and electrodialysis.

In this context, this Thesis is focused on the investigation the mechanisms, at the molecular scale, that govern the transport of neutral organic solute through a cation exchange membrane.

The objective is to understand the behavior of a CMX membrane by using combined computational and experimental approaches. More precisely, it is focused on the understanding of mechanisms and interactions by which the counter-ions, used for the conditioning of the cation-exchange membrane, affect the transfer of the organic solute.

On one hand, it is known from previous theoretical *ab-initio* studies that noncovalent interactions and in particular hydrogen bonds control different membrane properties [40] [41].

On the other hand, since previous work on ion exchange membranes pointed out that the fluxes modification was mainly due to some change in the membranes properties at the molecular level, the structural changes of the organic matter in electrolyte solutions will not be explored [25]. Thus, the computational investigation will consider the only interactions in which the membrane is concerned.

The *ab-initio* modeling of polymer chains within supramolecular complexes is always a difficult task due to the several possible conformers or windings of the chains. In addition, the presence of cations makes the complexity of the systems higher. In order to face these difficulties a specific procedure will be implemented. The system will be divided into fundamental pieces, called "building blocks", such as the hydrated glucose, the monomers and the electrolytes. Firstly, these building blocks will be investigated separately. Secondly, these building blocks will be merged into more complex systems. In particular, systems containing the hydrated glucose and polymer fragments equilibrated with different cations will be used to evaluate if noncovalent interactions, correlated to the sugar/membrane interaction, are cation dependent. Moreover, systems of two polymeric chains in interaction, equilibrated with different counter-ions, will be developed to investigate the chain-chain interactions and the possible effects of the cation on the properties of the polymer network.

Quantum calculations are required in order to assess accurately the aforementioned interactions. However, quantum calculations need long computational times, especially when large molecular models have to be investigated. In these cases, Quantum Mechanics and Molecular Mechanics (QM/MM) approaches have proven to be reliable [42] [43]. Consequently, two computational approaches will be adopted in this work. The single building blocks will be studied at the quantum level using accurate levels of theory, while larger systems will be investigated using the QM/MM approach.

Experimental methods will be also investigated to get an image of the membrane properties at the molecular scale. Molecular scale sensitive techniques such as Infra-Red Spectroscopy (IR), Differential Scanning Calorimetry (DSC) and contact angle measurements will be used to get physical properties and their variation according to the ionic composition. Computed and experimental values will be compared in order to check the molecular mechanisms involved. These results will be also correlated with those obtained at the system scale dealing with the mass transfer through the membrane.

The manuscript is outlined as follows.

In Chapter 2, the information concerning the computational and the experimental approaches will be detailed. The theoretical background of the computational theories will be presented and discuss. Moreover, the experimental techniques will be also described.

Chapter 3 will concern the investigation of the properties of ions in solution using a computational approach. The computed properties will be also correlated to the experimental values of the sugar fluxes through NF and ion-exchange membranes obtained in previous work.

The core of the computational study will be reported in Chapter 4. In the first part of this chapter, the building blocks construction will be reported as well as the accuracy of the theory level for both the computational methods, i.e. Quantum Mechanics and Molecular Mechanics. In the second part, the theoretical investigations of the polymer-sugar interactions and polymer-polymer interactions will be presented and discussed.

Chapter 5 will describe the characterization of the CMX membrane. IR spectra will be computed at Quantum Mechanics level and compared with IR experimental measurements. Then, additional experimental investigation involving DSC and Contact Angle measurements will be presented.

Finally, Chapter 6 will end the general conclusions and recommendations for future work.

I.4 References

[1] Global Footprint Network, "August 19th is Earth Overshoot Day: The date our Ecological Footprint exceeds our planet's annual budget," 2014.

[2] Global Footprint Network, "Earth Overshoot Day," 2014.

[3] A. I. Stankiewicz and J. A. Moulin, "Process Intensification: Transforming Chemical Engineering," *Chem. Eng. Prog*, pp. 22–34, 2000.

[4] B. Van der Bruggen, E. Curcio, and E. Drioli, "Process intensification in the textile industry: the role of membrane technology.," *J. Environ. Manage.*, vol. 73, no. 3, pp. 267–74, 2004.

[5] E. Drioli and E. Curcio, "Perspective Membrane engineering for process intensification: a perspective," vol. 227, pp. 223–227, 2007.

[6] E. Drioli, A. I. Stankiewicz, and F. Macedonio, "Membrane engineering in process intensification—An overview," *J. Memb. Sci.*, vol. 380, no. 1–2, pp. 1–8, 2011.

[7] M. Sadrzadeh and T. Mohammadi, "Sea water desalination using electrodialysis," *Desalination*, vol. 221, no. 1–3, pp. 440–447, 2008.

[8] G. M. Geise, D. R. Paul, and B. D. Freeman, "Fundamental water and salt transport properties of polymeric materials," *Prog. Polym. Sci.*, vol. 39, no. 1, pp. 1–42, 2014.

[9] M. A. Shannon, P. W. Bohn, M. Elimelech, J. G. Georgiadis, B. J. Mariñas, and A. M. Mayes, "Science and technology for water purification in the coming decades.," *Nature*, vol. 452, no. 7185, pp. 301–10, 2008.

[10] H. Strathmann, "Electrodialysis, a mature technology with a multitude of new applications," *Desalination*, vol. 264, no. 3, pp. 268–288, 2010.

[11] A. Elmidaoui, F. Lutin, L. Chay, M. Taky, M. Tahaikt, and M. R. Alaoui Hafidi, "Removal of melassigenic ions for beet sugar syrups by electrodialysis using a new anion-exchange membrane," *Desalination*, vol. 148, pp. 143–148, 2002.

[12] R. Bernstein, S. Belfer, and V. Freger, "Toward Improved Boron Removal in RO by Membrane Modification: Feasibility and Challenges," *Environ. Sci. Technol.*, vol. 45, pp. 3613–3620, 2011.

[13] Z. Wang, Y. Luo, and P. Yu, “Recovery of organic acids from waste salt solutions derived from the manufacture of cyclohexanone by electrodialysis,” *J. Memb. Sci.*, vol. 280, no. 1–2, pp. 134–137, 2006.

[14] C. Abels, F. Carstensen, and M. Wessling, “Membrane processes in biorefinery applications,” *J. Memb. Sci.*, vol. 444, pp. 285–317, 2013.

[15] X.-L. Wang, C. Zhang, and P. Ouyang, “The possibility of separating saccharides from a NaCl solution by using nanofiltration in diafiltration mode,” *J. Memb. Sci.*, vol. 204, no. 1–2, pp. 271–281, 2002.

[16] A. Bouchoux, H. Balmann, and F. Lutin, “Nanofiltration of glucose and sodium lactate solutionsVariations of retention between single- and mixed-solute solutions,” *J. Memb. Sci.*, vol. 258, no. 1–2, pp. 123–132, 2005.

[17] S. Bouranene, A. Szymczyk, P. Fievet, and A. Vidonne, “Influence of inorganic electrolytes on the retention of polyethyleneglycol by a nanofiltration ceramic membrane,” *J. Memb. Sci.*, vol. 290, no. 1–2, pp. 216–221, 2007.

[18] A. Escoda, P. Fievet, S. Lakard, A. Szymczyk, and S. Déon, “Influence of salts on the rejection of polyethyleneglycol by an NF organic membrane: Pore swelling and salting-out effects,” *J. Memb. Sci.*, vol. 347, no. 1–2, pp. 174–182, 2010.

[19] E. Singlande, “Procedes integres couplant l’electrodialyse et le traitement biologique : influence de la composition ionique et application au traitement des effluents salins,” Université Toulouse III - Paul Sabatier, 2006.

[20] G. Bargeman, J. M. Vollenbroek, J. Straatsma, C. G. P. H. Schroën, and R. M. Boom, “Nanofiltration of multi-component feeds. Interactions between neutral and charged components and their effect on retention,” *J. Memb. Sci.*, vol. 247, no. 1–2, pp. 11–20, F. 2005.

[21] C. Umpuch, S. Galier, S. Kanchanatawee, and H. R. Balmann, “Nanofiltration as a purification step in production process of organic acids: Selectivity improvement by addition of an inorganic salt,” *Process Biochem.*, vol. 45, no. 11, pp. 1763–1768, 2010.

[22] V. Boy, H. Roux-de Balmann, and S. Galier, “Relationship between volumetric properties and mass transfer through NF membrane for saccharide/electrolyte systems,” *J. Memb. Sci.*, vol. 390–391, pp. 254–262, 2012.

[23] L. X. Tuan and C. Buess-Herman, “Study of water content and microheterogeneity of CMS

cation exchange membrane," *Chem. Phys. Lett.*, vol. 434, no. 1–3, pp. 49–55, 2007.

[24] K. Zhuo, J. Wang, H. Wang, "Volumetric properties for the monosaccharide (D-xylose, Darabinose, D-glucose, D-galactose) –NaCl- water systems at 298.15K" *Carbohydrate Research,* vol 328, pp. 383-391, 2000.

[25] S. Galier, J. Savignac, and H. Roux-de Balmann, "Influence of the ionic composition on the diffusion mass transfer of saccharides through a cation-exchange membrane," *Sep. Purif. Technol.*, vol. 109, no. 0, pp. 1–8, 2013.

[26] J. Savignac, "Impact des interactions membrane/électrolyte sur la diffusion de sucres à travers des membranes échangeuses d'ions," Doctorat de l'Université Toulouse III - Paul Sabatier, 13 octobre 2010.

[27] M. A. Izquierdo-Gil, V. M. Barragán, J. P. G. Villaluenga, and M. P. Godino, "Water uptake and salt transport through Nafion cation-exchange membranes with different thicknesses," *Chem. Eng. Sci.*, vol. 72, pp. 1–9, 2012.

[28] J. P. G. Villaluenga, V. M. Barragán, B. Seoane, and C. Ruiz-Bauzá, "Sorption and permeation of solutions of chloride salts, water and methanol in a Nafion membrane," *Electrochim. Acta*, vol. 51, no. 28, pp. 6297–6303, 2006.

[29] C. E. Evans, R. D. Noble, S. Nazeri-Thompson, B. Nazeri, and C. a. Koval, "Role of conditioning on water uptake and hydraulic permeability of Nafion® membranes," *J. Memb. Sci.*, vol. 279, no. 1–2, pp. 521–528, 2006.

[30] P. N. Pintauro and D. N. Bennion, "Mass Transport of Electrolytes in Membranes. 2. Determination of NaCl Equilibrium and Transport Parameter for Nafion," *Ind. Eng. Chem. Fundam.*, vol. 23, no. 2, pp. 234–243, 1984.

[31] P. Długołęcki, B. Anet, S. J. Metz, K. Nijmeijer, and M. Wessling, "Transport limitations in ion exchange membranes at low salt concentrations," *J. Memb. Sci.*, vol. 346, no. 1, pp. 163–171, 2010.

[32] J. Lehn, "Supramolecular Chemistry - Scope and Perspectives. Molecules, Supermolecules and Molecular Device (Nobel Lecture)," *Angew. Chemie, Int. Ed. English*, vol. 27, no. 1, pp. 89–112, 1988.

[33] J.-M. Lehn, "Toward self-organization and complex matter.," *Science (80-.).*, vol. 295, no. 5564, pp. 2400–3, 2002.

[34] S. J. Grabowski, W. A. Sokalski, E. Dyguda, and J. Leszczyn, "Quantitative Classification

of Covalent and Noncovalent H-Bonds," *J. Phys. Chem. B*, vol. 110, pp. 6444–6446, 2006.

[36] R. M. Silverstein, F. X. Webster, and D. J. Kiemle, *Spectrometric identification of organic compounds*, 7th ed. John Wiley & Sons, Inc., 2005.

[37] G. De Luca, A. Gugliuzza, and E. Drioli, "Competitive Hydrogen-Bonding Interactions in Modified Polymer Membranes: A Density Functional Theory Investigation," *J. Phys. Chem. B*, vol. 113, pp. 5473–5477, 2009.

[38] T. H. Yu, Y. Sha, W.-G. Lui, B. V. Merinov, P. Shirvanian, and W. A. I. Goddard, "Mechanism for Degradation of Nafion in PEM Fuel Cells from Quantum Mechanics Calculations," *J. Am. Chem. Soc.*, vol. 133, pp. 19857–19863, 2011.

[39] G. De Luca, F. Bisignano, F. Paone, and S. Curcio, "Multi-scale modeling of protein fouling in ultrafiltration process," *J. Memb. Sci.*, vol. 452, pp. 400–414, 2014.

[40] G. De Luca, L. Donato, S. García Del Blanco, F. Tasselli, and E. Drioli, "On the cause of controlling affinity to small molecules of imprinted polymeric membranes prepared by noncovalent approach: a computational and experimental investigation.," *J. Phys. Chem. B*, vol. 115, no. 30, pp. 9345–51, 2011.

[41] A. Gugliuzza, G. De Luca, E. Tocci, L. De Lorenzo, and E. Drioli, "Intermolecular interactions as controlling factor for water sorption into polymer membranes.," *J. Phys. Chem. B*, vol. 111, no. 30, pp. 8868–78, 2007.

[42] V. V Barkaline, Y. V Douhaya, and A. Tsakalof, "Computer simulation based selection of optimal monomer for imprinting of tri-O-acetiladenosine in polymer matrix: vacuum calculations.," *J. Mol. Model.*, vol. 19, no. 1, pp. 359–69, 2013.

[43] X. Kang, Y. Song, Y. Luo, G. Li, Z. Hou, and J. Qu, "Computational Studies on Isospecific Polymerization of 1-Hexene Catalyzed by Cationic Rare Earth Metal Alkyl Complex Bearing a C 3 i Pr-trisox Ligand," *Macromolecules*, vol. 45, pp. 640–651, 2012.

Chapter II

Computational and Experimental approaches

II.1 Theoretical Background

II.1.1 Introduction

The link among computational methods and experiments is every day more prominent since modeling and simulation techniques can be a sort of eyes for experimentalists at nanoscopic and sub-nanoscopic levels, but also in case of trials carried out in unusual or dangerous procedure [1]. In addition, computational approaches allow to obtain quantities and knowledge that by means of the experimental methods are very long and difficult to obtain, and in some cases impossible with the current instrumentations. In fact, computational procedures can provide useful information that are not directly investigated by experimental techniques or can be tested but only by inaccurate approximations [2] [3]. The computational techniques, and in particular the investigation at atomic and sub-atomic scale, allow to make a leap forward in the knowledge since only by knowing the infinitesimally small, it is possible learn about the infinitely large.

Computational methods can be divided in 3 macro-categories depending on the scale of the simulation, from the molecular to the macro scale

The first category is that of Nano and Sub-nano models. In *ab initio* quantum mechanics calculations, the electron properties are taken in account breaking and forming of bonds interaction energies, spectral properties and noncovalent interactions. Quantum Mechanics allows also being free from adjustable or fitting parameters [4] [5]. Unfortunately, due to the high computational demand, quantum models cannot be used for systems exceeding hundreds of atoms. Instead, Molecular Mechanics has the advantages to be less computational demanding (number of atoms up to 10^9). Furthermore, dynamical properties can be computed as well as trajectories, conformers and packing. But, since information about electrons is lost, the forming and/or breaking of bonds (even those noncovalent) cannot be studied.

The second category is that of mesoscale models. In these models, the discrete composition of materials is considered. However, the entities used to describe the materials are not atoms but supra-atomic complexes in which the atomic properties are averaged. These techniques can be used for the investigation of thermal stability, morphological behavior, formation of domains and related properties. A non-trivial work about parameterization has to be done, and

information from the molecular scale is needed.

Finally, in macroscopic models the object of the investigation is described as a continuum unit cell. Crack propagation, heat and mass transport, permeation flux can be investigated as well as macroscopic structural behavior. Details about molecular interactions are not considered since they are included in the initial parameters, thus modifications at these levels cannot be investigated.

The objective of this Thesis is to investigate the phenomena, at molecular level, that govern the transport of neutral organic solutes through a membrane. Thus, an overview of the Quantum and Molecular Mechanics theories and their combination used in this Manuscript is presented below.

II.1.2 Quantum Mechanics: the Density Functional Theory (DFT)

In 1929 Paul Dirac stated that: "*The fundamental laws necessary for the mathematical treatment of large parts of physics and the whole of chemistry are thus fully known, and the difficulty lies only in the fact that application of these laws leads to equations that are too complex to be solved.*"

He was referring that a complete mathematical description of a generic N-electron molecular system can be provided by the Schrödinger equation:

$$H\psi = E\psi \qquad \text{(II.1)}$$

in which H is the Hamiltonian operator, E is the system energy and ψ is the wave function. It is worth noting that the modulus squared of the wave function is a real number interpreted as the probability density of finding a particle in a given place at a given time [6].

In practice, analytic solutions of these equations are available only for a single particle that it is not in interaction with any other, while the Schrödinger equations of many-body systems are extremely complex to be solved. Indeed, taking as example the evaluation of the energy for a single benzene molecule, the Schrödinger equation that must be solved has 162 variables deriving from the spatial coordinates of the 54 bodies, i.e. 12 nuclei and 42 electrons, of its molecular structure. Thus, approximations are essential to solve the Schrödinger equation.

One of the most important approximations in Quantum Mechanics is that of Born -

Oppenheimer (BO). It deals with the fact that nuclei are very slow in their movements with respect to electrons due to the high ratio among the electron and nuclear masses. Thus, nuclei can be considered as fixed and represented by a potential energy. This means that their contribution can be neglected from the Schrödinger equation resulting in a decreasing of variable [6].

However, even if the nuclei are not considered, the number of variables related to the electron is still high. Always taking the example of benzene, without the nuclei contribution, its Schrödinger equation has 126 variables due to the coordinates of its 42 electrons. Furthermore, the case of benzene is very a simple case. Just to give an idea, in this Thesis the systems to be treated have about 1000 electrons.

To overcome this problem, another approach is necessary: the independent electron approximation. This approach is based on the possibility to express the multi-electron molecular Hamiltonian by using *n* mono-electron Hamiltonians, where *n* is the number of electrons present in the system. Thus, the molecular Hamiltonian becomes the sum of n mono-electron Hamiltonians, that each one of those provides the kinetic energy of one electron in interactions with the nuclei. In this way, the Schrödinger equation becomes easy to calculate. Unfortunately, this approximation does not consider the inter-electron interactions and this lack leads to wrong results [7].

At this point, during the development of Quantum Mechanics, there was an impasse: the independent electron approximation leads to wrong results, the multi-electron Hamiltonian is irresolvable. In the early '30s, the solution of this problem was found by Vladimir Fock, one of the fathers of the Quantum Mechanics technique named: Hartree - Fock (HF) method. He proposed to use the independent electron approximation, but using an additional operator for upgrading each mono-electron Hamiltonian, the Fock operator, that is the sum of two operators. One is called the Coulomb term and it concerns the repulsion potentials among the electrons. This term gives an average local potential of the electrostatic interactions. The other is the exchange potential. It reduces the repulsive electrostatic potential among two electrons belonging to two different orbitals with the same spin. It is strictly related to the second Hund's rule.

It is worth noting that in the Coulomb term, the use of an average potential is less reliable than the solution of the Schrödinger equation that includes the electron-electron interactions. Since the correlations among the electrons in the systems is lost, the difference among the values obtained with the use of the Fock operator and the real value is called *correlation energy [6]*

[7]. Considering that this energy expresses our incapacity to find the exact solution resolving the Schrödinger equation, Feynman named it *stupidity energy [8]*.

At this point, the bases of Quantum Mechanics were set and the first calculations in its frame could be performed. The use of the approximations briefly discussed in this paragraph is known as Hartree -Fock method (HF).

In practice, analytic solutions of these equations are available only for a single particle that it is not in interaction with any other. The solution of equations describing "real systems" needs sophisticated numerical approaches, i.e. the HF method (and progenies), dealing with the approximation concerning the study of the quantum many-body systems partially discussed above. Thus, in the early '30s, the progress of computational chemistry on real systems was deadlocked for scientific reason (advancement of numerical methodologies/ approximations) and technological (development of *High Performance Computing, parallelization*).

The development of supercomputers able to run Quantum Mechanics calculations was reached only in the '90s with the Fujitsu Numerical Wind Tunnel in Japan and the Intel Paragon in USA. However, concerning the Quantum Mechanics theories, something new came within the '60s. In these years, precisely in 1964 and 1965, Walter Kohn laid the foundations of the Density Functional Theory (DFT) by two papers, the first published with Pierre Hohenberg [9], the second with Lu J. Sham [10].

Density Functional Theory is an alternative way to investigate the electronic structure of molecules since it is based on the investigation of electron density (ρ_{el}) of the system instead of its wave function. This, as it has been mentioned by the same Kohn during its Nobel lecture, gave two contributions to Quantum Mechanics [11].

The first is on the fundamental understanding of the QM theories. In fact, to achieve the resolution of the Schrödinger equation, physicists were mainly focused on the mathematical problems and due to the extreme complexity of the equations, the physical meaning was lost. Instead, DFT focuses always on real quantities easily viewable/imaginable also for large systems. This different point of view allows a better comprehension of the quantum phenomena, and consequently, it allows making further progress.

The second is a more practical contribution. Quantum Mechanics calculations are in general computationally expensive, either HF or DFT. However, the computational time of a DFT calculation rises much more slowly with the number of atoms (electrons) in the system than a HF calculation. This decreasing in computational times directly depends from the use of the

density function instead of the wave function, but, it is also influenced by the more simple conceptual and mathematical ways used to treat the correlation energy.

Recapping, the HF method deals with the approximation concerning the study of the quantum N-body systems computing the many-electron wave function. On the other hand, Density Functional Theory is based on the investigation of the electron density (ρ_{el}) of the system. It should be emphasized that the two systems are complementary. In fact, electron density and wave function are completely interconnected since ρ_{el} can be obtained by the electron wave function. Furthermore, the integration of ρ_{el} in the space gives the number of electron present in the system. The main advantage of using DFT is that ρ_{el} is dependent on only 3 spatial coordinates, while ψ (and thus the methods related to it) is dependent upon 3N coordinates representing the N electrons in the system [12] [13].

The physical legitimations of the use of electron density as basic variable instead of wave function are two theorems. Quoting the paper of Hohenberg and Kohn from 1964, the first theorem states: "*The external potential $V_{ext}(\mathbf{r})$ is (to within a constant) a unique functional of $\rho(\mathbf{r})$. Since, in turn $V_{ext}(\mathbf{r})$ fixes H, we see that the full many particle ground state is a unique functional of $\rho(r)$.*"[9]. In other terms it asserts that the energy can be express like a functional of electron density:

$$E= E[\rho_{el}] \qquad \text{(II.2)}$$

The second theorem is the variational principle: "*The functional that delivers the ground state energy of the system, delivers the lowest energy if and only if the input density is the true ground state density.*":

$$\rho^{trial} \geq 0 \text{ and } \int \rho^{trial}(\mathbf{r})d\mathbf{r} = N \rightarrow E[\rho^{trial}] \geq E^0 \qquad \text{(II.3)}$$

or rather "*given a trial electron density ρ^{trial} that integrated in the space gives the number of electrons in the system, the related energy will be higher or at the limit equal at the true energy system*" [13] [14]. From this it is possible to evince that only with the exact ρ_{el} is possible to calculate the exact energy, while, approximations in ρ give rise to higher energies E.

$E[\rho]$ is the DFT energy functional that can be defined as the sum of the electron kinetic energy T_{el}, iso-electronic non-interacting system, an attractive force nucleus-electron $V_{nu\text{-}el}$ and the interelectronic repulsion $V_{el\text{-}el}$ and can thus be expressed as:

$$E[\rho] = -T_{el}[\rho] - V_{nu\text{-}el}[\rho] + V_{el\text{-}el}[\rho] \qquad \text{(II.4)}$$

These terms are not ordinary functions, but composition of those, since they are functions that

in their turn are dependent from the electron density function. This equation can be also written as:

$$E[\rho] = F_{HK}[\rho] + \int \rho(\mathbf{r})\, v(\mathbf{r})\, d\mathbf{r} \qquad \text{(II.5)}$$

where v(r) is the external potential of the quantum system and $F_{HK}[\rho]$ is the universal functional expressed as :

$$F_{HK}[r] = -T_{el}[r] - V_{el\text{-}el}[r] \qquad \text{(II.6)}$$

where $V_{el\text{-}el}[\rho]$ can be defined by a classical term V_{coul} coulomb representing the repulsion energy easily computable by the coulomb's equation and two non-classical terms:

$$V_{el\text{-}el}[\rho] = V_{coul} + V_{exc\text{-}corr} \qquad \text{(II.7)}$$

$V_{exc\text{-}corr}$ is known as exchange - correlation energy which represents the difference between the kinetic energies of non-interacting and the real interacting systems. Without entering in further mathematical details of the theory, as aforementioned, the role of this term has to be emphasized since they are key-points in the calculations of the system energy. In fact, it defines the specific functional of the method used. The functional calculation is the main problem in DFT, since the exact form is known only for the free electron gas. Fortunately, the computation of physical quantities can be performed by accurate approximations. The development of new functional or the improvement of existing ones is an active field since the use of one or the other depends on the system and the properties under investigation. A more precise $E[\rho]_{exc\text{-}corr}$ increases the reliability and the accuracy of the calculated properties and can enlarge their number and kinds. There are two kinds of functionals, i.e. pure and hybrid. The "pure" functionals are derived by a specific approximation, while the hybrid ones are derived by terms originated by different kinds of approximation or by Hartree-Fock (HF) methodologies. In fact, HF does not consider the correlation energy, but on the other hand the exchange energy is computed in an exact way.

In DFT, the energy of a quantum system is correlated to its electron density by the universal functional and the external potential.

The electron density (ρ) can be expressed as function of molecular orbital (ψ), or more precisely, as the sum of the squares of the molecular orbitals. The molecular orbitals can be approximated as linear combination of atomic orbitals (ϕ) centered on the atomic nuclei coordinates. The latter, with their positions and charges, define the external potential v(**r**). Thus, the atomic orbital are useful terms to express the electron density:

$$r = \sum_i |\psi_i|^2, \quad \psi = \sum_m a_m \phi_m \rightarrow r = r(\phi_1, \phi_2, \phi_3, ..., \phi_m) \qquad \text{(II.8)}$$

The set of atomic orbitals used to describe each molecular orbital is called basis set. The atomic orbitals are proportional to the exp (-r) and functions with the same dependence are called Slater-type orbitals (STO). However, the use of this kind of functions makes the calculation of some terms difficult from a mathematical point of view. For this reason, another kind of mathematical representation is used, the Gaussian type orbitals (GTO). The GTO functions are mathematically easy to treat, but they are proportional to exp ($-r^2$), thus they do not have the same trend of atomic orbital, while it is well represented by STO orbitals. Consequently, linear combinations of those are used in order to increase their reliability as basis functions. The single Gaussian function is also named "primitive". Of course, the number of primitive functions increases the approximation of the calculus, but at the same time, the computational time increases. To summarize, the electron density can be described by molecular orbitals, which are represented by atomic orbital using the basis sets, that are composed by basis functions expressed as linear combination of Gaussian functions called "primitives" [13] [14].

Over the years, a huge number of basis sets has been implemented for many different chemical computational investigations. In this Thesis the *multiple-ζ split-valence basis sets* will be used, and only a brief explanation of those will be given. When an atomic orbital is represented by only one basis function it is called single- ζ. If more primitives are used to describe the same atomic orbital, a raise in the modeling accuracy is reached. It was also noticed that for a given number of primitives, higher accuracy is achieved if the primitives are partitioned into more basis functions. When more than one basis function is used to represent an atomic orbital, it is called multiple-ζ. Because this is true especially for the valence atomic orbital, it is a common practice to use single-z to describe core atomic orbitals and multiple–ζ for valence atomic orbitals. For example, the structure of the 6-311G basis sets, a common basis set used also in this work, is illustrated. The name of this basis set is self-explanatory and it is composed by 3 different parts: the number (6) before the dash, the digits (311) after the dash and the G that means Gaussian-type functions. The first digit indicates the number of primitives used in a single basis function to represent the core atomic orbitals. In this case, 6 primitives are linearly combined in a single basis function. Indeed, since the number after the dash is composed by three digits, three are the basis functions used to approximate the valence atomic orbitals. Each basis function is composed by a different number of primitives that is expressed by the value of the digit. In the 6-311G basis set, the valence orbital are thus modeled by 3 basis functions.
The first one is represented by 3 Gaussian-type functions (3 is the first digit after the dash).
The second one is composed by a single Gaussian function (as the second digit after the dash).
The third is also expressed by a single Gaussian function (last digit).

Furthermore, some specific basis functions such as polarization and/or diffusion can be added to increase the reliability for the investigation of some particular systems.

As established by the Kohn-Sham theorem, the variational method is applicable also in the frame of Density Functional Theory. Thus, the minimization of the total energy functional respect to the density function gives an exact value only if the exchange-correlation energy is exact, while if $V_{exc\text{-}corr}$ is approximated, also the computed system energy will be approximated. Furthermore, since the density function is expressed as a linear combination of molecular orbitals, which are expressed by linear combination of atomic orbital, the minimization of the total energy functional represented in function of the same molecular orbitals gives the coefficients of the linear combination by which the density function is expressed.

The equations that deal with the optimization of the coefficients used to minimize the total functional describing the density of the system and its other properties are the Kohn-Sham equations. These equations are the core of the calculations in Density Functional Theory.

From the discussion above, it is possible to define what is the necessary information to perform a calculation in DFT. First of all, the external potential, thus the information about the system geometry and the nuclei charge, should be defined. The number of electrons present in the system is also essential as well as the spin of the system. A core exchange-correlation functional able to treat the properties under investigation should be selected/implemented. Then the basis sets have to be assigned for each nucleus.

Concerning the definition of the external potential, thus on the initial geometry, it should be mentioned that a particular disposition of the atoms does not provide the lowest total energy of the molecular system. The initial geometries have to be physical and chemical consistent but they have to be treated as guesses, thus an optimization to find the nuclei arrangement corresponding to a minimum in the potential energy surface must be performed. Moreover, the potential surface energy of a molecule has several minima corresponding to the possible conformers of that molecule. The scanning of the potential surface energy to characterize the probability of existence of the different conformers for a big molecule with numerous rotamers is a very difficult task in the frame of Quantum Mechanics due to the high computational demand and the need of initial definition of the geometries. The issue of the initial geometry definition could be addressed by the use of Quantum Dynamics, but the computational demand for systems like those investigated in this Thesis is extremely high. Anyway, the conformational research can be carried out also using other molecular theories such as in the frame of Molecular

Mechanics (as in this Manuscript) or its combinations with Quantum Mechanics (QM/MM). Conformational researches in pure MM or QM/MM are both reliable and less computational expensive compared to a Quantum Dynamics calculation. An adequate analysis of the potential energy surface (PES) is an important preliminary step for the investigation of the vibrational properties of the molecule (Infra-Red and Raman spectra). In many typical algorithms used to investigate the potential energy surface based on the calculation of the first derivative, it is difficult to distinguish if the geometry is related to a minimum or to a saddle point. Saddle points refer to transition geometries, particularly interesting during reaction studies in QM, but at the same time computational studies on them could give information non comparable with the experimentally investigated samples in equilibrium as the case of this Thesis. In fact, the geometries related to the saddle points of a PES are unstable geometries, while stable and highly probable geometries have to be used in the QM investigated IR spectra in order to be comparable with the experimental IR analysis.

By mean of Quantum Mechanics, the characteristic vibrational properties of molecules can be investigated. Thus, the Infra-Red Spectrum can be computed and compared with experimental data. The vibrational mode investigation strictly regards the nuclear displacement. The information about the nuclei displacements is already included in the potential energy, but unfortunately, it is not completely examined during the geometry optimization by Quantum Mechanics theories. In fact, due to the optimization algorithms, only the minimum or the saddle points of the potential energy surface are known. Thus, in order to perform a vibrational analysis by computational methods, the internal motions of the nuclei are approximated with a harmonic behavior. Assuming this, each atom is perturbed in the three dimensions and in positive and negative directions. Then, the changes in the system energy are used a second derivative matrix of the system energy. The diagonalization of this matrix and the associated eigenvalues provide *k*, the force constants of the vibrational modes. From k and using the harmonic approximation, the vibrational frequencies (ν), can be calculated by the equation:

$$\nu = \frac{1}{2\pi}\sqrt{\frac{k}{\mu}} \qquad \text{(II.9)}$$

where μ is the reduced mass of the atoms, and the associated intensity (I) can be expressed as:

$$I = \frac{1}{2}kx^2 \qquad \text{(II.10)}$$

where *x* represents the nuclei displacements. The Infra-red simulations should be performed in

a high level of theory since the above formulas require that the geometry is in the minimum or in a saddle point of the potential energy surface. Furthermore, the calculation of the matrix for the calculation of *k* has to be also performed in the same level of theory since a change in the functional or basis sets implies a change in the profile of the potential energy surface.

Vibrational analysis gives also information about the reliability of the optimized geometry by the presence or the absence of negative values in the matrix diagonal (related to *k* values). In fact, the presence of negative values means that some vibrational modes can decrease the system energy, what means that the geometry in object of the vibrational investigation does not correspond to a minimum of the potential energy surface. There are two possible cases in this situation, the presence of more than 1 negative value or the presence of only 1. If the analyzed geometry has more than one negative value, a new optimization should be performed with stricter convergence criteria or higher level of theory, since the presence of more than one vibrational mode means that the geometry is unstable. Instead, in the case of only 1 negative value the evaluated geometry is related to a transition state, thus could be interesting to be analyzed.

Finally, it should be mentioned that the vibrational analysis by Quantum Mechanics are affected by an error of 5-10% on the computed intensities due to the assignment in the frequency modes. This will have to be taken into account for further discussions and comparison.

II.1.3 Molecular Mechanics (MM)

Molecular Mechanics is another chemical computational technique. In MM, the system energies are computed by the typical equation of the classical mechanics. Atoms and bonds are respectively treated as "balls" and "springs" with defined mass, charge and force constants. This means that electron effects are considered in the force constants of the springs representing the bonds between the atoms or the partial charges distributed over the latter. However, given the polarization effects (important specially when dealing with ions and water molecules) as well as noncovalent interactions guided by the electrons of the system, significant changes on the atomic charge of the bond strengths are possible depending on the system under study. It is thus difficult to use data-base to describe these properties. Nevertheless, MM approach requires much less computational time compared to quantum methods thus allowing the study of systems with thousands of atoms, an unachievable goal by QM.

The system energy E in MM depends on the position of the atoms in the space (**r**) and it is the sum of three terms:

$$E(\mathbf{r}) = E_{\text{bonded}}(\mathbf{r}) + E_{\text{non-bonded}}(\mathbf{r}) + E_{\text{special}}(\mathbf{r}) \quad \text{(II.11)}$$

- E_{bonded} ($\mathbf{r}$) refers to the effect of the force constants of the springs between atoms that are covalently bounded. Thus it is linked to bond stretching, angle bending, torsion/distortion angle rotations. Their mathematical representations are similar to the very well-known Hooke's law in harmonic form for the stretching, bending and distortion terms and in trigonometrically form for the torsional term. The following term regarding the bond stretching is used as example:

$$E_{str}(\boldsymbol{r}) = \sum \frac{1}{2} k_b (b - b_o)^2 \quad \text{(II.12)}$$

where k is the force constant, *b* is the bond length under analysis, b_0 is the reference bond length. Thus, the contributions of the bounded terms are computed as the change in energy of each atom when moving away from the equilibrium position.

-The second term in the system energy, $E_{\text{non-bonded}}$ ($\mathbf{r}$), comes from the interaction energies among two atoms spaced by at least 3 bonds. It can be explained by two characteristic terms, the Leonard-Jones term and the Coulomb term. The first deals with the van der Waals interactions, while the second with the interactions among atoms due to their partial charges. Thus, $E_{\text{non-bonded}}$ ($\mathbf{r}$) is the energy that describes the repulsion or the attraction among atoms due to the electrostatic and London interactions.

-Finally, E_{special}, in real, encloses all the "special" terms useful to characterize the modeling. It can contain terms that help the correlation among E_{bonded} and $E_{\text{non-bonded}}$ as well as terms referring to possible external potentials [7] [13] [15].

Therefore, in order to perform molecular mechanics calculations, several parameters such as force constants, bond length, equilibrium angles, partial charges and Leonard-Jones term are needed. Since these parameters are function of the chemical environment of the atoms, many molecular mechanics methods include different parameters for the same atom but of different kind e. g. carbon in an aliphatic chain or in benzene or in an aldehyde. The coupling among the set of all the parameters and the mathematical function used to correlate them gives rise to what is known as Force Field (FF). Although MM is a great tool to describe systems in which thousands of atoms are present, due to the structure of FFs themselves, MM presents some crucial limitations. The absence of the electronic properties of the atoms reduces the capability to model chemical reactions or an overall in the electron distribution in the molecule e. g. when polarization effects are important. Even if these parameters are carefully derived for one system, it does not mean that they are adequate for another system. For this reason, preliminary tests

(FF calibration) on their accuracy are usually required before using them outside of their "comfort-zone" [1].

In this Thesis, Molecular Mechanics theories are used combined with QM to investigate large systems (see next paragraph) and to carry out conformational analysis. In fact, conformational analysis is essential for an accurate modeling of polymer chains. But as explained an *ab-initio* approach is difficult and computational expensive due to the large number of atoms and the several possible conformers or windings of the chains. Thus, Molecular Mechanics will be used for the scanning of the potential energy surface, but the optimization of the selected geometries will be refined by QM.

II.1.4 Quantum Mechanics/Molecular Mechanics

As pointed out before, each quantum or classical molecular modeling theory has its strength and weakness. On one hand Quantum Mechanics is needed to describe the formation and break of chemical bonds or to assess noncovalent interactions in which strong effects of electron polarization are present avoiding adjustable parameters. But it requires long computational times, especially when macromolecules have to be investigated. On the other hand, Molecular Mechanics requires less computational power, but it shows some limitations regarding the accuracy on the noncovalent investigations. In case of large systems, it is reasonable to think to use a method that could merge the strength points while reducing the weaknesses. For this, Quantum Mechanics/Molecular Mechanics (QM/MM) methods were implemented and they have become a familiar tool for the modeling of large atomic systems. In 1976, Wardhel and Levitt were the first researchers to introduce the concept of QM/MM used to investigate enzymatic reactions. However, the use of this method started to grow only in the last two decades [16].

In general in QM/MM approaches a large system is divided in two regions: one classical and the other quantum. The quantum region is usually defined to be the as small as possible while at the same time considering all the aspect of the performed chemical investigation. For this reason, generally some preliminary trials on smaller systems are necessary to determine the atoms that should be included in this region. The classical region is defined by all the atoms not directly involved in the noncovalent interactions under study, but helpful to consider the environment or structural modifications in the molecules.

In Figure II.1, the quantum and classical regions of a molecular model used in the calculations are shown. In this system, water molecules, counter-ion (i.e. Na^+) and SO_3^- groups interact by

means of strong noncovalent interactions. Then, as explained previously, they are treated at the QM level. The functionalized phenyls are also treated by QM to include the properties of the electron delocalization of the π orbitals in the quantum effects. As a result, the MM zone is composed by the carbon and hydrogen atoms of the backbone and unfunctionalized phenyls. In Figure II.1, to understand the division among QM and MM zones, the carbon and hydrogen atoms treated in MM are represented in blue and light blue respectively.

The bonds between the two zones, i.e. the boundary of QM region (light green in Figure II.1), are replaced by bonds with fictitious atoms, hydrogen atoms in this Thesis. The position of the hydrogen atoms, describing the boundary of the quantum part, is evaluated by the following relationship:

$$\boldsymbol{R}_{Hlink} = (1 - g)\boldsymbol{R}_{QM} + g\boldsymbol{R}_{MM} \qquad \text{(II.13)}$$

where g is a scale factor set at 0.709, $\mathbf{R}_{\text{Hlink}}$ [17] the coordinate of the fictitious hydrogen, while $\mathbf{R}_{\text{QM}}$ and $\mathbf{R}_{\text{MM}}$ are the coordinates of the atoms defining the bond between the quantum and classical (MM) sides of the system [18], respectively. The total energy of the macromolecular models is calculated as the sum of the energies of the classical and quantum parts, respectively:

$$E = E_{qm}^{int}(\mathbf{r}, \rho) + E_{qm}^{ext}(\mathbf{r}, \mathbf{R}, \rho) + E_{mm}(\mathbf{r}, \mathbf{R}) \qquad \text{(II.14)}$$

where **r** represent the coordinates in the QM region, **R** the coordinates of the atoms defining the MM region and ρ the electron density. E_{qm}^{int} is expressed as the vacuum phase energy of the QM region, E_{qm}^{ext} denotes the influence of the electrostatic interactions among the electron density of QM region and the classical charges of MM zone and E_{mm} is function of all the classical interactions computed in MM zone by means of the selected FF as above described [19].

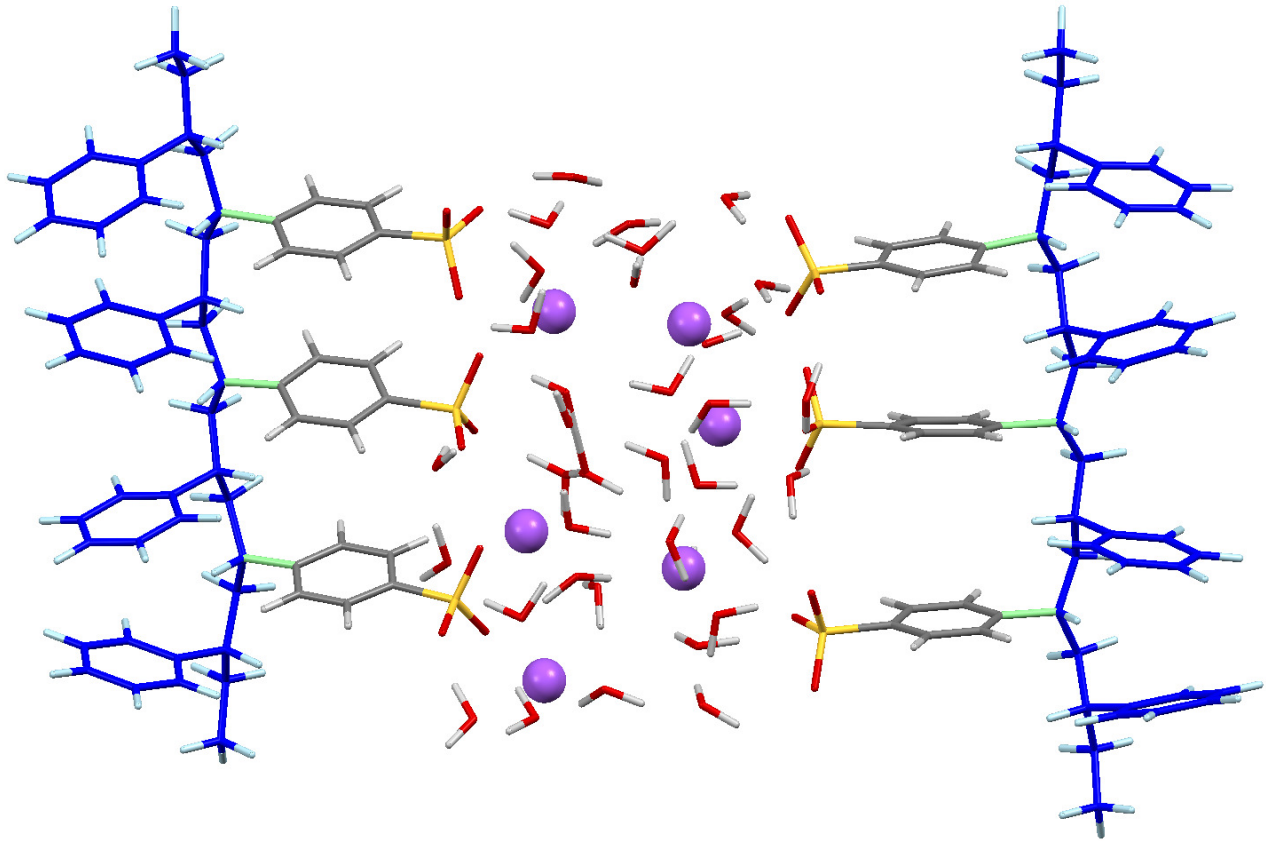

Figure II.1: QM/MM zone-sharing example. C and H atoms of classical region are in blue and light blue colors, the other atoms are part of QM region. The bonds in light green are the boundary of QM region.

Concerning the geometries optimizations, a step by step energy minimization of the two separated regions is carried out in the QM/MM method. In the first step, the QM region is optimized fixing the MM atoms and an electrostatic quantum potential is computed by using the optimized QM region. A successive MM step is run for the optimization of the classical region with the QM atoms represented by the quantum potential. The cycle, formed by the two steps, is repeated until the convergence criteria are reached.

In this Chapter, the bases of the computational methods used in this Thesis were described. In addition, the computational details (e. g. theory level, models), used to characterize the noncovalent interactions in different systems, will be reported later in each Chapter where they will be used.

II.2 Experimental Methodologies

II.2.1 Membrane and membrane conditioning

The membrane used in this work is a CMX membrane (Neosepta), cationic exchange membrane of sulfonated polystyrene-divinylbenzene. Before any characterization, the membrane samples were conditioned following the NF X 45-2000 standard procedure [20]. This treatment consists of a washing cycle with acid (HCl), base (NaOH) and the equilibrating electrolyte solutions to clean the membrane from eventual impurities due to the manufacturing process and to equilibrate it with the different cations. The equilibrated membranes were stored in their own electrolyte solutions. Before performing the analysis such as Infra-Red spectroscopy (IR) and Differential Scanning Calorimetry (DSC), the membrane was washed in ultrapure water to remove the excess of salts.

For the electrolyte solutions, salts containing chloride as anion were used in order to avoid secondary effects coming from a different anion: LiCl, KCl, NH_4Cl, NaCl, $CaCl_2$ and $MgCl_2$. All the chemicals were provided by Sigma Aldrich.

II.2.2 Infrared Spectroscopy

Infrared (IR) spectroscopy is a technique used to investigate material properties by means of the interaction among matter and light in the IR spectrum (wavenumbers range 10 - 13000 cm^{-1}). It is a very well-known technique due to its remarkable quality to be a non-destructive method. IR spectroscopy is based on the phenomenon that chemical bonds can vibrate but only when they are irradiated by a specific IR radiation. In particular, the radiation should have a specific energy, the amount of energy that allows the transition of a covalent bond from its ground vibrational level to an excited one. This change in the energetic level causes a rotational or vibrational motion of the involved atoms and it gives rise to a change in the dipole moment of the molecule.

Two are the most important vibrational modes in a molecule: the stretching (variations on interatomic distances) and the bending (variations in bonds angle). Combinations of those are possible and the most common have specific names (e. g. rocking twisting).

A good model to understand the phenomenon of molecular vibrations is to consider the atoms as ball and the bonds like springs. The combinations of the balls movements in the three directions are the possible vibrations, while the force constants of the springs represent the bond

strengths. In fact, using the Hooke's law, it is possible to give an approximate allocation of the vibrational frequencies by the formula:

$$\nu = \frac{1}{2\pi c}\sqrt{\frac{f}{(M_x M_y)/(M_x+M_y)}} \qquad \text{(II.15)}$$

in which ν (cm^{-1}) is the vibration frequency of a certain vibrational mode, c (cm s^{-1}) the speed of light, M_x (g) and M_y (g) are the atoms mass and f (dyne cm^{-1})is the force constant of the bond. The value of *f* for approximate calculations can be taken as $5*10^{-5}$ dyne/cm (=$5*10^{-8}$ N/m) for single bond, 2 or 3 times this value for double or triple bonds [21]. This formula does not predict the exact value because the environment and coupled interactions are not taken into account. However it is useful to estimate the frequency assignment reliability. Experimentally, the spectra are solved by using tables and databases in which are reported the characteristic vibrational frequencies of the chemical groups, as well as by comparison with previous works.

Some information about the IR spectra of CMX membranes soaked in different electrolytes can be obtained from previous studies on Nafion membranes. Indeed, even if the two polymers used to prepare the Nafion and the CMX membrane are quite different, both have in common SO_3^- as functional groups. Then, since the cation mainly interacts as counter ion with the functional groups, and since the molecular vibrational modes are affected only by very local perturbations, we can expect that the two membranes can show a similar behavior. Falk [22] noticed that in Nafion membranes spectra there is a change in the OH stretching in the H_2O zone with different electrolytes. It should be noticed that the spectra were recorded in low water content condition, about one water molecule for each sulfonate group. Further work with Nafion membrane has shown that also the stretching of the S-O bond in the functional group at about 1060 cm^{-1}, is sensitive to the different counter-ions used to equilibrate the membrane [23].

In the present work, the IR spectra were recorded by a Nexus Diamant spectroscope equipped by an ATR accessory. The spectra were obtained by averaging 20 acquisitions over a range of wavenumber of 600 cm^{-1} to 4000 cm^{-1} with a resolution of 4 cm^{-1}. Since the broad absorption of the water in the bulk and on the surface could overlay the whole spectra range, the samples were dried in an oven at 50°C for 48h before the data acquisition. The low temperature was decided to exclude possible influences of thermal stress on the samples, but at the same time to exclude modification due to the presence of water. The data elaboration was performed using OMNIC software.

II.2.3 Contact angle

The contact angle is the angle that exists, at the thermodynamic equilibrium, among a solid

surface, a drop of fluid in contact with this surface and the fluid in which the surface and the drop are immersed. It is an interesting parameter, since it can be used to study the membrane surface characteristics such as hydrophilic/hydrophobic properties and surface free energies can be extrapolated.

In this work, the contact angles of CMX membranes soaked in different electrolyte solutions were studied by the captive bubble technique. In this technique, the contact angle between a bubble of air and a flat membrane in solution is measured as shown in Fig. II.2 [24] [25]. The captive bubble technique was chosen because it allows the study of the membrane properties in its environmental conditions, avoiding any drying process that could affect the membrane characteristics.

Figure II.2: Example of contact angle measurement by the captive bubble technique

The thermodynamics of contact angles between a liquid and a solid (membrane) is well described by the Young's equation [26] and the output of his work was crucial for the development of Good and Girifalco [27] [28] equation by which the surface free energy of the membrane can estimated:

$$\gamma_s = \frac{\gamma_l(1+cos\Theta)^2}{4\Phi^2} \qquad \text{(II.16)}$$

where γ_s (mJ m^{-2}) is the surface tension of the membrane, γ_l (mJ m^{-2}) is the surface tension of the liquid, θ (°) is the equilibrium contact angle and Φ is an interaction parameter related to intermolecular forces (polar, dispersive, etc.). In this work, Φ can be approximated to 1 due to the close matching between the molecular properties and the intermolecular forces of both phases [27], while the values of γ_l for the different electrolyte solutions are calculated by the Dutcher - Wexler - Clegg method [29]. Thus, it is possible to estimate the surface free energy of the CMX membrane soaked in LiCl, KCl, NH_4Cl, NaCl, $CaCl_2$ and $MgCl_2$ solutions by measuring the contact angles in the different environments.

The contact angle measurements were performed at room temperature blowing 6 µl of air to the

underside of the membrane by the computer controlled micro syringe of the Dataphysics contact angle system OCA 20. The measurements were repeated at least five times in different spots resulting in 10 data points since two angles were determined for each measure (left and right sides). In Chapter 5, the mean values and the standard deviation of these measurements will be presented.

II.2.4 Differential Scanning Calorimetry

The Differential Scanning Calorimetry (DSC) is a routine technique to study the thermal properties of materials. It is based on the physical principle that during a phase transition (e. g. glass transition, melting, freezing), more or less energy is exchanged with the environment, depending if the process is exothermic or endothermic. The thermal history of the sample is observed applying well-defined heating-cooling conditions. In practice, two samples (one being the reference) are submitted to the same heating-cooling cycle and they are maintained to the same temperature. When the temperature of a phase transition is reached, the sample absorbs or releases energy. Then, observing the different heat flows between the sample and the reference, it is possible to determine the amount of energy needed to go through the phase transition. Thus, from this analysis, the thermal properties of the membrane can be investigated. The cooling and heating cycles of the CMX membrane conditioned following the NF X 45-2000 standard procedure [20] in KCl, NaCl, LiCl, NH_4Cl, $CaCl_2$ and $MgCl_2$ were measured on a Perkin Elmer DSC 8000. The surface of each membrane was lightly wiped using “parafilm” to remove superficial water. The “parafilm” was used instead of paper to avoid possible dehydration of the membrane due to capillary forces. Thus, samples with a weight in the range of 8 to 12 mg were sealed in an aluminum pan and equilibrated for 1 minute at 30°C. Subsequently, each sample was cooled at -60°C with a scanning rate of 5°C/min, stabilized for 3 minutes at this temperature and then heated to 30°C with the same scanning rate. The cycle was repeated three times for each sample. The repetition of the cycles was necessary because in the first cycle, the peak at the freezing temperature was not found in a stable position. The phenomenon is clearly shown in Fig. II.3. Indeed, one can see that peak 1 that is related to the first cooling cycle is distinct from peak 2 and 3 obtained for the subsequent cycles that are completely in overlap. It should be noticed that peak 1 could be obtained at lower as well as at higher temperature with respect to the other peaks. This incertitude can be attributed to different responses of the polymer network to the water volume expansion due to the transition phase. However, after the first cycle, the peaks are reproducible. This means that, after the first mechanical stress (enlargement of the chain-chain distances due to the water expansion), the

membrane structure reaches a stable configuration.

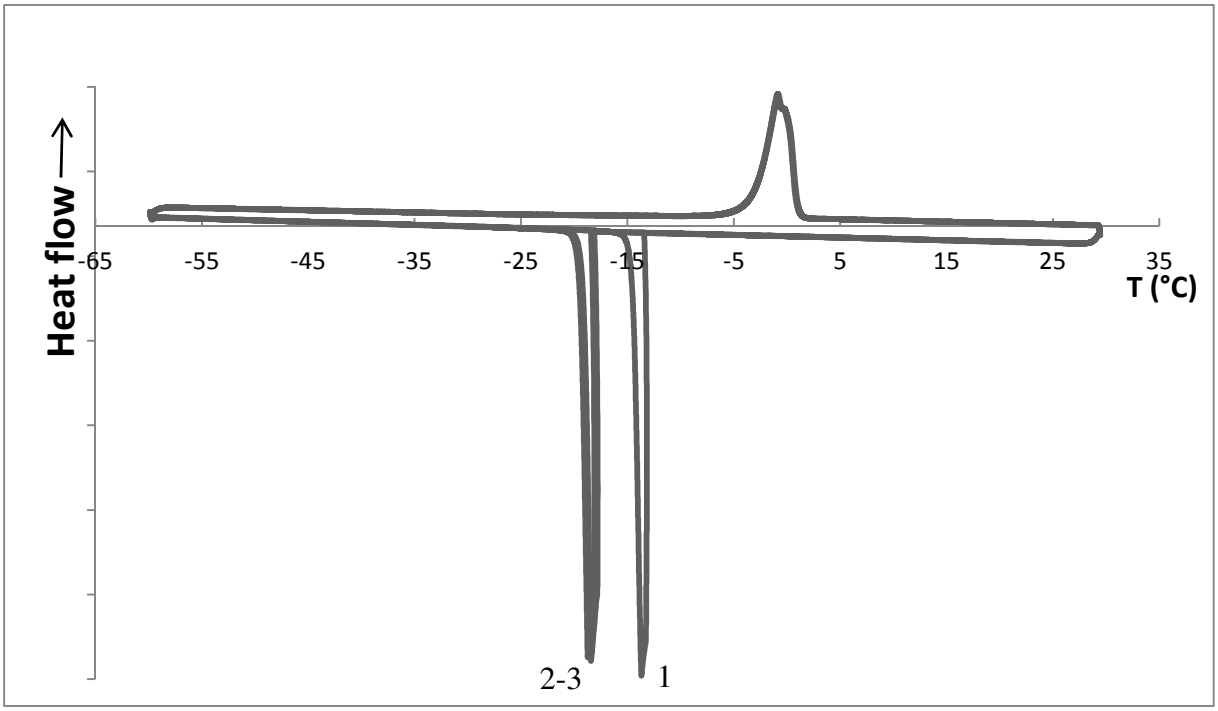

Figure II.3: Example of DSC measurement on CMX membrane equilibrated by Mg^{2+}. Peak 1 is related to the first cycle while peaks 2 and 3 are the successive and reproducible peaks.

II.3 References

[1] J. A. Elliott, “Novel approaches to multiscale modelling in materials science,” *Int. Mater. Rev.*, vol. 56, no. 4, pp. 207–225, 2011.

[2] D. Hofmann and E. Tocci, “Molecular Modeling, A Tool for the Knowledgr-Baed Design of Polymer-Based Membrane Materials,” in *Membrane Operations. Innovative Separations and Transformations*, E. Drioli and G. Lidietta, Eds. Wiley-VCH Verlag GmbH & Co., 2009.

[3] R. Ball and G. Goldbeck, *Materials Modelling: Where do we want to go?* European Union, 2014.

[4] G. De Luca, A. Gugliuzza, and E. Drioli, “Competitive Hydrogen-Bonding Interactions in Modified Polymer Membranes: A Density Functional Theory Investigation,” *J. Phys. Chem. B*, vol. 113, pp. 5473–5477, 2009.

[5] G. De Luca, F. Bisignano, F. Paone, and S. Curcio, “Multi-scale modeling of protein fouling in ultrafiltration process,” *J. Memb. Sci.*, vol. 452, pp. 400–414, 2014.

[6] Attila Szabo and N. S. Ostlund, “Modern Quantum Chemistry Introduction to Advanced Electronic Structure Theory.” Dover Publications, 1996.

[7] W. J. Hehre, “A guide to Molecular Mechanics and Quantum Chemical Calculation,” Wavefun Inc., 2003.

[8] R. P. Feynman, *Statistical Mechanics*. Benjamin, Read- ing, 1972, p. 249.

[9] P. Hohenberg and W. Kohn, “Inhomogeneous Electron Gas*,” *Phys. Rev.*, vol. 136, p. B864, 1964.

[10] W. Kohn and L. J. Sham, “Self-Consistent Equations Including Exchange and Correlation Effects,” *Phys. Rev.*, vol. 140, p. A1133, 1965.

[11] W. Kohn, “Nobel Lecture: Electronic structure of matter—wave functions and density functionals *,” *Rev. Mod. Phys.*, vol. 71, no. 5, pp. 1253–1266, 1999.

[12] K. M. Dunn, “Introduction to Quantum Mechanics: In Chemistry, Material Science, and Biology (S. M. Blinder),” *J. Chem. Educ.*, vol. 82, no. 3, p. 383, 2005.

[13] F. Jensen, *Introduction to Computational Chemistry,*, II. , John Wilwy & Sons, 2007.

[14] W. Koch and M. C. Holthausen, *A Chemist’s Guide to Density Functional Theory*, II., vol.

3. 2001.

[15] I. N. Levine, *Quantum Chemistry*, V. Prentice-Hall inc, 2000.

[16] W. Thiel, "QM/MM Methodology: Fundamentals, Scope, and Limitations," in *Multiscale Simulation Mehods in Molecular Sciences*, 2009, vol. 42, pp. 203–214.

[17] V. V. Barkaline, Y. V. Douhaya, and A. Tsakalof, "Computer simulation based selection of optimal monomer for imprinting of tri-O-acetiladenosine in polymer matrix: vacuum calculations.," *J. Mol. Model.*, vol. 19, no. 1, pp. 359–69, 2013.

[18] "http://www.nwchem-sw.org/index.php/Release61:QMMM_Parameters accessed on 4-nov-2013." .

[19] M. Valiev, E. J. Bylaska, N. Govind, K. Kowalski, T. P. Straatsma, H. J. J. Van Dam, D. Wang, J. Nieplocha, E. Apra, T. L. Windus, and W. A. De Jong, "NWChem: A comprehensive and scalable open-source solution for large scale molecular simulations," *Comput. Phys. Commun.*, vol. 181, no. 9, pp. 1477–1489, 2010.

[20] J. Savignac, "Impact des interactions membrane/électrolyte sur la diffusion de sucres à travers des membrane échangeuses d'ions," Doctorat de l'Université Toulouse III - Paul Sabatier, 13 octobre 2010.

[21] R. M. Silverstein, F. X. Webster, and D. J. Kiemle, *Spectrometric identification of organic compounds*, 7th ed. John Wiley & Sons, Inc., 2005.

[22] M. Falk, "An infrared study of water in perfluorosulfonate (Nafion) membranes," *Can. J. Chem.*, vol. 58, pp. 1495–1501, 1980.

[23] R. M. Blanchard and R. G. Nuzzo, "An infrared study of the effects of hydration on cation-loaded nafion thin films," *J. Polym. Sci. Part B Polym. Phys.*, vol. 38, no. 11, pp. 1512–1520, 2000.

[24] A. W. Neumann, "Contact Angles and their temperature dependece:thermodynamic status, measurement, interpretation and application," *Adv. Colloid Interface Sci.*, vol. 4, pp. 105–191, 1974.

[25] M. J. Rosa and M. N. de Pinho, "Membrane surface characterisation by contact angle measurements using the immersed method," *J. Memb. Sci.*, vol. 131, no. 1–2, pp. 167–180, 1997.

[26] C. J. Van Oss, M. K. Chaudhury, and R. . Good, "Interfacial Lifshitz-van der Waals and

Polar Interactions in Macroscopic Systems," *Chem. Rev.*, vol. 88, pp. 927–941, 1988.

[27] R. Good and L. A. Girifalco, "A theory for estimation of surface and interfacial energies. III. Estimation of surface energies of solid from contact angle data," *J. Phys. Chem.*, vol. 64, pp. 561–565, 1960.

[28] A. W. Neumann, R. J. Good, C. J. Hope, and M. Sejpal, "An equation-of-state approach to determine surface tensions of low-energy solids from contact angles," *J. Colloid Interface Sci.*, vol. 49, no. 2, pp. 291–304, 1974.

[29] C. S. Dutcher, A. S. Wexler, and S. L. Clegg, "Surface tensions of inorganic multicomponent aqueous electrolyte solutions and melts.," *J. Phys. Chem. A*, vol. 114, no. 46, pp. 12216–30, 2010.

Chapter III

Ions properties in solution and their correlation with the solute transfer through Nanofiltration and ion-exchange membranes

The aim of this Chapter is oriented on the understanding of what are the ion properties that could affect the separation process of organic matter through membranes. It is based on previous experimental correlations between the hydration properties of ions and the modification of the transfer of organic solutes through different kinds of membranes used in nanofiltration and electrodialysis. Thus, water-cation clusters are modeled at various hydration levels to investigate the effect of the water-water interactions on the solvation properties by computational methods.

The study of electrolytes in solution is a very large field. Furthermore, in many cases, the results depend on the different methods used to characterize that property [1]. For example during the evaluation of coordination number by experimental techniques, one generally obtains data for the total salt and not for the single ions. Thus the criteria used to split the different contributions can confer some differences. With the development of the computing technology, Quantum Mechanics and Molecular Mechanics were also used to investigate the ions properties in solution [2]. Several theoretical works are already available in the literature, but also in these cases, some differences can be found in the results due to the kind of method used to compute the ions in solution, or to some kind of assumption such as the difference between the coordination number and hydration number.

In the first part of the Chapter, an evaluation of the ions properties in interaction with water clusters, such as the coordination and hydration numbers and the interaction energy, are evaluated and compared with literature data. In the second part, the computed properties are correlated with experimental data obtained in previous works [3] [4] concerning the sugar transfer through nanofiltration and ion-exchange membranes.

III.1 Computational methods

The investigation on the hydration properties of ions was carried out in the framework of Density Functional Theory (DFT) by using X3LYP potential and energy functional. This functional is well known for its reliability in describing H-bonds in clusters also involving ions [5] [6]. All the ion-clusters structures were fully optimized using analytical energy gradients and the quasi-Newton optimization with approximate energy Hessian updates [7]. Optimization convergence was based on the maximum and root-mean-square gradient thresholds of (4.5 and 3.0) $x10^{-4}$ a.u., respectively, in conjunction with the maximum and root-mean- square of the Cartesian displacement vectors with thresholds of (1.8 and 1.2) 10^{-3} a.u. respectively. The energy convergence threshold for the self-consistent field procedure was set to 10^{-6} a.u., and the

root-mean-square of the electron density was set to 10^{-5} a.u. The 6-31+G* atomic orbital basis sets were used for all the atoms, i.e. H, O, Na, Mg, Ca, Cl, S. Polarization orbitals were used since it gives appreciable contributes for the hydrogen bonding modeling [8], while the diffuse function is required for a better description of cations and oxygen-containing systems [9] [10]. Interaction energy between the cation and the water molecules, ΔE_i^w, is calculated from the difference between the energy of the complex, $E_{Complex}$, and those of the two single fragments, i.e. the ion, E_{ion}, and the optimized water cluster, $E_{Hyd.shell}$.

$$\Delta E_i^w = E_{Complex} - E_{ion} - E_{Hyd.shell} \qquad \text{(III.1)}$$

Basis Set Superposition Error (BSSE) correction [11] was applied to increase the accuracy on the calculated interaction energy [12] [13].

In quantum optimizations of large or medium molecular structure, containing noncovalent interaction/bonds, the initial geometry is a crucial point. Thus, the starting geometries of each target molecular systems, containing an increasing number of water molecules (from 1 to 16) around the considered ions, were built each time *ex-novo*. In particular, in the initial highly symmetrical structures as shown in Fig III.1, the distance between the cation and the oxygen of the water molecules was set at 2.3Å. Regarding the Cl^- and SO_4^{2-} anions, the distances between Cl^- or S atom and the reference hydrogen of the water molecule were set at 2.1 Å and at 3.6Å, respectively. These distances were chosen to avoid orbital overlaps between ions and/or water molecules.

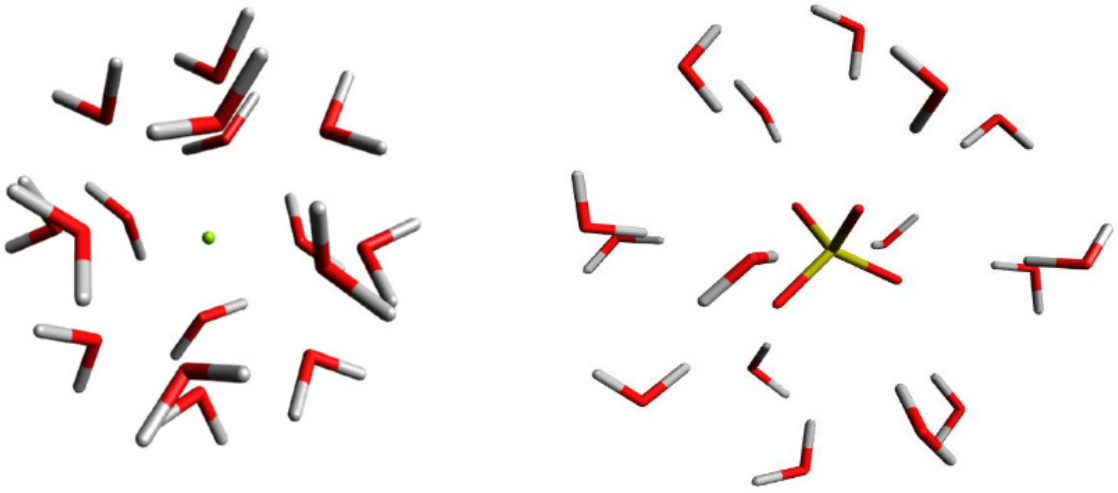

Figure III.1: Initial structure with 16 H_2O for the Mg^{2+} cation, on the left, and the SO_4^{2-} anion on the right

The main objective of the quantum optimizations of the hydrated ions was to investigate the differences in their properties. More precisely, in this work, the coordination number (CN) indicates the total number of water molecules directly interacting with the ions and it can be also defined as the first hydration shell. A water molecule is considered in direct interaction with the central ion if the water-ion distance is lesser than 2.8 Å for monoatomic ions [14] while for SO_4^{2-} anion, a hydrogen bond has to be established between the water molecules and an oxygen of the ion. The geometrical parameters used to establish the presence of a hydrogen bond are a donor-acceptor distance set at 2.1 Å and a cutoff angle of 120° [15]. On the other hand, the hydration number is defined as the number of water molecules required achieving the asymptotic convergence of the interaction energy as defined by equation (III.1). Then, it corresponds to the starting point of the plateau in the curves representing the variation of the interaction energy *versus* the number of water molecules. Thus, the total hydration shell of the ion is formed by the coordination number (i.e. the first hydration shell) and an eventual second/successive shell.

III.2 Computed ions properties

III.2.1 Coordination numbers and average ion-water distances

Three cations and two anions interacting with an increasing number of water molecules were investigated. Table III.1 shows the values of the coordination number CN as function of the added water molecules for each target ion, as well as the average lengths between the ion and the water molecules comprised in the first hydration shell. The maximum number of water molecules added is 16. In Table III.2, several properties of the hydrated ion structure, optimized at QM level, were summarized. Literature data were also reported to validate these calculations. In the following, for each investigated ion the computed properties will be briefly discussed.

For the Na^+ cation, coordination numbers of 5 and 6 are obtained. These values are in agreement with the literature data. Also, the average Na^+-water distance of 2.43 Å is in agreement with previous experimental work. The optimized structure with 5 water molecules is the more stable when the initial structure is composed by up to 9 H_2O, whereas the structure with 6 water molecules is more probable with starting geometries containing more water molecules. Changes in the structural form of the water coordination cluster are obtained as for an increasing number

of water molecules. A square based pyramid (shown in Fig III.2) is the most common structure at low water concentration.

Then, the coordination structure evolves in a trigonal dipyramid (Fig. III.3) when the sodium is surrounded by 11 water molecules, while the octahedral form (Fig. III.4) is favored for higher numbers of water molecules. It is worth noting that for Na^+ the coordination and hydration numbers match, showing that the interaction between Na^+ and the water in its second hydration shell are negligible.

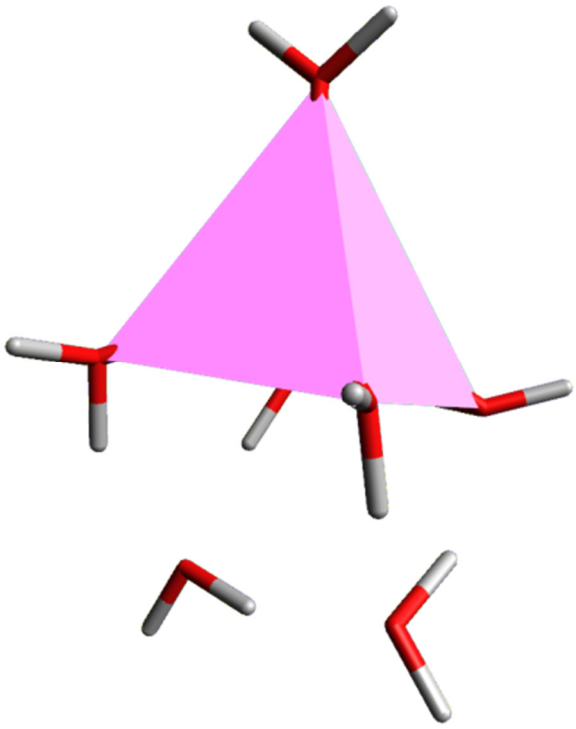

Figure III.2: Optimized structure of the Na^+ surrounded by 7 water molecules, with its coordination structure: a square based pyramid.

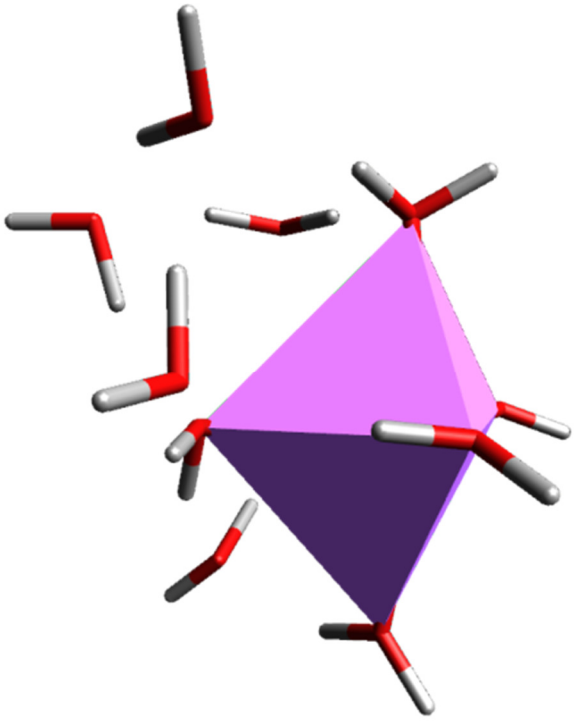

Figure III.3: Optimized structure of Na^+ surrounded by 11 water molecules, with its coordination structure: a trigonal dipyramid.

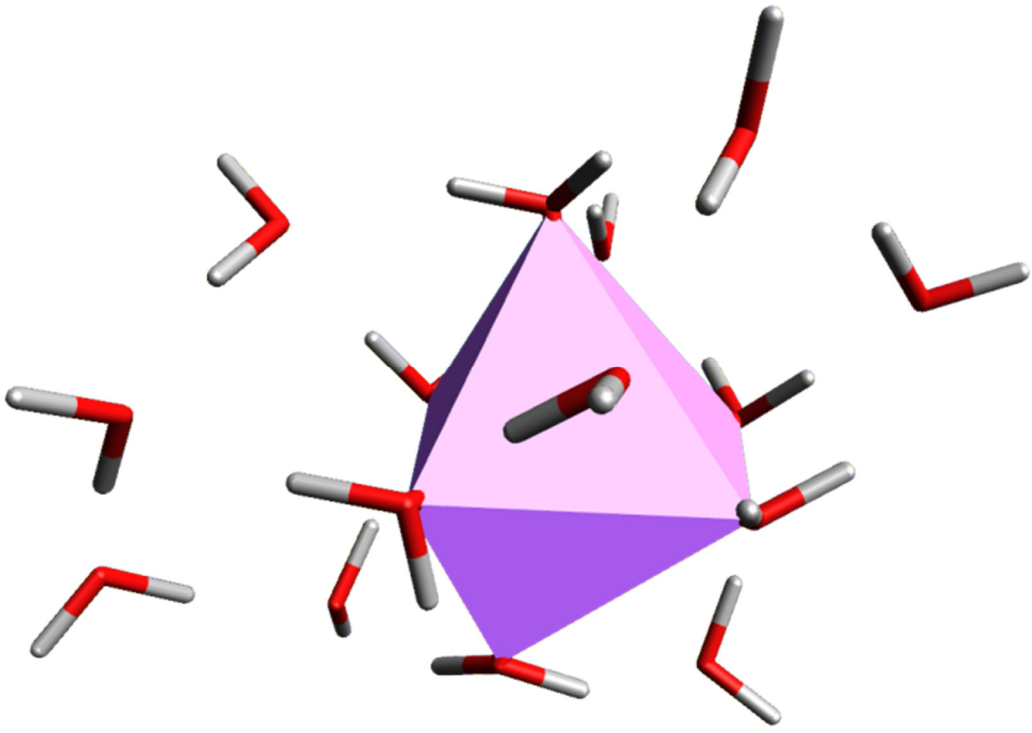

Figure III.4: Optimized structure of Na^+ surrounded by 15 water molecules, with its coordination structure: an octahedral form.

	Na^+		Ca^{2+}		Mg^{2+}		Cl^-		SO_4^{2-}	
N° H2O	CN	d_{Na-O} (Å)	CN	d_{Ca-O} (Å)	CN	d_{Mg-O} (Å)	CN	d_{Cl-H} (Å)	CN	d_{SO4-H} (Å)
1	1	2.21	1	2.33	1	1.94	1	2.20	1	1.89
2	2	2.23	2	2.25	2	1.96	2	2.25	2	1.91
3	3	2.36	3	2.37	3	1.98	3	2.27	3	1.88
4	4	2.28	4	2.39	4	2.02	4	2.42	4	1.81
5	5	2.34	5	2.41	5	2.07	4	2.34	5	1.96
6	5	2.36	6	2.44	6	2.10	5	2.41	6	1.91
7	5	2.39	7	2.48	5	2.06	4	2.29	7	1.93
8	6	2.42	8	2.54	6	2.10	5	2.36	8	1.89
9	4	2.32	8	2.53	6	2.10	6	2.48	9	1.89
10	6	2.45	7	2.48	6	2.10	5	2.34	10	1.93
11	5	2.37	8	2.54	6	2.10	5	2.36	10	1.92
12	6	2.46	8	2.53	6	2.11	6	2.38	10	1.90
13	5	2.39	7	2.49	6	2.10	6	2.36	10	1.90
14	6	2.46	8	2.57	6	2.12	7	2.50	11	1.90
15	6	2.43	7	2.48	5	2.06	5	2.32	11	1.91
16	6	2.46	8	2.55	5	2.05	5	2.33	11	1.89

Table III.1: Coordination number (CN) of Na^+, Mg^{2+}, Ca^{2+}, Cl^- and SO_4^{2-} and average distances, d(Å), between the ions and the water molecules at several hydration level. Computed values obtained in this work.

	Na^+	Mg^{2+}	Ca^{2+}	SO_4^{2-}	Cl^-
CN	**5-6**	**5-6**	**7-8**	**≈10-11**	**≥ 5-6**
CN_{ref}	**6** *[16]*, **5.85** *[17]*	**6** *[16]*, **5.1, 6.0** *[23]*	**8** *[16]*, **4.8-8.2** *[23]*	**11.2** *[24]*	**6.25** *[17]*
d(Å)	**2.40**	**2.09**	**2.52**	**1.91**	**2.37**
d_{ref}(Å)	**2.43** [16]	**2.10** *[16]*,**2.07** *[15]*,**2.13, 2.07** *[23]*	**2.46** *[16]*, **2.35** *[15]*, **2.42, 2.52** *[23]*	n.a.	**2.24-2.42** *[2]*
N_H	**5-6**	**11-12**	**10-11**	**12-13**	**7-8**
$N_{H\ ref}$	**6.5***[18]*, **5.97** *[19]*,	**11.7***[18]*	**10.4***[18]*	**3.9***[18]* , **12** *[25]*, **< 13** *[25]*	**5.3** *[18]*, **8.36** *[16]*, **4-9** *[9]*
ΔE_i^w (Kcal/mol)	**-99**	**-446**	**-342**	**-215**	**-71**
ΔH (Kcal/mol)	**-99***[20]*	**-465***[20]*	**-382***[20]*	**-247** *[20]*	**-87** *[20]*
r (Å)	**1.02** *[21]*	**0.72** *[21]*	**1.00** *[21]*	**2.40** *[21]*	**1.81** *[21]*
$r_{hyd.}$ (Å)	**3.58** *[22]*	**4.28** *[22]*	**4.12** *[22]*	**3.79** *[22]*	**3.32** *[22]*

Table III.2: Computed solvation properties in this work (grey rows) of the target ions and some key properties from Literature (white rows): CN, ion-water distance, hydration number (N_H), ΔE_i^w Interaction energy, ΔH hydration enthalpy, r and $r_{hyd.}$ are ionic radius and the hydrate radius of the ions.

The systems with Mg^{2+} ion present also coordination numbers between 5 and 6 with a preference on 6. However, the same number of water molecules in the first hydration shell does not mean that the interaction properties of Na^+ and Mg^{2+} with water are the same. In fact, as it will be shown in the following, the Mg^{2+} has a higher capability to interact with the water molecules, and its hydration number is higher than the hydration number of Na^+. The higher interaction energy with the water clusters exhibited by Mg^{2+} is visible by the shorter distances among the water and the Mg^{2+} with respect the systems containing Na^+ (see Tables III.1 and III.2). As shown in Table III.1, the first hydration shells of Mg^{2+}, at increasing number of water molecules, are very compact with an average of the water-cation distance of 2.09 Å (Table III.2). This is an indication of a strong attraction interaction between the Mg^{2+} cation and the water molecules. Concerning the equilibrium structures of the coordination shell, two geometries are found. A high symmetric octahedral structure (Fig. III.5) is the favorite structure when 6 water molecules are surrounding the Mg^{2+}, while a trigonal dipyramid (Fig.III. 6) with 5 water molecules is more probable.

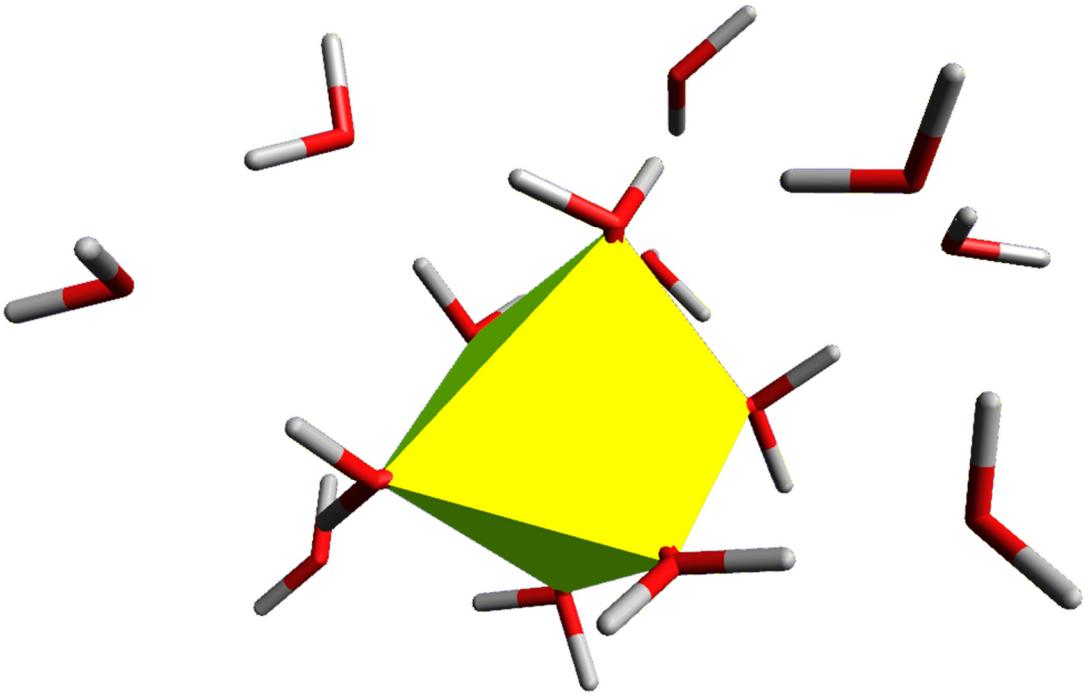

Figure III.5: Optimized structure of Mg^{2+} surrounded by 14 water molecules, with its coordination structure: an octahedral form.

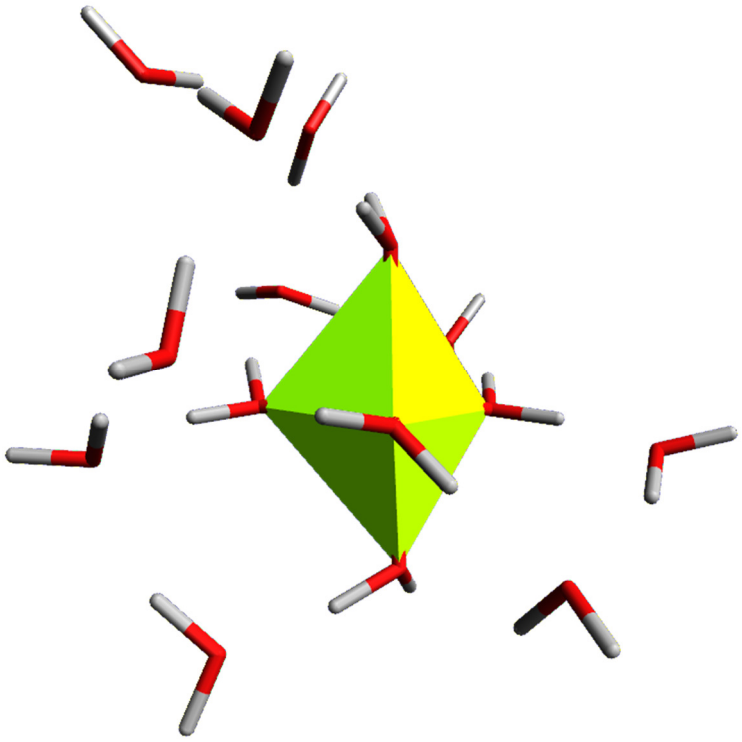

Figure III.6: Optimized structure of Mg^{2+} surrounded by 15 water molecules, with its coordination structure: a trigonal dipyramid.

For the water cluster around the Ca^{2+}, the computed coordination number obtained in this work fluctuates between 7 and 8, as illustrated in Table III.1. This is in agreement with the literature (Table III.2). A detailed analysis of the optimized structures gives some information on the stable geometry of the first coordination shell, as reported in Figure III.7. A square antiprismatic with an average distance of 2.52 Å between the Ca^{2+} and the water molecules is the favorite when 8 water molecules are present in the coordination shell. The square antiprismatic geometry is the more stable structure also when 7 water molecules are present in the coordination shell, but due to the absence of one water molecule, the structure presents a vacancy in one vertex. In the case of the cluster containing 13 water molecules, it is found 7 molecules in the coordination structure in a pentagonal bypiramid structure. However, this different form can be due to the asymmetry in the second hydration shell, since, a different arrangement of the external water can affect the stable geometry of the first shell.

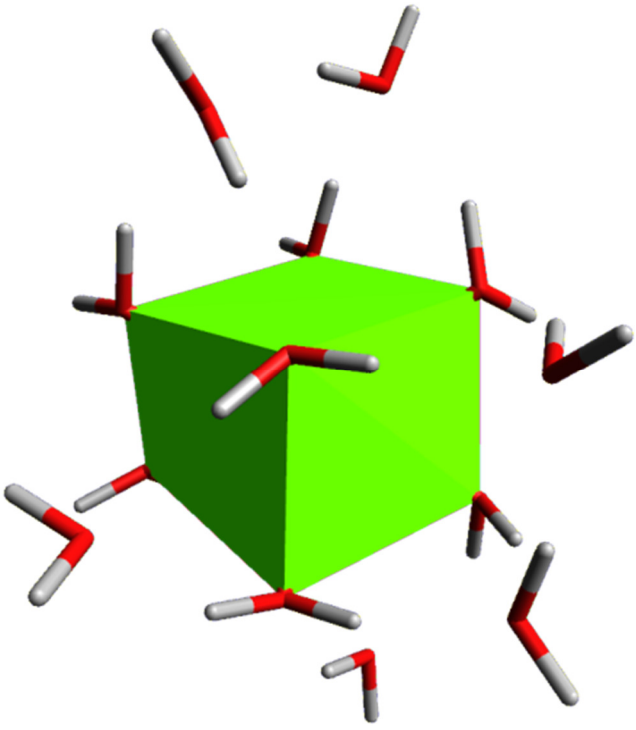

Figure III.7: Optimized structure of Ca^{2+} surrounded by 14 water molecules, with its coordination structure: a square antiprismatic.

In Figure III.8 the optimized structure of a solvated chloride ion containing 16 water molecules is reported. In this Figure, one can observe a strong difference of the Cl^- hydration shell with respect to the previous results concerning the cations. Then, in order to compare the properties of this hydrated ion with the other analyzed, the results were reported. A coordination number close to that in the literature value is obtained. Also the average Cl^--water distance, computed

by using the first hydration structures, is equal to 2.37 Å, a value comparable with the literature data. Moreover, by comparing the computed values with corresponding literature data (see Table III.1) it is possible to affirm that the coordination and hydration number as well as the computed interaction energy are reliable. However, other calculations are needed to understand the reasons for the asymmetrical structure.

Figure III.8 Optimized structure of Cl^- surrounded by 16 water molecules.

In Figure III.9 the hydration shell of SO_4^{2-} composed by 16 H_2O is reported. The sulfate differs from the other investigated ions because it is a multi-atomic. Indeed, due to its point group with a tetrahedral symmetry, T_d, it is always a highly symmetrical ion. From Figure III.9, it is possible to note how the structure and the symmetry of the ion affect the structure of the water cluster. The H_2O molecules build a regular network of hydrogen bonds around the ion in which the oxygen atoms of the sulfate are used as contact spots among the ion and the water cluster. Furthermore, the interaction between the water molecules and the sulfate are established by well-defined hydrogen bonds. A coordination number of 10 water molecules is found when 10 to 13 water molecules are surrounding the SO_4^{2-}. It increases to 11 with more water molecules added. Probably, the first hydration shell of the SO_4^{2-} could have some adjustments in presence of more water molecules in the second hydration shell. It should be also remarked the different kind of interactions occurring between the SO_4^{2-} and the water molecules with respect to those observed with the systems with the other ions. In this case, the interaction are H-bonds, while

in the systems with the other ions, the interactions were more in the form of electrostatic ones. In fact, in the optimized structures with SO_4^{2-}, the average distance of the water molecules is 1.91 Å from the nearest oxygen, which it is in the range of hydrogen bonds distances [26].

Figure III.9: Optimized structure of a SO_4^{2-} surrounded by 16 water molecules.

III.2.2 Hydration numbers and interaction energies

The aim of this Chapter is to compare some key properties of hydrated ions, evaluated at high quantum mechanics level, with experimental values of sugar fluxes, and to verify if any correlation exists. Since a correlation with the hydration number was highlighted in previous works [3] [4], and due to the strict correlation among hydration number and hydrated ions interaction energies, ΔE_i^w, the interaction energy for each target ion was investigated.

The computed interaction energies of the cations obtained in this work are reported in Figure III.10 as function of the increasing number of coordinating water molecules, i.e. different hydration levels (from 1 to 16 water molecules). Two different regions can be observed for each curve. In the initial stage, the interaction energy decreases as the number of water molecules increases. The energy step between two consecutive points, in the graph, is the contribution of the last added water molecule to build a stable water cluster around the ion. When the curve reaches a plateau, it means that the last added molecule has no impact on the energy of the water cluster surrounding the ion, more precisely the contribute decreases asymptotically. Once

reaching the plateau, one can consider that the hydration shell is completed, since the energy of the complex, ΔE_i^w, formed by the ion and its hydrated shells, is not significantly influenced by the presence of more water molecule. Hence, as pointed out above, the ion hydration number is the number of water molecules at the starting point of the plateau in Fig. III.10 and III.11. The interaction energy of the ion hydration, i.e. ΔE_i^w, corresponds to the average value of the energy reached at the plateau. The calculated values are reported in Table III.2. One can observe that the hydration numbers taken from literature (N_{Href} in Table III.2), are in good agreement with the values obtained in this work, still showing a good accuracy of the computational method used.

In Fig. III.10 and III.11, for Na^+ and Cl^- respectively, it is possible to note that there are two plateau values of the energy, one at a low hydration level and the second one with an increased number of water molecules in the cluster. The presence of these two plateau values is due to the formation of the second hydration shell for the Na^+ and Cl^- ions. They are found when the 10^{th} or the 12^{th} water molecule is added to the Na^+ and Cl^- structures, respectively. In this work only the interaction energies of the hydration shell are taken into account and compared with the sugar fluxes. Thus, in the cases of Na^+ and Cl^-, the energies of the structure with higher hydration level are not used during the evaluation of the ΔE_i^w. The calculated values are reported in Table III.2.

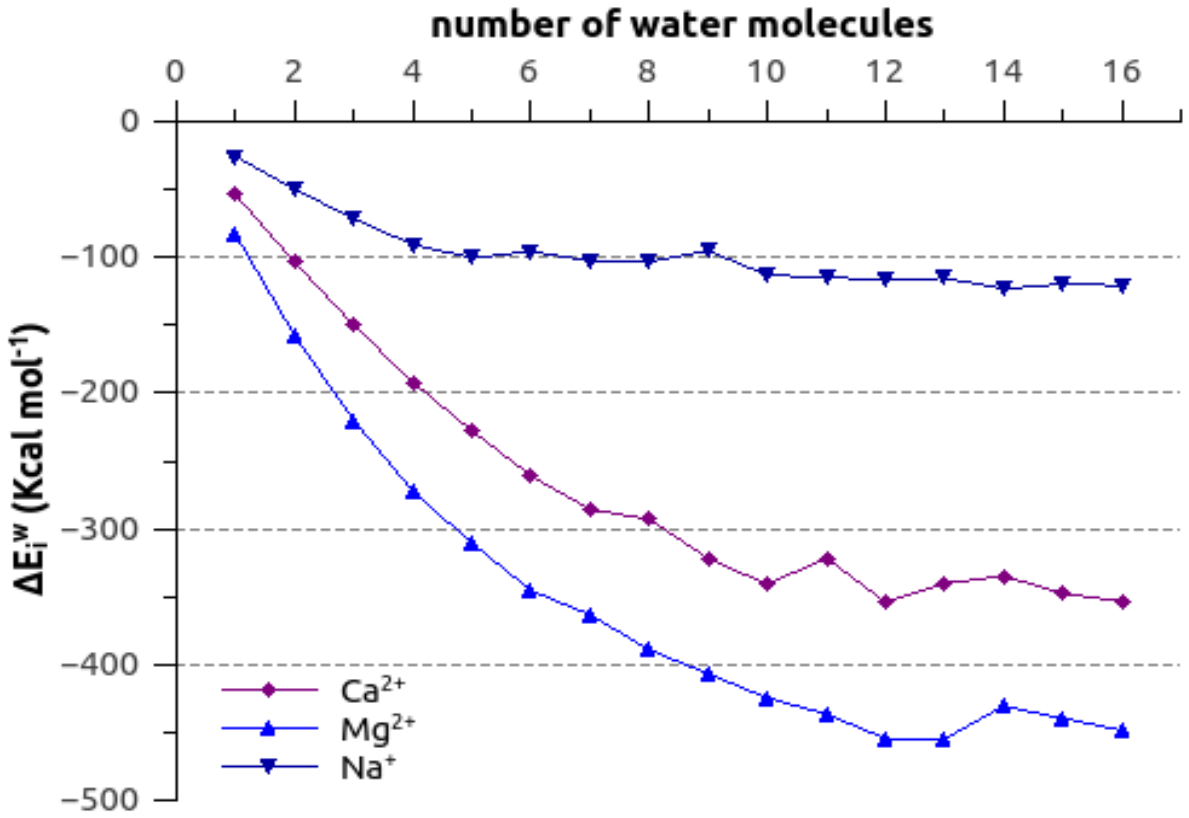

Figure III.10: Variation of the interaction energy (ΔE_i^w) between the cation and the water cluster versus the hydration level (from 1 up to 16)

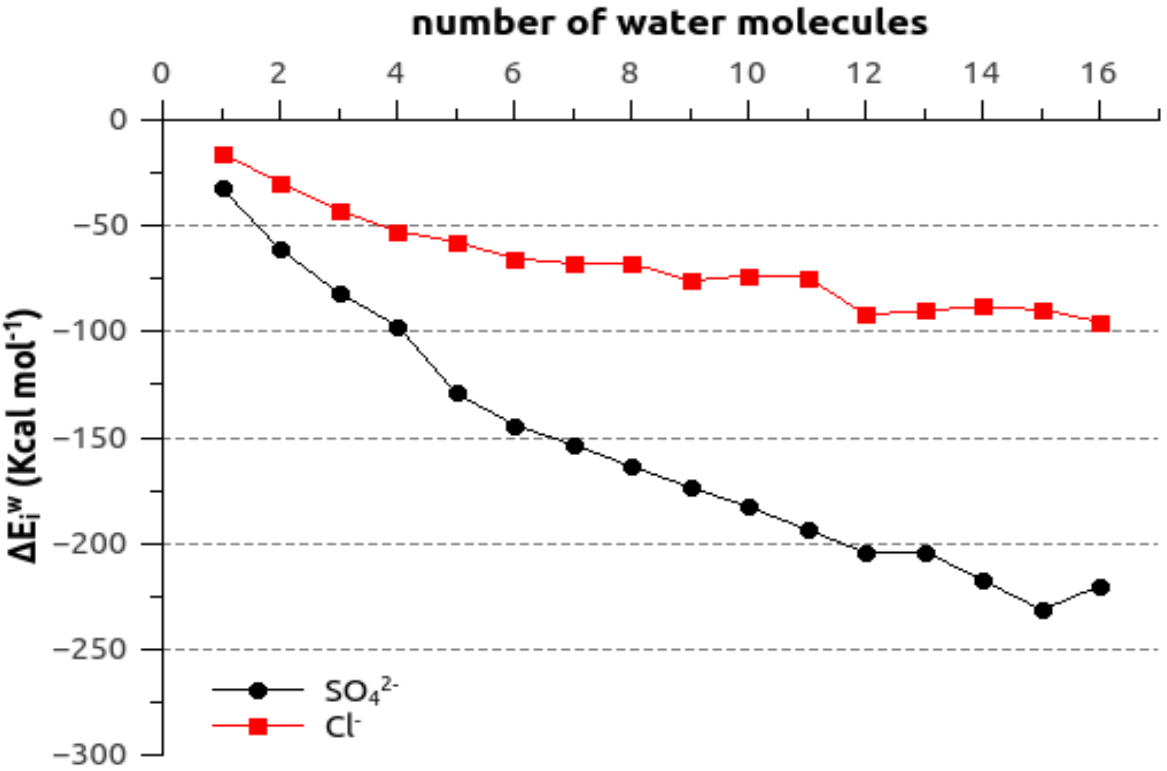

Figure III.11: Variation of the interaction energy (ΔE_i^w) between the anion and the water cluster versus the hydration level (from 1 up to 16)

In general, the interaction energy is related to the thermodynamic properties, like the Gibbs free energy of hydration and/or the hydration enthalpy of those ions in water. In fact, taking as example the hydration enthalpy, it is the sum of the interaction energy and the necessary energy to spread the ions or hydrated ions into the solvent medium, which has a dielectric constant different from vacuum. The semi-quantitative comparison between the computed ΔE_i^w, and the experimental hydration enthalpy, ΔH_{ref}, presented in Table III.2, shows, again, that the computational method used in this work to characterize the properties of ions in interaction with water molecules is sufficiently accurate. Starting from this preliminary validation of the computed key properties of hydrated ions, in the next section, a correlation between the computed interaction energies and the experimental mass transfer of neutral organic molecules through Nanofiltration and Ion-exchange membranes will be carried out.

III.3 Ions properties vs solute flux in NF or ED systems

In previous experimental works, the impact of the electrolytes on organic matter separations using nanofiltration and electrodialysis was correlated to the hydration of the ions present in solutions [3] [4]. In any case, a strong variation of the flux of organic matter (xylose, glucose and sucrose) was observed according to the hydration of the ions in the system. It was highlighted that the influence of the ions on the transfer of sugars follows the ion hydration trends in solution. However, different mechanisms were pointed out regarding the impact of the ions. In Nanofiltration systems, it was found that the presence of more hydrated ions causes an increase of the sugar fluxes ($J_S^{Na+} < J_S^{Ca2+} < J_S^{Mg2+}$ and $J_S^{Cl-} < J_S^{SO42-}$). On the contrary the flux of a given solute through an Ion-Exchange Membrane was found to decrease when the membrane is equilibrated with a more hydrated counter-ion ($J_S^{Na+} > J_S^{Ca2+} > J_S^{Mg2+}$ for a cation exchange membrane CMX and $J_S^{Cl-} > J_S^{SO42-}$for an anion exchange membrane AMX). Using appropriate methodologies [27] [28], it was possible to distinguish the influence of the ions in the solution and the influence of the ion on the membrane properties. More precisely, an important difference was found between the two kinds of membrane. In fact, in the case of Nanofiltration, the ion effect on the solute flux was mainly due to the modifications in the solution itself, i.e. to the variation of the sugar hydration according to the electrolyte composition. A stronger dehydration of sugars was observed in presence of highly hydrated ions using macroscopic methods (determination of the Apparent Molar Volume). The reduction

of the sugar hydration shell implying a shrinking of the kinetic diameter of the sugar, thus it leads to an increase of the sugar flux. On the contrary, in the case of Electrodialysis a decrease of the solute flux was measured when the Ion-Exchange membranes were soaked with increasingly hydrated ions in solution. Thus the influence of the ions was mainly due to a change in the membrane properties, mainly fixed according to the membrane counter-ion. Indeed, a different counter-ion in the Ion-exchange membrane can affect the interactions at different levels, like the solubility of the sugar in the membrane, i.e. sugar-polymer interaction, or the inter-chain interactions taking place inside the polymer network constituting the membrane.

In the first step, the correlation between the coordination number and/or the hydration number (in solution) of the ions and sugar fluxes was investigated. Concerning the coordination numbers of the different cations, it was found that 5-6 water molecules form the coordination structure for Na^+ as well as for Mg^{2+}, while 7-8 is the coordination number for a cluster containing Ca^{2+} (see Table III.2). Thus, a trend as follow is found: $CN_{Na+} \approx CN_{Mg2+} < CN_{Ca2+}$. If the coordination number is taken as reference to characterize the hydration of the ions in relationship with the transfer, similar values of the flux should be obtained for Na^+ and Mg^{2+}. This is not the case for both the investigated systems. But, if the hydration numbers of the ions are taken into account, it is possible to find a correlation with the sugar fluxes since 5-6, 10-11 and 11-12 are the values for Na^+, Ca^{2+} and Mg^{2+} respectively and 5-6 and 10-11 for Cl^- and SO_4^{2-}. In the case of the hydration numbers, the trend is equal to the trend on the strength of the ion impact: $N_H^{Na+} < N_H^{Ca2+} < N_H^{Mg2+}$ for cations and $N_H^{Cl-} < N_H^{SO42-}$ for anions (Table III.2). A higher hydration number of the ion corresponds to a higher impact on the sugar flux, increasing flux values in NF and decreasing ones in IEM. The fact that the fluxes can be correlated to the hydration number and not to the coordination number of the ions, shows that even if these two quantities are strictly related, the use of one or the other can discriminate, or not, the impact of the ions in the environment at molecular-scale. Probably, the different behavior is due to the fact that the coordination number takes into account only very local interactions, while the hydration number is also related to long range interactions.

In a previous work [3], changes in the apparent molar volume (AMV) of the investigated sugars were measured. AMV values are usually interpreted in terms of the structural hydration model developed by Gurney [29] to investigate saccharide/electrolyte or amino-acid/electrolyte

interactions [30] [31] [32]. According to the hydration model, increasing AMV reveals a dehydration of sugars in presence of electrolytes in solution.

In Table III.3 the variation of the apparent molar volume, ΔV, associated to three sugars when different electrolytes are present in solution are reported. ΔV is the difference between the AMV of a sugar in the electrolyte solution and in water. Considering the method used to evaluate ΔV, positive values mean that there the hydration of the sugar decreases. More details on the methodology are given in literature [3] [27]. One can observe that all ΔV values reported in Table III.3 are positive, therefore the increase of fluxes is attributable to a dehydration of the considered sugars. A direct correlation between sugar dehydration and interaction energies of the ions in solution can be also identified. Indeed, Figure III.11 shows that higher sugar fluxes are obtained in presence of ions with higher ΔE_i^w. Cations with higher interaction energy could subtract one or more water molecules from the sugar hydration shell thus producing a modification in the AMV, as observed. However, xylose and glucose on one hand, and sucrose on the other hand show different trends. The two small sugars are less affected by the presence of electrolytes, and the influence is not strongly electrolytes dependent, even if both sugars are less hydrated in presence of Ca^{2+}. In the case of sucrose, ΔV is strongly influenced by the interaction energies of the cations and it varies with a linear trend following the cation hydration energy. Moreover, the presence of divalent ions in solution gives rise to a very strong impact on the AMV of sucrose.

Electrolyte	**ΔV (cm^3 mol^{-1}) xylose**	**ΔV (cm^3 mol^{-1}) glucose**	**ΔV (cm^3 mol^{-1}) sucrose**
Na_2SO_4	1.4	2.0	2.4
NaCl	0.9	1.3	1.5
$CaCl_2$	1.3	1.9	10.1
$MgCl_2$	1.0	1.6	13.7

Table III. 3: variation of the AMV of saccharides, ΔV, in presence of different electrolytes [m_s = 1mol Kg^{-1}; T=25°C]. Sugar fluxes measured in diffusion regime [Sugar] =1 mol L^{-1} [electrolyte]= 1equiv. L^{-1} [3]

It can be assumed that the hydration shell of the sugar is composed by two kinds of water molecules: one kind that is in strong interactions by hydrogen bonding with the OH groups present in the sugars structure, while the second kind of water molecules have only weak interactions with the whole structure. These two kinds of water molecules could behave in very

different ways according to environmental factors. One can imagine that the weak interacting water molecules can be lost by the sugar while transferring through the membrane. On the contrary, the water molecules interacting by strong H-bonds can be still clinging to the sugar even in a confined space, i.e. during the transfer in the membrane. When the ions and the sugars are sufficiently close to be at interaction distance, like at the solution-membrane interface, one can expect that the ions modify the energy of noncovalent interactions among these strongly bounded water molecules and the sugars. In particular, cations with stronger interaction energy can reduce the strength of the sugar-water interactions, reducing, *de facto*, the hydration shell of the sugar, since the sugar can lose one or more water molecules affected by the cation presence during the permeation through the membrane. Furthermore, the cations do not interact only with the hydration shell of sugar but they could cause some change in its structural properties, like for instance induce the transformation into a different conformer/isomers[33]. Thus, more specific studies on the water - sugar interactions in presence of different electrolytes should be carried out in order to have a deeper knowledge of the observed phenomena at the molecular-scale.

Figure III.12 shows the variation of the fluxes of xylose, glucose and sucrose versus the interaction energies of the different cations ΔE_i^w, or compared by the ΔE_i^w of the anions (Cl^- and SO_4^{2+}) present in the electrolyte solutions used during the experiments. Two information can be obtained from this Figure. Firstly, increasing interaction energy ΔE_i^w of the ions in solution are related to increasing values of the sugar flux for each investigated sugar. This statement is valid both for cations and anions. Thus, the interaction energies between ions and water molecules, in solutions, correlate with the experimental fluxes of the sugars. This correlation suggests that the interaction between ions and water molecules coordinating the organic molecules (although not linear in the case of sucrose) can be the origin of their influence on the AMV of sugars. Secondly, the slope of the curves in Figure III.12 is correlated with the sugar size. In particular, bigger is the sugar, steeper is the slope of the curve correlating the interaction energy of ions and the sugar fluxes. This can be easily noticed by the intersection of the lines concerning xylose and glucose in presence of different cations. Though xylose and glucose have similar chemical structures, the glucose ($C_6H_{12}O_6$) is bigger than xylose ($C_5H_{10}O_5$), and it has one more OH group in its structure. This makes that the glucose hydration shell is bigger than the xylose hydration shell, since the OH groups can build a hydrogen bonding with the water that surrounds the sugar. The presence of an ion at interaction bonding distance, even for a very short time, can induce a change in the strength of these H-bonds,

modifying the hydration shell of the sugars. More are the preferential interactions sites of the sugar, i.e. OH groups, stronger the ion effect could be. However, these conclusions should be confirmed by accurate calculations whereas accurate experimental measurements of these interactions are very difficult. In presence of divalent cations, bigger sugars are more permeable than smaller sugars (i.e. $J_{xylose} < J_{glucose} < J_{sucrose}$). This trend does not respect the initial supposition, based on molecular size discrimination theory with the sugars in dried or fully hydrated form, in which at smaller sugar dimension should correspond a higher flux. However, as previously mentioned, a sugar moves in the membrane surrounded by its hydration shell, or part of it, if there is a partial dehydration caused by the presence of ions in solution. Thus, the electrolytes could affect the kinetic diameter of the sugar resulting smaller respect a second sugar, even if in their respective dried or fully hydrated forms, the second sugar is smaller. This could be the cases of Ca^{2+} and especially with Mg^{2+}, in which a clear trend reversal (i.e. $J_{sucrose} > J_{glucose} > J_{xylose}$) is observed.

Particular is the trend of the sucrose since a nonlinear behavior is found. It is probably due to specific interactions occurring between this sugar and Ca^{2+}. In fact, specific interactions among electrolytes and sugar were already observed, especially among fructose and Ca^{2+} [34] [35]. Because the sucrose is composed by two subunits, glucose and fructose, it is reasonable to extend the interactions among divalent cations and fructose, also to the sucrose.

Nanofiltration is not the only membrane process influenced by the presence of ions, but recently, it was pointed out that Electrodialysis is also sensitive to the composition of electrolyte solutions used to equilibrate the membrane. As previously discussed, it was possible to discern the contributions of the ions to a change in the solute dimension or to a modification of the membrane properties using specific experimental methods [4] [23]. Thus, it was found that in the case of Ion- exchange Membrane operating in diffusion condition, the ions act prevalently on the membrane transport properties.

However, the effect of the electrolytes on this membrane process is completely different with respect to the one observed for NF. In fact, in case of CMX and AMX, the presence of electrolytes with higher interaction energy with the water cluster, ΔE_i^w, induces a decrease in the sugar fluxes.

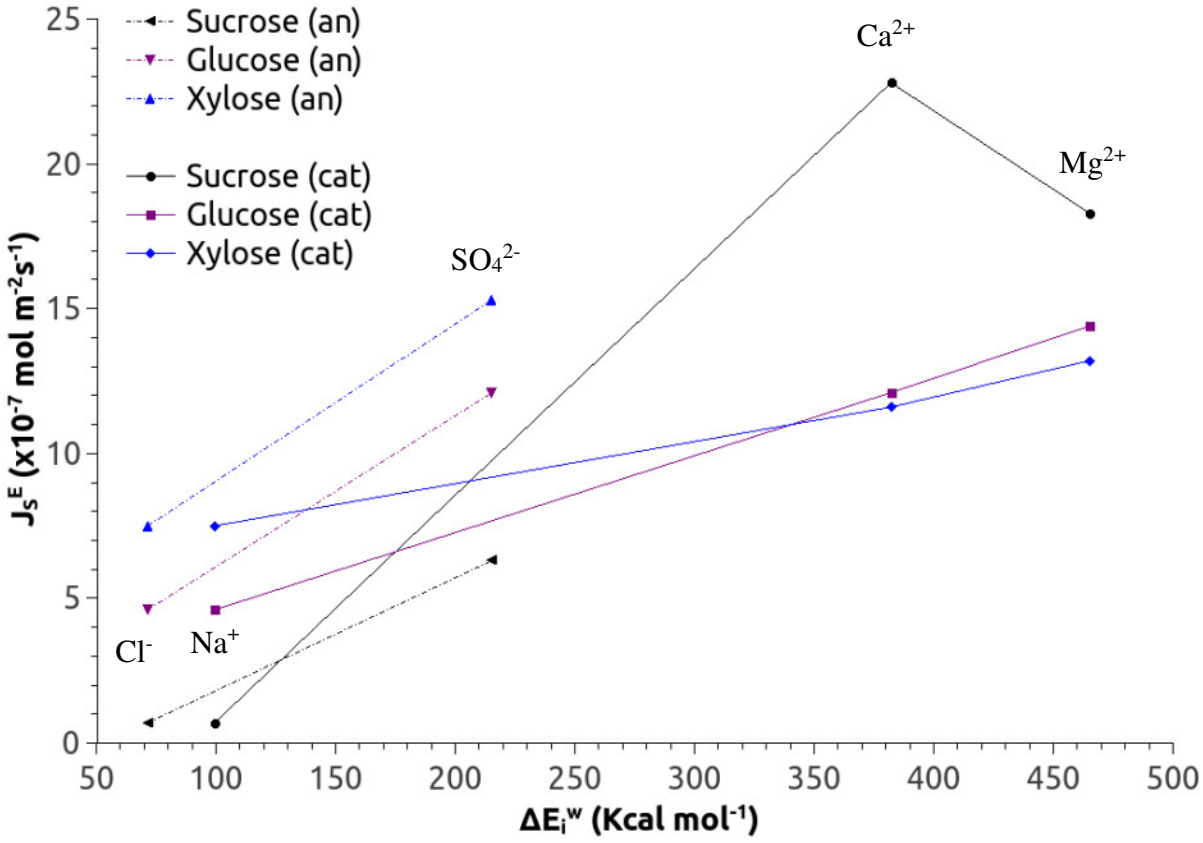

Figure III.12: Sugars fluxes J_S through nanofiltration membrane versus interaction energy ΔE_i^w of ions. Curves at fixed anion, thus considering the cation effect (cat), or considering the effect of the anion (an). Sugar fluxes measured in diffusion regime [Sugar] =1 mol L^{-1} [electrolyte]= 1equiv. L^{-1} [3]

In Figure III.13 the fluxes of the three investigated sugars, obtained with ion-exchange membranes in diffusion regime, are reported as function of the ΔE_i^w of the ions used to equilibrate the membrane. It is interesting to note that the fluxes linearly decrease with respect to the energy of the interaction between ion and water molecules, without any constrain around the ion-water complex, for both the CMX and AMX membranes [4]. A correlation between the computed interaction energies and the experimental sugar fluxes can be observed. The two quantities are inversely proportional:

$$J_a \propto \frac{1}{\Delta E_i^w} \qquad \text{(III.2)}$$

where J_a is the experimental flux of a sugar measured through a membrane equilibrated with a given counter-ion, and ΔE_i^w is the interaction energy between the counter-ion and the water without considering any influence of polymer fragments. It is essential to pay close attention

on the analysis of the correlation (2), since the two quantities are referred to completely different chemical environments: J_a is related to the flow of the sugar through a dense membrane whereas ΔE_i^w refers to the interactions between the ion and a fixed number of water molecules. It goes without saying that when the same ion interacts with the polymer fragments and at same time with the water molecules, the interaction energy changes due to the presence of functional monomers. For this reason, the correlation should be considered simply as a numerical relationship between two experimental and theoretical quantities. Hence, no extrapolation about the mechanisms, at the molecular level, can be deduced from it. In fact, in the next chapter of this Thesis, the energies associated to the interactions between ions, water and polymer fragments will be analyzed in details.

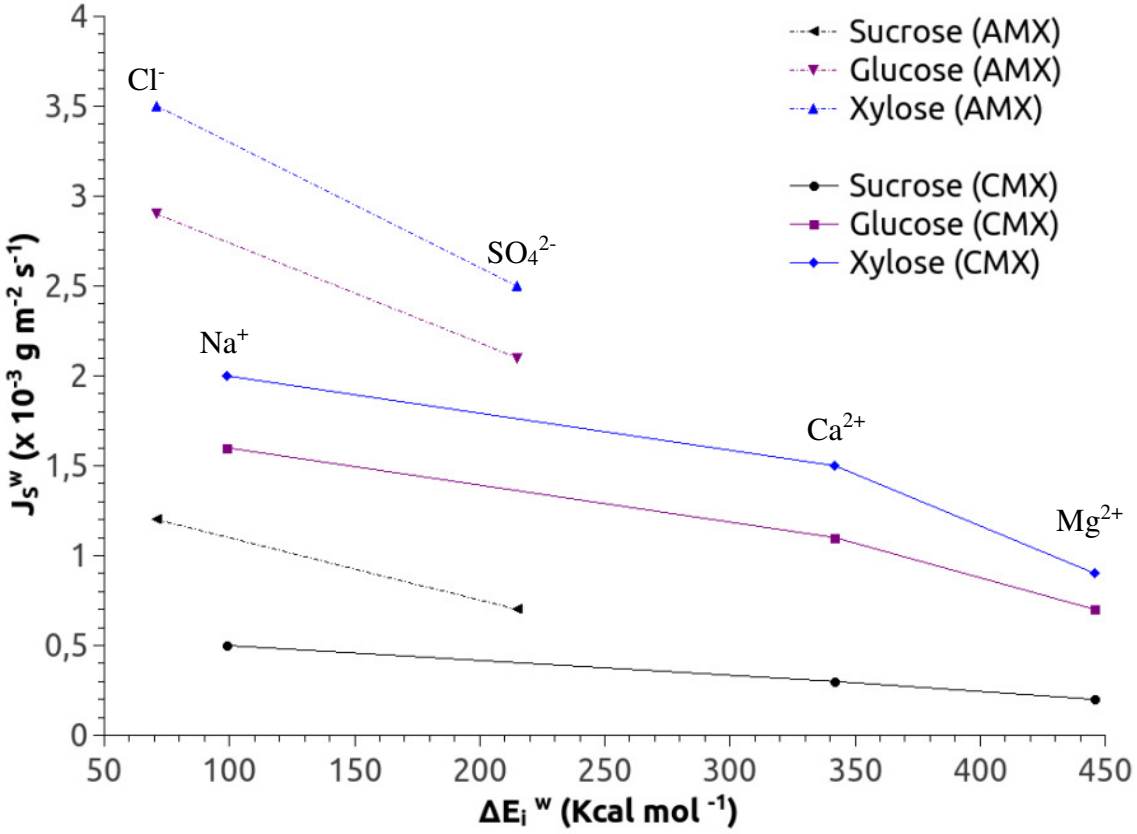

Figure III.13: Sugars fluxes J_S through ion-exchange membranes, versus interaction energy ΔE_i^w of ions. Sugar fluxes measured in diffusion regime [Sugar] =1 mol L^{-1} [electrolyte]= 1equiv. L^{-1} [10].

Considering the inverse proportionality between fluxes and the computed interaction energies among the ion and the clusters of water, ΔE_i^w, and the formal charge of the ions, z, an empirical mathematical correlation can be written between the ions properties and the sugar fluxes:

$$\frac{J_a}{J_b} \approx \frac{\Delta E_{ib}^{w} / z_b}{\Delta E_{ia}^{w} / z_a} \qquad \text{(III.3)}$$

where J_a and J_b are the sugar fluxes related to CMX or AMX membrane equilibrated with a given counter ion and ΔE_{ia}^{w}, ΔE_{ib}^{w} and z_a, z_b are the ion properties. It is worth nothing that the valence of the ions is used since from this value depends the number of functional groups that can be equilibrated by the counter-ion. In Table III.4 the ratio between the experimental sugar fluxes (normalized with respect to the one obtained with the membranes soaked with Na^+ or Cl^- , for CMX and AMX respectively) are compared with the corresponding considered electrolyte properties. For both membranes, the simple empirical relationship allows to have a quasi-quantitative evaluation of the sugar flux in presence of a given ion if the sugar flux in presence of another ion is known. For example, in the best case (J_{Na+}/J_{Mg2+} and $(\Delta E_{iMg2+}^{w}/z_{Mg2+})/(\Delta E_{iNa+}^{w}/z_{Na+})$), for a computed value of 2.25, the experimental values are 2.22, 2.28 and 2.5. Moreover it can be noticed that also in the case of Ca^{2+} the values are similar. Instead, in the case of the AMX membrane the accuracy is lower with respect to the CMX values. However, the empirical relation (III.3) can also give an idea of the anion's effect on the ED membrane, in fact for a ratio between the anion properties of 1.51 the ratios between the fluxes are 1.11, 1.2 and 1.42 for xylose, glucose and sucrose respectively. However, one can observe that the bigger ion dimensions of SO_4^{2-} (in comparison with the monoatomic ions size) could affect the free volume available for the diffusion of the sugar in the membrane, while the presence of S-O bonds, could encourage H-bond interactions among the anion and the solute, the water and the polymer network.

The good agreement between the ratio of the hydration energy and the ions and the ratio between fluxes at given counter-ion present in Table III.4 shows that the relation (III.3), used to obtain the values of this Table, is useful because it allows to estimate the ion influence on the sugar fluxes through an IEM from the ion properties. However, it is important to emphasize that the aforementioned relations are empirical, hence not based on an established molecular mechanism by which they must be validated.

Anyway, though the mechanisms at molecular level explaining the anion influence are still not known, as in the CMX also in the case of AMX membrane, the empirical formula certifies the influence of ions, although in solution, on the transfer of neutral organic molecules.

Cation (CMX)				
Counter-ion (b)	**$(\Delta E_{ib}^{w}/z_b)$ $/(\Delta E_{iNa+}^{w}/z_{Na+})$**	**J_{Na+}/J_b (Xylose)**	**J_{Na+}/J_b (Glucose)**	**J_{Na+}/J_b (Sucrose)**
Ca^{2+}	1.72	1.33	1.45	1.66
Mg^{2+}	2.25	2.22	2.28	2.50

Anions (AMX)				
Counter-ion (b)	**$(\Delta E_{ib}^{w}/z_b)$ $/(\Delta E_{iCl-}^{w}/z_{Cl-})$**	**J_{Cl-}/J_b (Xylose)**	**J_{Cl-}/J_b (Glucose)**	**J_{Cl-}/J_b (Sucrose)**
SO_4^{2-}	1.51	1.11	1.2	1.42

Table III.4: Summary of the normalized ions properties and sugar fluxes measured for CMX or AMX membrane soaked in the same electrolytes.

III.4 Conclusion

The aim of this Chapter was to compare some key properties of hydrated ions, calculated in the frame of Density Functional Theory, with the experimental fluxes of three sugars (xylose, glucose, and sucrose) measured through different kinds of membranes, Nanofiltration and Ion-Exchange membranes.

In the first part of this Chapter, a computational approach to calculate the ions properties in interaction with water was proposed and validated by a comparison with data from the literature. Specifically, the coordination and hydration numbers of ions were computed as well as the water-ion distances and the interaction energies between the investigated ions and the water molecules inside their hydration shell. A good agreement among the computed and the literature data is found. Then, this agreement allowed the study on the geometrical structures of the coordination shells.

In the second part, correlations between the interaction energy of the different ions with the water clusters and the transfer of sugars in Nanofiltration and Ion-Exchange Membranes have been investigated. In Nanofiltration, the influence of the electrolyte in solution acts mainly on the hydration shell of the sugars. For all the sugars, an increasing of the flux is observed with ions having a higher energy of interaction with the water clusters constituting their hydration shell. As previously investigated using macroscopic thermodynamic characteristics obtained from experimental measurements, this is due to a dehydration of the sugars. A stronger effect is detected on the sucrose probably for particular interactions among this hydrated sugar and the cations. Furthermore, in the case of sucrose, specific interactions could affect not only the hydration shell of the sugar, but also its molecular structure. However these conclusions extrapolated from the correlation pointed out in this work should be proven with *ad hoc* accurate calculations if necessary.

It is on Ion-Exchange membranes that the ion properties have a crucial role. In previous studies, carried out in diffusion conditions, it was pointed out that the electrolyte composition affects the membrane transport properties. Here an empirical correlation between the properties of ions in solution and the sugar fluxes was shown. This empirical relation correlates the fluxes of sugars through the CMX membrane, where the counter-ions balance the negative charges along the polymer chains, and the interaction energies of these counter-ions dissolved in water. Although the interaction energy between the ions and the water are different with respect to the interaction occurring in the polymer matrix, a roughly prevision about the effect of the

investigated ion is given. In general, the higher is the interaction energy, the lower are the sugar fluxes. This conclusion has nevertheless to be considered with caution because the molecular mechanisms governing the flux are complex and they probably cannot simply be reduced to a correlation with the energy between ion and water molecules.

The ion influence on the mass transfer through a membrane is a challenging field. This preliminary finding has highlighted that correlations between ions properties, in solution, and sugar fluxes can be drawn, showing that the ions play an important role. This *ab-initio* computational investigation on ion hydration is important because it provides information useful for future studies concerning the molecular mechanisms through which ions in solution and in membrane affect the transport of organic solutes.

This Chapter encourages further work that should be carried out to better understand the involved mechanisms especially those taking place at the molecular-scale. In particular, for Nanofiltration the dehydration of sugars should be investigated as function of the nature of ions present in solution, since it was demonstrated to be the key factor. On the other hand, to better understand the ions effect on Ion-Exchange membranes, the structural modification of the membrane polymer network should be further investigated since it was observed that it is this kind of modification fixes the membrane performances. This will be the objective of the following Chapter.

III.5 References

[1] J. Zhou, X. Lu, Y. Wang, and J. Shi, "Molecular dynamics study on ionic hydration," *Fluid Phase Equilib.*, vol. 194–197, pp. 257–270, 2002.

[2] A. Tongraar and B. Michael Rode, "The hydration structures of F- and Cl- investigated by ab initio QM/MM molecular dynamics simulations," *Phys. Chem. Chem. Phys.*, vol. 5, no. 2, pp. 357–362, 2003.

[3] V. Boy, H. Roux-de Balmann, and S. Galier, "Relationship between volumetric properties and mass transfer through NF membrane for saccharide/electrolyte systems," *J. Memb. Sci.*, vol. 390–391, pp. 254–262, 2012.

[4] S. Galier, J. Savignac, and H. Roux-de Balmann, "Influence of the ionic composition on the diffusion mass transfer of saccharides through a cation-exchange membrane," *Sep. Purif. Technol.*, vol. 109, no. 0, pp. 1–8, 2013.

[5] V. S. Bryantsev, M. S. Diallo, A. C. T. van Duin, and W. a. Goddard, "Evaluation of B3LYP, X3LYP, and M06-Class Density Functionals for Predicting the Binding Energies of Neutral, Protonated, and Deprotonated Water Clusters," *J. Chem. Theory Comput.*, vol. 5, no. 4, pp. 1016–1026, 2009.

[6] G. De Luca, A. Gugliuzza, and E. Drioli, "Competitive Hydrogen-Bonding Interactions in Modified Polymer Membranes: A Density Functional Theory Investigation," *J. Phys. Chem. B*, vol. 113, pp. 5473–5477, 2009.

[7] M. Valiev, E. J. Bylaska, N. Govind, K. Kowalski, T. P. Straatsma, H. J. J. Van Dam, D. Wang, J. Nieplocha, E. Apra, T. L. Windus, and W. A. De Jong, "NWChem: A comprehensive and scalable open-source solution for large scale molecular simulations," *Comput. Phys. Commun.*, vol. 181, no. 9, pp. 1477–1489, 2010.

[8] V. V. Barkaline, Y. V. Douhaya, and A. Tsakalof, "Computer simulation based selection of optimal monomer for imprinting of tri-O-acetiladenosine in polymer matrix: vacuum calculations.," *J. Mol. Model.*, vol. 19, no. 1, pp. 359–69, 2013.

[9] J. V. Burda, M. Pavelka, and M. Šimánek, "Theoretical model of copper Cu(I)/Cu(II) hydration. DFT and ab initio quantum chemical study," *J. Mol. Struct. THEOCHEM*, vol. 683, no. 1–3, pp. 183–193, 2004.

[10] M. Pavlov, P. E. M. Siegbahn, and M. Sandstrom, "Hydration of Beryllium, Magnesium,

Calcium, and Zinc Ions Using Density Functional Theory," *J. Phys. Chem. A*, vol. 102, pp. 219–228, 1998.

[11] E. R. Davidson and S. J. Chakravorty, "A possible definition of basis set superposition error," *Chem. Phys. Lett.*, vol. 217, no. 1–2, pp. 48–54, 1994.

[12] W. Koch and M. C. Holthausen, *A Chemist's Guide to Density Functional Theory*, II., vol. 3. 2001.

[13] A. Szabo and N. S. Ostlund, "Modern Quantum Chemistry Introduction to Advanced Electronic Structure Theory." Dover Publications, 1996.

[14] C. D. Cappa, J. D. Smith, K. R. Wilson, B. M. Messer, M. K. Gilles, R. C. Cohen, and R. J. Saykally, "Effects of Alkali Metal Halide Salts on the Hydrogen Bond Network of Liquid Water," *J. Phys. Chem. B*, vol. 109, pp. 7046–7052, 2005.

[15] A. Gugliuzza, G. De Luca, E. Tocci, L. De Lorenzo and E. Drioli "Intermolecular Interactions as Controlling Factor for Water Sorption into Polymer Membranes" J. Phys. Chem. B, *vol*. 111, no. 30, pp. 8868–8878, 2007.

[16] I. Persson, "Hydrated metal ions in aqueous solution: How regular are their structures?," *Pure Appl. Chem.*, vol. 82, no. 10, pp. 1901–1917, 2010.

[17] G. O. Karlstrom and Anders, "A Combined Quantum Chemical Statistical Mechanical Simulation of the Hydration of Li + , Na + , F - , and Cl -," *J. Phys. Chem. B*, vol. 108, pp. 8452–8459, 2004.

[18] *Y. Marcus*, *Ion Properties*, Marcel Dekker, New York, *1999*.

[19] M. Mezei and L. D. Beveridge, "Monte Carlo studies of the structure of dilute aqueous sclutions of Li+, Na+, K+, F−, and Cl−," *J. Chem. Phys.*, vol. 74, no. 12, p. 6902, 1981.

[20] Y. Marcus, "The Thermodynamics of Solvation of Ions. Part 2. The Enthalpy of Hydration at 298.15 K," *J. Chem. Soc. Faraday Trans.*, vol. 83, pp. 339–349, 1987.

[21] Y. Marcus, "A simple empirical model describing the thermodynamics of hydration of ions of widely varying charges, sizes, and shapes," *Biophys. Chem.*, vol. 51, no. 2–3, pp. 111–127, 1994.

[22] G. M. Geise, D. R. Paul, and B. D. Freeman, "Fundamental water and salt transport properties of polymeric materials," *Prog. Polym. Sci.*, vol. 39, no. 1, pp. 1–42, 2014.

[23] T. Ikeda, M. Boero, and K. Terakura, “Hydration properties of magnesium and calcium ions from constrained first principles molecular dynamics.,” *J. Chem. Phys.*, vol. 127, no. 7, p. 074503, 2007.

[24] A. Musinu, G. Paschina, and G. Piccaluga, “On the structure of the NH+4 ion in aqueous solution,” *Chem. Phys. Lett.*, vol. 80, no. 1, pp. 163–167, 1981.

[25] R. L. Wong and E. R. Williams, “Dissociation of SO 42 - (H 2 O),” no. 1, pp. 10976–10983, 2003.

[26] S. J. Grabowski, W. A. Sokalski, E. Dyguda, and J. Leszczyn, “Quantitative Classification of Covalent and Noncovalent H-Bonds,” *J. Phys. Chem. B*, vol. 110, pp. 6444–6446, 2006.

[27] V. Boy, “Rôle de la composition ionique sur le transfert de sucres à travers des membranes de nanofiltration,” Doctorat de l'Université Toulouse III - Paul Sabatier, 7 mars 2012.

[28] J. Savignac, “Impact des interactions membrane/électrolyte sur la diffusion de sucres à travers des membrane échangeuses d’ions,” Doctorat de l'Université Toulouse III - Paul Sabatier, 13 octobre 2010.

[29] R. W. Gurney, *Ionic Processes in Solution*. New York: McGraw-Hill Book Company, Inc., International Chemical Series, 1953.

[30] Y. Jiang, M. Hu, J. Wang, K. Zhuo, and S. Xia, “Volumetric properties and volumetric interaction parameters for the CsCl–monosaccharide (d-galactose, d-xylose and d-arabinose)–water systems at T=298.15 K,” *J. Chem. Thermodyn.*, vol. 36, no. 8, pp. 671–676, 2004.

[31] P. K. Banipal, T. S. Banipal, J. C. Ahluwalia, and B. S. Lark, “Partial molar heat capacities and volumes of transfer of some saccharides from water to aqueous sodium chloride solutions at T=298.15K,” *J. Chem. Thermodyn.*, vol. 34, no. 11, pp. 1825–1846, 2002.

[32] K. Zhuo, J. Wang, Y. Yue, and H. Wang, “Volumetric properties for the monosaccharide (D -xylose, D -arabinose, D -glucose, D -galactose) – NaCl – water systems at 298.15 K,” *Carbohydr. Res.*, vol. 328, pp. 383–391, 2000.

[33] H. A. Tajmir-Riahi, “Interaction of D-Glucose with alkaline-earth metal ions. Synthesis, Spectroscopic, and structural characterization of metal-ion binding on anomeric configuration of the sugar.” *Carbohydrate Research*, vol 163, pp 35-46, 1988.

[34] I. Pedruzzi, E. a. B. da Silva, and a. E. Rodrigues, “Selection of resins, equilibrium and sorption kinetics of lactobionic acid, fructose, lactose and sorbitol,” *Sep. Purif. Technol.*, vol. 63, no. 3, pp. 600–611, 2008.

[35] C. Nobre, M. J. Santos, a Dominguez, D. Torres, O. Rocha, a M. Peres, I. Rocha, E. C. Ferreira, J. a Teixeira, and L. R. Rodrigues, “Comparison of adsorption equilibrium of fructose, glucose and sucrose on potassium gel-type and macroporous sodium ion-exchange resins.,” *Anal. Chim. Acta*, vol. 654, no. 1, pp. 71–6, 2009.

Chapter IV

Role of noncovalent interactions on the transfer of sugar through a CMX membrane: a Quantum Mechanics/Molecular Mechanics analysis

Recent experimental studies have demonstrated that the ionic composition of the solution, i.e. the nature and concentration of the ions have a significant impact on the transport of neutral organic matter through ion exchange membranes like those used in electrodialysis [1]. The solvent (water) and organic matter (saccharides of different molecular weights) transfer were measured, in a diffusion regime, through a CMX cation exchange membrane (sulfonated polystyrene-divinylbenzene, Neosepta Tokuyama corp. Japan) soaked in different electrolyte solutions NaCl, $CaCl_2$, $MgCl_2$ and NH_4Cl. It was found that the xylose, glucose and sucrose fluxes, through the membrane soaked with NaCl, are twice compared to those obtained when the same membrane is soaked in $MgCl_2$ and about 1.5 those when it is soaked in $CaCl_2$ (see Table I.2). Hence, the understanding of mechanisms, at the molecular level, and interactions governing such trend is crucial to optimize the Electrodialysis process

Therefore, in this Chapter a theoretical analysis is carried out by a combined molecular modeling free from adjustable parameters. Previous *ab-initio* (quantum) investigations have highlighted the crucial role of noncovalent interactions, and in particular hydrogen bonding, on the polymeric membrane properties, such as the ion exchange capacity, molecular affinity and the non-linear increase of the water sorption as function of additive content in polymer[2], [3], [4] and [5]. More precisely, the present Chapter is focused on the noncovalent interactions and molecular mechanisms by which the counter-ions, used to soak a cation-exchange membrane, affect the fluxes of sugars. Building blocks, such as the sulfonated phenyl group, hydrated polystyrene monomers neutralized with the different cations, Na^+, Mg^{2+} and Ca^{2+}, and the hydrated glucose were assembled in supramolecular structures, i.e. glucose-polymer complexes and double polymer chain fragments, representing different parts of the macroscopic system. The building blocks were first studied at a high level of quantum theory, before being assembled in supramolecular models which were then studied by means of a combined Quantum and Molecular Mechanics approach (QM/MM).

Then the trend of the interaction energies between the sugar-polymer and the chain-chain in polymer network are compared to those of the sugar flux in order to identify the transfer driven mechanisms.

IV.1 Computational approaches, building blocks structures and force field validation.

In order to accurately assess the aforementioned interactions quantum chemical calculations are mandatory. However, considering the size of the investigated systems, as well as the discussion

in Chapter 2, Quantum Mechanics and Molecular Mechanics approaches are adopted. Single building blocks were first studied at quantum level, using an accurate level of theory, and when the systems have become too large (more than 100-150 atoms) then a QM/MM approach was used. The QM/MM calculations were performed by NWChem software [6] [7].

An *ab-initio* modeling of polymer chains is always a difficult task due to the large number of atoms and the several possible conformers or windings of the chains. The presence of cations makes the complexity of the system still higher. A conformational research of polymer fragments was then required. This research was performed at Molecular Mechanics level by using the Avogadro code [8] and the Universal Force Field [9]. A weighted rotor search of the more probable conformers (i.e. the scan of the potential energy surface of the molecular model) and subsequently MM optimizations (500 steps and convergence energy criterion at 10^{-8}a.u.) was carried out. This procedure was repeated for five times, for each target structure, then the energy of each found conformer was calculated at quantum level to select the most stable among them.

IV.1.1 Sulfonated styrene monomers

The quantum mechanics calculations were carried out in the frame of Density Functional Theory (DFT). Two functionals, BP86 [10] and X3LYP [11], were used to optimize the sulfonated phenyl group neutralized with sodium ion. The dual optimization of the same structures was made to evaluate the functionals reliability. In fact, as it has been discussed in Chapter 2, DFT calculations can be affected by the used functional. Thus, two well-known functionals were compared to evaluate the more suitable for the systems investigated in this Chapter. The structures, shown in Figure IV.1, were fully optimized using the analytical energy gradients and the quasi-Newton optimization with the updating of approximate Hessian energy [6]. The maximum and root-mean-square of the energy gradients were set to 4.5 10^{-4} and 3.0 10^{-4} a.u., while the thresholds of the maximum and root-mean-square of the Cartesian displacement vectors were 1.8 10^{-3} and 1.2 10^{-3} a.u, respectively. The energy convergence threshold for the self-consistent field procedure was set to 10^{-6} a.u. and the root-mean-square of the electron density was set to 10^{-5} a.u. Triple -ζ basis sets were employed and in particular 6-311G basis set was used for C and H atoms, 6-311G* for S atom, 6-311++G(2d,2p) for O atoms and Na^+ ion. Polarization orbitals were necessary to better describe the hydrogen bond while the diffuse functions were required to better model cations [12] and oxygen-containing system

[13]. A conformational research of the sulfonated phenyl group was carried out before quantum optimizations according to the procedure described above.

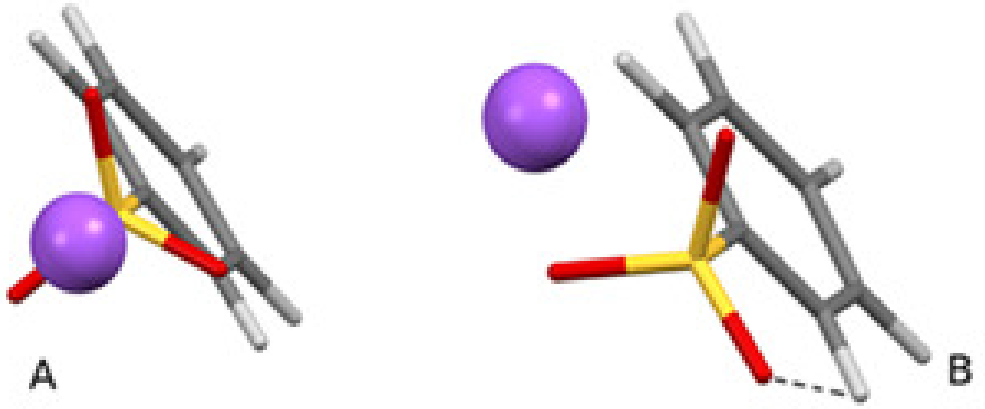

Figure IV.1: Equilibrium (QM optimized) structures of more probable conformers of sulfonated phenyl group: on the left, geometry with oxygen atoms *out* of phenyl ring, i.e. out-plane conformer, and structure with one oxygen *in* the same phenyl plane, i.e. in-plane conformer, on the right. Red color indicates oxygen atoms, violet Na^+ counter-ions, yellow S atoms, grey and white C and H atoms.

The interaction energies, ΔE_{int}, were then calculated by using the optimized QM geometries. In the entire paper, the interaction energies are defined as:

$$\Delta E_{int} = E_{tot} - E_1 - E_2 \qquad \text{(IV.1)}$$

where, E_{tot} is the energy of the total adduct, in this case formed by sulfonated phenyl and cation, E_1 and E_2 are the energies of the two isolated subsystems in interaction. For this section, E_1 and E_2 are the energy of sulfonated phenyl and cation, respectively. The Basis Set Superposition Error (BSSE) correction was also applied in the calculations of ΔE_{int} according to the counterpoise method [14].

Two conformers were found for the smallest building block, i.e. the sulfonated styrene. In the first conformer, all the oxygen atoms are outside the plane of phenyl ring, as shown in IV.1a. In the second structure, one oxygen atom is in the same plane as the phenyl ring, Fig. IV.1b, in interaction with one hydrogen atom of the phenyl by means of a hydrogen bonding. The interaction energies between the Na^+ and the sulfonated phenyl were then evaluated. The values, reported in Table IV.1, show that the functional X3LYP yields interaction energies smaller than the BP86 one. In addition, the energy of ionic bond in the in-plane conformer is smaller than that of the out-plane structure when X3LYP is used. On the contrary, BP86 functional gives the same interaction energies for both conformations. This is not physically consistent because in the structure with one oxygen in-plane, the intra molecular interaction (O···H, Fig IV.1b) produces an asymmetry on the electron density of the sulfonic group and this should result in a

different interaction with Na^+. Then, X3LYP was chosen for the subsequent quantum calculations in addition to the optimized Ph-SO_3^-···Na^+ in-plane conformer which defines the starting geometry of the smallest building block.

Functional	*Complex*	*ΔE_{int} (Kcal/mol)*
BP86	*Ph-SO3--Na+ (in-plane)*	*-127,39*
X3LYP	*Ph-SO3--Na+ (in-plane)*	*-138,37*
BP86	*Ph-SO3--Na+ (out-plane)*	*-127,38*
X3LYP	*Ph-SO3--Na+ (out-plane)*	*-131,82*

Table IV.1: Energies of the sulfonated phenyl…Na^+ ionic interaction (bond) evaluated using two DFT functionals.

Nevertheless, to evaluate the noncovalent interactions, involved in the sugar transport through a cation exchange membrane, the role of water molecules has to be taken into account. Thus, the in-plane conformation was used to evaluate the hydration level of each considered counter-ion. Precisely, the hydration of each counter-ion was computed using a two steps procedure, in which the water molecules were first inserted one by one, then the entire adduct, obtained after each insertion, being optimized at QM level. Each inserted water molecule was directly attached to the target cation at a bond distance of 2.2 Å until reaching the saturation of "steric" space (i.e. the available space) around the cation. It is worth noting that the full quantum optimizations, after each water molecule insertion, allow the relaxing of the entire water cluster around the cation. Thus, after each optimization, a new arrangement of the water molecules was found. Then, the new optimum water arrangement was used as starting geometry to bind a new water molecule, if there was available free space around the cation. To evaluate the space available for the water molecules, the van der Waals radii [15] of the involved atoms were used. Finally, the basis sets, used to perform the QM optimizations with the criteria already described above, were: 6-31G* for C, H, S, O and 6-31++G for Na^+, Mg^{2+} and Ca^{2+}.

The results, concerning the hydration of the cations, are summarized in Fig. IV.2 and in Table IV.2. In particular, the number of water molecules added around each cation until reaching the saturation limit is reported in the first column of Table IV.2. One can observe that the saturation limit depends on the kind of cation, respectively 10 water molecules for Na^+ and Ca^{2+} and 8 for Mg^{2+}. This difference is due to the more wedged position of the Mg^{2+}cation between the two SO_3^- groups compared to Na^+ or Ca^{2+}. The analysis of the optimized structures, after each water molecule insertion, reveals that they are arranged in two shells. In the first shell, the water molecules still remain directly linked to the cations, as shown in Fig. IV.2 (spacefill atoms).

Whilst, those of the second shell, even though placed close to the cation before the QM optimization, are moved in a farther position (sticks in Fig. IV.2), where they do not interact directly with the cation since they are shielded by the ones in the first shell.

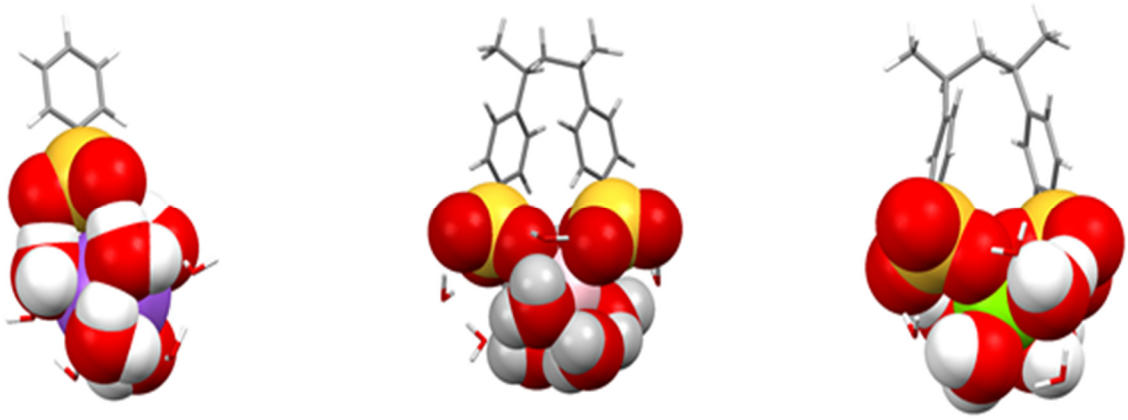

Figure IV.2: Sulfonated styrene monomers neutralized by Na^+ (in violet), Ca^{2+} (in pink) and Mg^{2+} (in green). Spacefill and stick atoms indicate the water molecules of the first and second hydration shell, respectively.

Number of H_2O molecule	***1st shell Na^+***	***1st shell Ca^{2+}***	***1st shell Mg^{2+}***
1	*1*	*1*	*1*
2	*2*	*2*	*2*
3	*3*	*3*	*3*
4	*3*	*3*	*4*
5	*4*	*4*	*4*
6	*4*	*5*	*4*
7	*6*	*5*	*4*
8	*5*	*5*	*4*
9	*6*	*5*	*nd*
10	*6*	*5*	*nd*

Table IV.2: Number of water molecules added around each counter-ion, until saturation limit, and 1st hydration shell.

Again the number of water molecules belonging to the first shell depends on the cation: 6 water molecules for Na^+, 5 for Ca^{2+} and 4 for Mg^{2+}. In the case of divalent cations, the deformation of the sulfonated styrene monomers was taken into account in the quantum optimizations, hence the Ph-SO_3^--Na^+···$(H_2O)_6$, (Ph-SO_3^-)$_2$-Ca^{2+}···$(H_2O)_5$ and (Ph-SO_3^-)$_2$-Mg^{2+}···$(H_2O)_4$ were chosen as the starting geometries of the slightly larger successive building blocks. The energies, associated to the interactions between the first hydration shell and the monomers-cation build blocks, is high: -87.43 Kcal/mol for Ph-SO_3^--Na^+···$(H_2O)_6$, -146.78 Kcal/mol and -157.44 Kcal/mol for the (Ph-SO_3^-)$_2$-Ca^{2+}···$(H_2O)_5$ and (Ph-SO_3^-)$_2$-Mg^{2+}···$(H_2O)_4$ complexes, respectively. These high values demonstrate that these complexes can be considered as stable substructures within the CMX polymer matrix. Conversely, since all the water molecules belonging to the second hydration shell displayed lower adhesion energy to the inner core, they were not included in the building block structures. Indeed, some of them can move or rearrange during the sugar diffusion.

The examination of the optimized building block structures can give some preliminary correlation between the experimental fluxes and the number of water molecules in the first hydration shell. On one hand, it should be remembered that the sugar fluxes in a CMX membrane equilibrated with Na^+ are higher than the ones obtained with the membrane equilibrated by Ca^{2+} and that an even bigger difference was detected with Mg^{2+} used as counter-ion. On the other hand, the computed building blocks with Na^+, Ca^{2+} and Mg^{2+} reveal that 6, 5 and 4 water molecules are, respectively, involved in the first hydration cluster around the cation. Thus, at this stage, one can state that the decrease of the sugar fluxes with the type of counter-ion can be related to the decrease of the number of water molecules involved in the first hydration shell of the polymer fragments-cation build block.

IV.1.2 Hydrated Glucose

The last building block necessary to analyze the target noncovalent membrane/solute interactions is the hydrated glucose. As with the previous blocks, the calculations were carried out in the frame of DFT. Energy and optimization convergence criteria were set as described in the previous section, while the 6-31G* basis set for all the atoms (i.e. O, H, C) was used. The glucose, in β-anomeric form, was chosen as initial structure for its highest presence in aqueous solution at room temperature [16]. In this case, two computational procedures were followed to evaluate the hydration level of glucose. The first one is that used for evaluating the hydrated structures of the neutralized sulfonated styrene monomers, i.e. a step by step insertion of water molecules and subsequently quantum optimization. However, the starting geometry was a glucose with 6 water molecules, glucose···$(H_2O)_6$, because using 6 water molecules all the -OH

groups and the ether oxygen interact with at least one water molecule, through H-bond, without any overlapping. Conversely, in the second used approach, all the structures were prepared without considering the optimized structures of lower hydrated glucose. This means that, for example, in the initial structure for the optimization of glucose with 7 water molecules, all the 7 molecules were added to a dried sugar without considering the previous optimized structure with 6 water molecules.

The 5 hydroxyl groups and the ether oxygen were considered as preferential interaction sites. In addition, since each -OH group can be considered as a partial donor and acceptor of proton, it can interact, *via* hydrogen bonding, with at least 2 H_2O. In the first insertion step, the water molecules were attached to the H atoms until the saturation of the hydroxyl hydrogen is reached. Then, further water molecules were added to the oxygen atoms of the -OH groups. All the water molecules were added at a distance of 2.1 Å from the reference atoms. The hydration shell of the sugar was considered to be achieved when the interaction energy between glucose and water molecules reaches a plateau. The results of the quantum calculations are shown in Fig. IV.3. The overlap between the interaction energies, evaluated with the two methods, for complexes containing up to 6 water molecules is due to the fact that, for the first procedure, the geometry with 6 water molecules was chosen as starting point.

Otherwise, a significant difference between the results obtained with the two approaches can be observed. Indeed, the structures obtained by the step by step method are more stable. The differences of about 10 kcal/mol for the structures with 7, 8 and 9 water molecules and of about 20 kcal/mol for the structure with 10 H_2O are significant since the average energy of the H···O bonds is in the range of 7-12 Kcal/mol. But, the most significant difference is in the value of the water molecule number above which the interaction energy reaches a plateau. In the step by step optimizations, the plateau starts from 11 H_2O whereas according the second method, it starts from 9 H_2O. Then, considering the most stable structures provided by the first method, the glucose···$(H_2O)_{11}$ is retained and chosen as the building block to model the hydrated sugars in the description of the membrane/solute interactions. In Fig. IV.4, the glucose···$(H_2O)_{11}$ complex is shown. The interaction energy, corresponding to the plateau, is -101.5 Kcal/mol, which roughly means an average energy of 9 Kcal/mol for each single water molecule -glucose interaction. Considering that the energy of stable H-bonds are in the order of 10 Kcal/mol [17], as in the case of the neutralized sulfonated styrene monomers, the hydrated sugar can be considered as another stable building block. Thus, the glucose···$(H_2O)_{11}$ complex has defined the initial geometry of the building blocks used to prepare larger models treated in QM/MM.

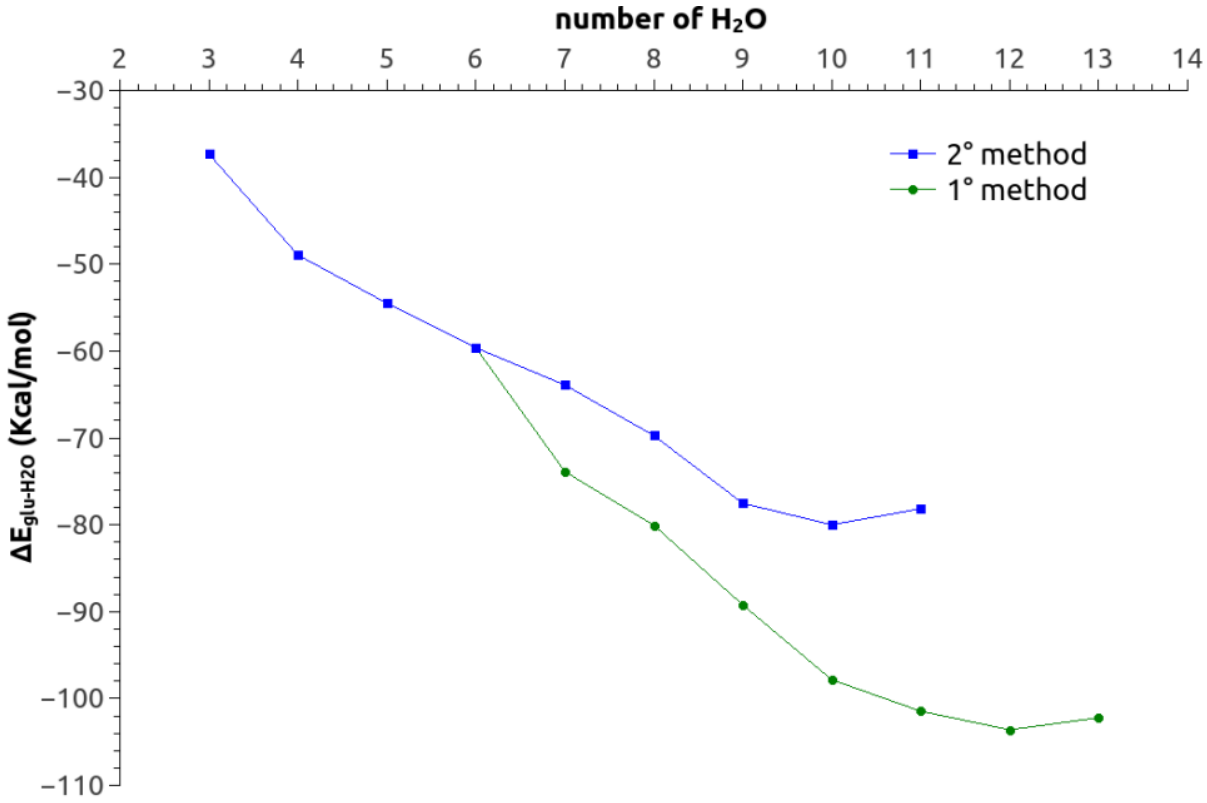

Figure IV.3: Interaction energy between glucose and water as function of the number of water molecules. In first method the glucose hydration shell is built "step by step"; in the second method the water molecules were added from scratch for each hydration level.

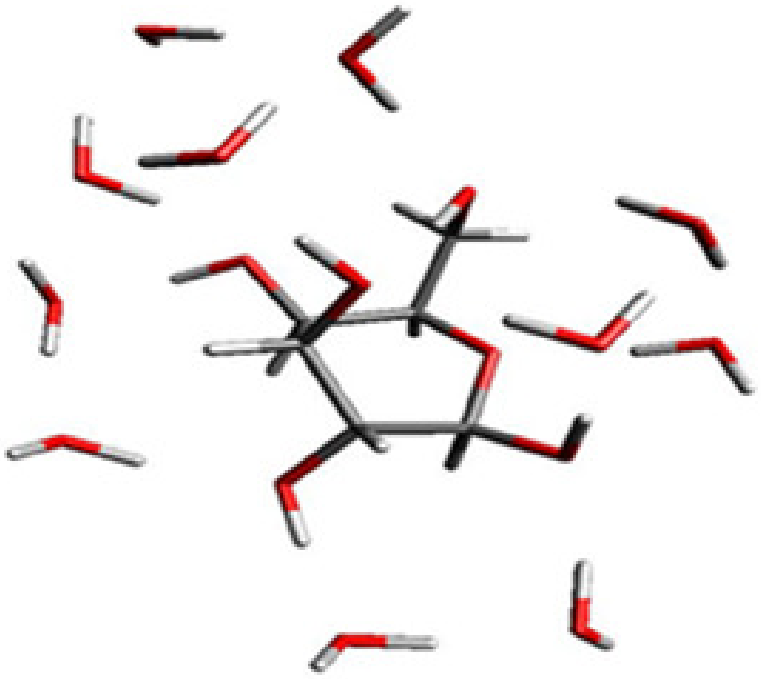

Figure IV.4: QM optimized structure of hydrated glucose, i.e. the glucose···$(H_2O)_{11}$.

An additional structure of a glucose molecule surrounded by 20 'randomly' arranged water molecules was also investigated to assess if the arrangement of the first hydration shell is influenced by the water molecules in the second shell. The computed interaction energy, among the glucose and 20 H_2O, is similar to the plateau energy achieved through the second method as well as the water arrangement in the first hydration shell. Thus, this glucose···$(H_2O)_{20}$ is also less stable than the former glucose···$(H_2O)_{11}$ selected structure, found by a "step by step" procedure.

More generally, one can suggest to use the "step by step" method for further investigation on the hydration shell of molecules.

A dimensional analysis of the sugar, at different hydration levels obtained by the "step by step" method, was also carried out. Then, the minimal molecular size, d_{min}, and the effective diameter, d_{eff}, of several glucose···$(H_2O)_n$ structures were calculated using a home-made algorithm described in previous works[18] and [19]. The values are reported in Table IV.3.

N° H_2O-Glucose	***d_{min}(Å)***	***d_{eff} (Å)***
6	*7.32*	*14.86*
7	*7.32*	*14.88*
8	*7.96*	*14.92*
11	*8.05*	*16.28*

Table IV.3: Minimal molecular size, d_{min}, and effective diameter, d_{eff}, of glucose at various hydration levels.

One can state that both size parameters have similar trends, i.e. increasing values for hydration higher than 7 water molecules. However, there is a great difference between the values of the minimal molecular size and that of the effective diameter of the solute, whatever the hydration level. This is an important point to take into account since, regarding the investigation of the transfer phenomena, the size of the hydrated solute d_{eff} is probably the most relevant value to be considered. However, as previously explained, the hydration shell of the transferring solute can be modified with respect to that in the solution.

IV.1.3 Force Field assessment

As pointed out, the optimization of macromolecules and the calculation of the related interaction energies required a QM/MM computational approach. In this case, the choice of an appropriate Force Field to describe the energy of classical regions is mandatory.

The Amber [20] and Charmm [21] force fields, well known and largely used in atomistic simulations, were chosen and compared to evaluate their reliability for the investigated systems. Some monomers, i.e. fragments, of the target polymer were first optimized. Then, the fragment-cation interactions were computed at DFT, DFT/Charmm and DFT/Amber levels and compared. Structural properties of the optimized fragments were finally investigated. The structures, used to evaluate the fragment-Na^+ and fragment-Mg^{2+} interactions, were formed from 1 to 5 monomers and from 2 to 4 monomers, respectively. An additional model, formed by 7 monomers, was also used to describe the fragment-Mg^{2+} system. A maximum of three SO_3^- groups was considered in the Na^+ models and four SO_3^- in the fragments with Mg^{2+}, as shown in Fig. IV.5. The positions of the sulfonic groups along the fragments were chosen by a random function. For each fragment, a conformational search was carried out using the procedure described in Section IV.1. Hence, the geometries of the most probable conformers were optimized at QM and QM/MM level, respectively. The updated Charmm parameters for the cations, defined by Beglov and Roux [22], were used.

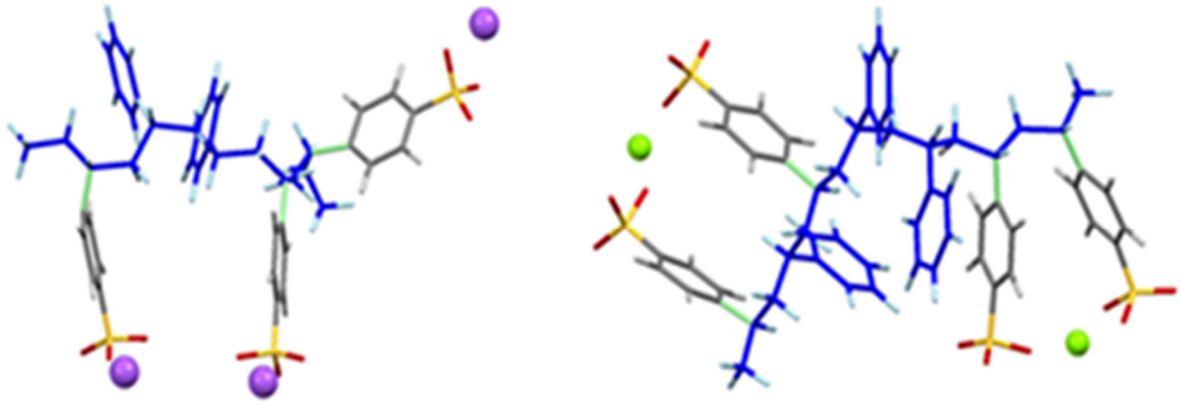

Figure IV.5: Polymer fragments of different lengths containing Na^+ (left) and Mg^{2+} (right) used in the Force Field calibration. MM region is represented in different shades of blue, in green the boundary bonds while the atoms, in the other colors, were treated at QM level.

As shown in Fig. IV.5, the QM regions were the -Ph-SO_3^-···Na^+ and (-Ph-SO_3^-)$_2$···Mg^{2+}, whereas the polymer backbone and the non-functionalized phenyl defined the classical region of the models. The convergence criteria for the QM zone were set as previously described in paragraph IV.1.1, while concerning the classical calculations, the criteria were 10^{-4} nm for the threshold on the step size and 10^{-4} a.u for the total energy in the QM/MM optimizations. BSSE correction was only applied to the quantum calculations of the interaction energies since it is not implemented in the QM/MM module of the NWChem version used. Anyway the possible error due to the absence of BSSE correction will be included in the differences between DFT and DFT/MM values.

The ΔE_{int} values, obtained at DFT, DFT/Charmm and DFT/Amber levels as a function of the monomers number, are reported in Fig. IV.6. A systematic shift to smaller interaction energies with respect to the DFT values for the two QM/MM methods can be observed. Nevertheless, the interaction energies, evaluated by the two classic force fields, show a good correlation with the reference QM values. The DFT/Charmm method gives ΔE_{int} values closer to quantum values compared to the DFT/Amber approach. Furthermore, DFT/Amber method does not reproduce the minimum and maximum ΔE_{int} values found for the Na^+ models containing 2 and 4 monomers, respectively. On the contrary, the DFT/Charmm approach is capable to represent this trend. Finally, a stronger overestimation of the interaction energies of more than 10 Kcal/mol is observed using the DFT/Amber approach for the models containing Mg^{2+} as counter-ion.

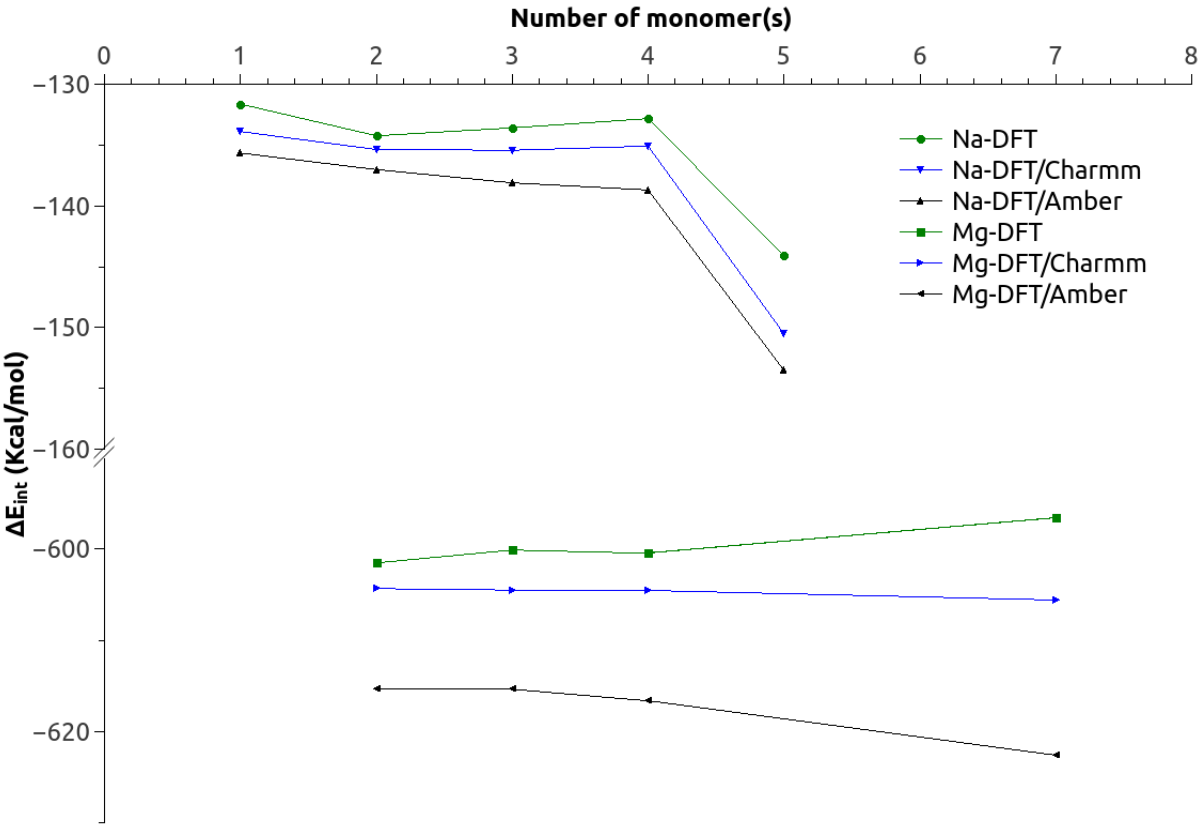

Figure IV.6: Interaction energies evaluated at DFT, DFT/Charmm and DFT/Amber levels as a function of the increasing number of monomers in the polymer fragments, illustrated in Fig IV.5.

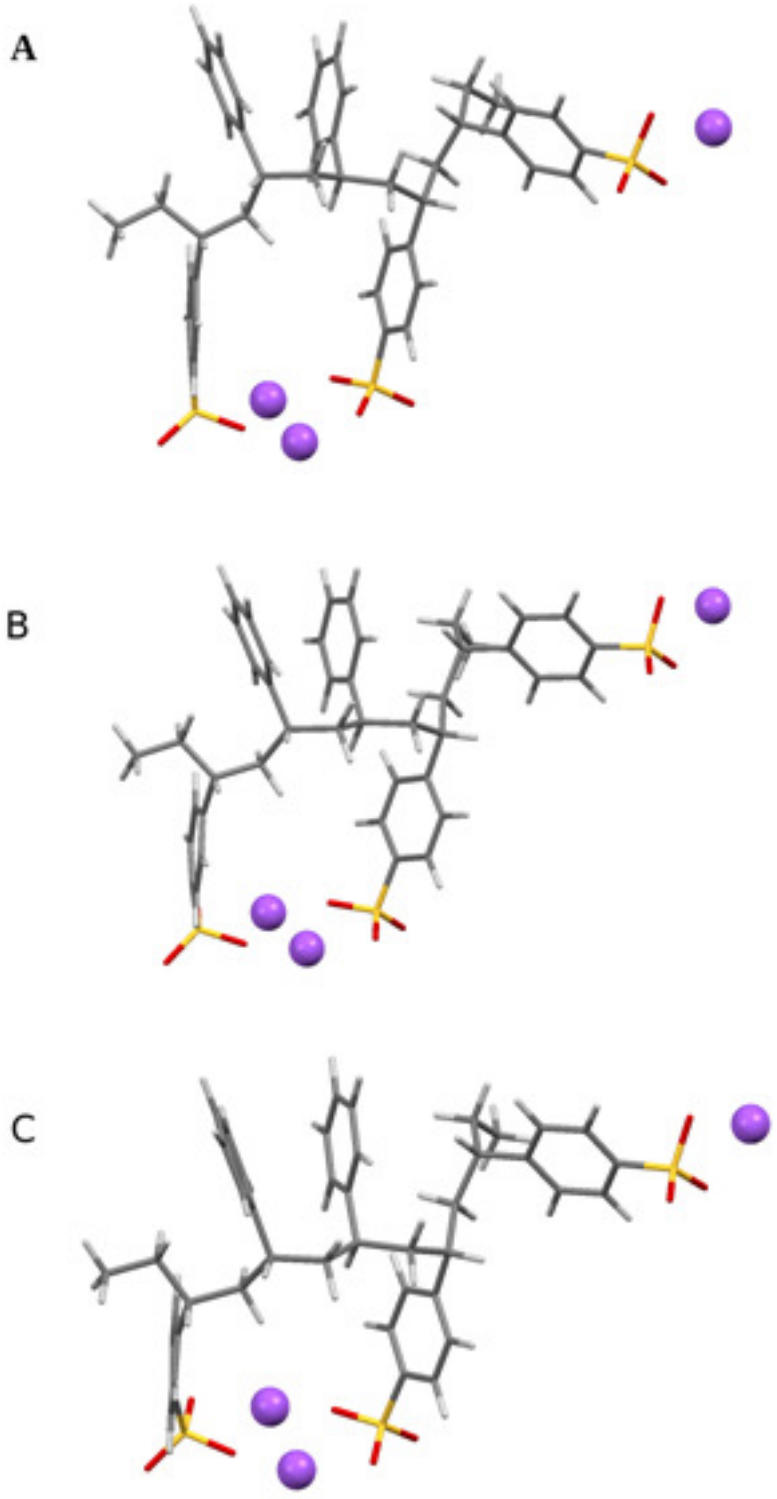

Figure IV.7: Polymer fragments equilibrium geometries formed by 5 monomers and Na^+: optimized geometry from DFT (A), from DFT/Charmm (B) and from DFT/Amber (C) approaches, respectively.

Also the optimized geometries, formed by 5 monomers and Na^+ (as indicated in Fig. IV.7) were compared. All the computational approaches give almost the same structures with the two SO_3^- groups and sodium closer than in the starting (initial) geometries, shown in Fig. IV.5 and obtained by assembling the build blocks described previously.

It is worth noting that the ability of DFT/Charmm and DFT/Amber to reproduce the quantum equilibrium structure is a marker of the reliability of the adopted QM/MM method. In Table IV.4, some geometrical parameters were shown for a better comparison. The selected lengths represent the different regions of the models, i.e. MM, boundary and QM. In particular, the average lengths of the C-H and C-C bonds, along the aliphatic chain (MM region), were reported. In addition, the main lengths related to C-Ph-$SO_3^-\cdots Na^+$ building block were chosen as representatives of the boundary and QM zone. The worst difference among the calculated average lengths is 3 hundredths of Angstrom in the C-C distance, while there are no significant differences in the bond lengths of the QM region. This result is important for the purpose of the Chapter. Though, from a geometrical point of view, the three computational approaches are in agreement, the DFT/Charmm method is the better to reproduce the quantum interaction energies. Therefore, the Charmm Force Field was preferred for the further analysis.
Always taking as example the structure containing five monomers and Na^+, 400 hours/cpu (Intel Xeon E3-1245) were required to obtain the equilibrium geometry, by means of a QM optimization, of a model containing 103 atoms. Instead, only 125 hours/cpu were necessary to complete the geometry optimization by using the hybrid QM/MM methods. Indeed, among the 103 atoms, only 45 were treated at quantum level while the others 58 were treated by Molecular Mechanics. In general, in a QM/MM simulation, only the QM region has a strong influence on the computational time.

Computational Approach	C-H (Å) ***(MM)***	C-C (Å) ***(MM)***	C-Ph (Å) ***(Boundary)***	Ph-S (Å) ***(QM)***	S-O (Å) ***(QM)***	O-Na^+ (Å) ***(QM)***
DFT	1.10	1.55	1.53	1.79	1.51	2.16
DFT/Charmm	1.11	1.58	1.53	1.79	1.51	2.17
DFT/Amber	1.09	1.58	1.52	1.79	1.51	2.17

Table IV.4: Meaningful bond lengths in the polymer fragment equilibrium geometries formed by 5 monomers and Na^+ and used in the Force Field calibration.

IV.1.4 Large models for the key interactions evaluation

After selecting the building blocks, their assembly in larger structures like macromolecules was performed. The geometries of these large structures were optimized at QM/MM level and the key interactions were assessed. The interactions between the sugar and the polymer were evaluated by using the complexes shown in Fig. IV.8, IV.9 and IV.10, composed by the monomers, defined in paragraph IV.1.1, and the hydrated sugar, as described in section IV.1.2. The contact spots between the hydrated glucose and the functionalized monomers were chosen as function of the steric hindrance. Different arrangements of the monomers around the hydrated sugar were taken into account in the QM/MM calculation of the glucose-monomers interactions. In this calculation, the hydrated glucose and the $(Ph\text{-}SO_3^-)_n$-cation define the QM region, while the other atoms of the complexes constitute the MM part. Regarding the computational criteria, the only changes with respect to the parameters used in the aforementioned quantum optimizations of the single building blocks concerned the maximum and root-mean-square of the Cartesian displacement vectors, now with thresholds of 5.4 and 3.6 10^{-3} a.u., respectively. The used basis sets were the 6-31G* on the H, O, C, S atoms and 6-31++G on the cations. The interaction energies between glucose and functionalized monomers as well as that between glucose and its hydration shell were then evaluated. Once defined the hydrated glucose-monomers complexes, the hydrated monomers, as described in the second part of the section IV.1.1, were used to build some fragments of the polymer chain. For each fragment, 7 monomers of styrene with 3 sulfonic groups, neutralized with Na^+, were used in the calculations as shown in Fig. IV.11. Meanwhile, 4 functional monomers with Ca^{2+} and Mg^{2+} were used to describe the interactions between the polymer chains containing these bivalent ions as shown in Fig. IV.12 and IV.13. The optimizations of the geometries of single fragment were first carried out, with the basis sets and criteria given before and following the described conformational analysis. Then, each optimized fragment was used to build a larger system formed by two fragments posted as a mirror image. These structures, shown in Fig. IV.11, IV.12 and IV.13, were further used as initial geometries for subsequent optimizations and the evaluation of the related interaction energies.

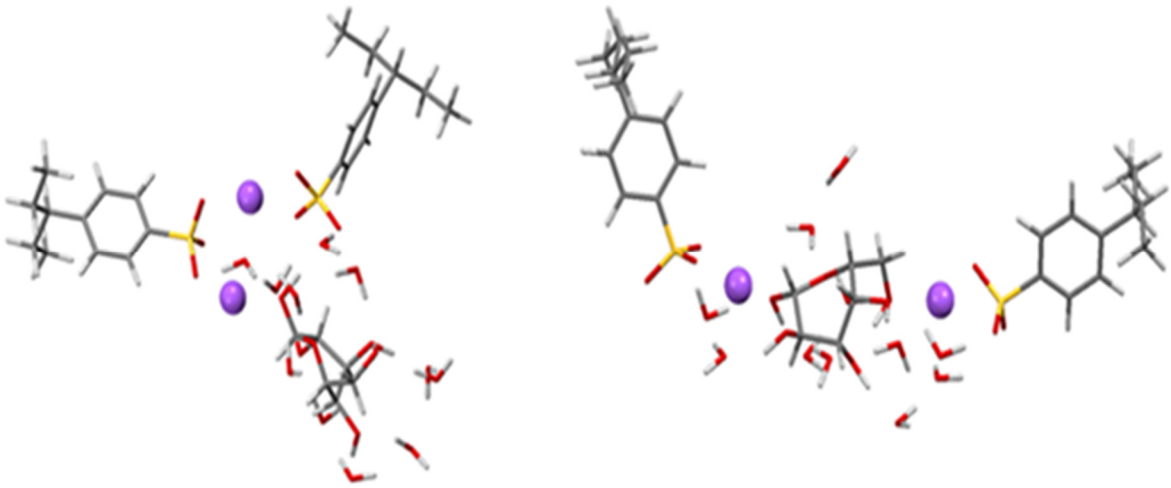

Figure IV.8: Equilibrium (optimized) arrangements of monomers with Na^{+} around the hydrated glucose.

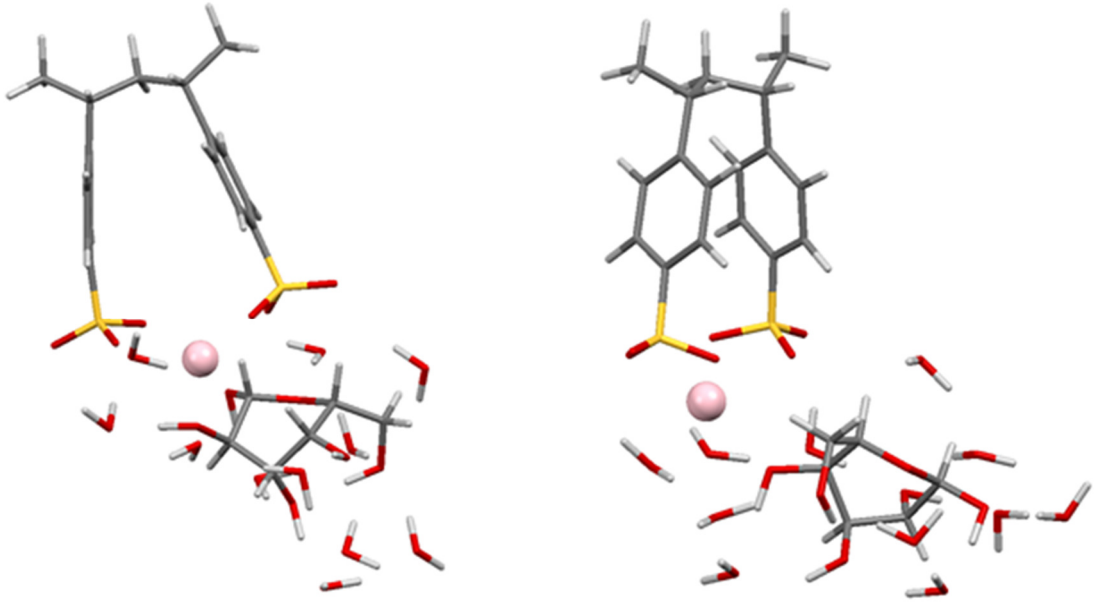

Figure IV.9: Equilibrium arrangements of monomers containing Ca^{2+} around the hydrated glucose.

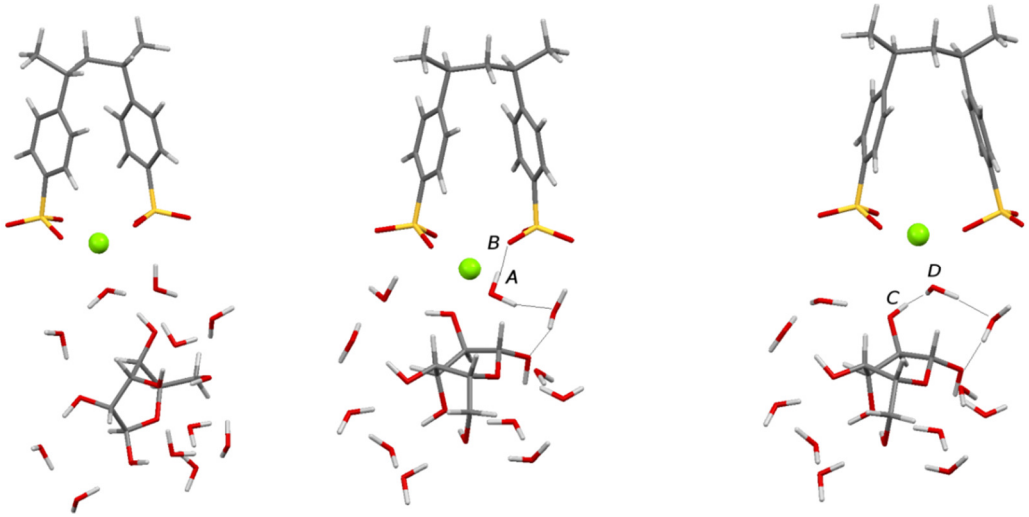

Figure IV.10: Equilibrium arrangements of monomers containing Mg^{2+} around hydrated glucose (left and center). Unstable complex used as starting geometry for the QM/MM optimizations (right).

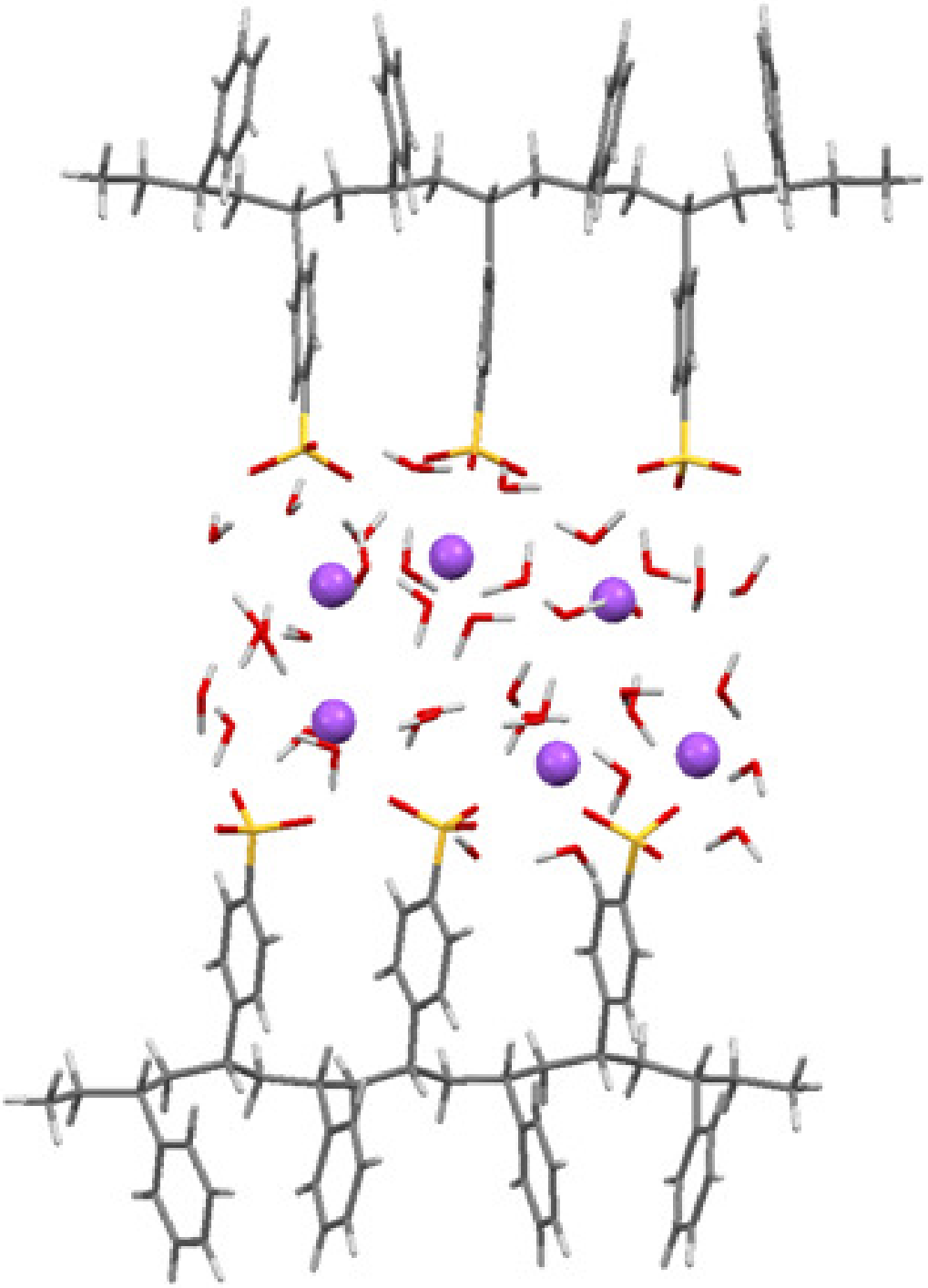

Figure IV.11: Optimized geometry of macromolecular model formed by two polymer fragments equilibrated by Na^+.

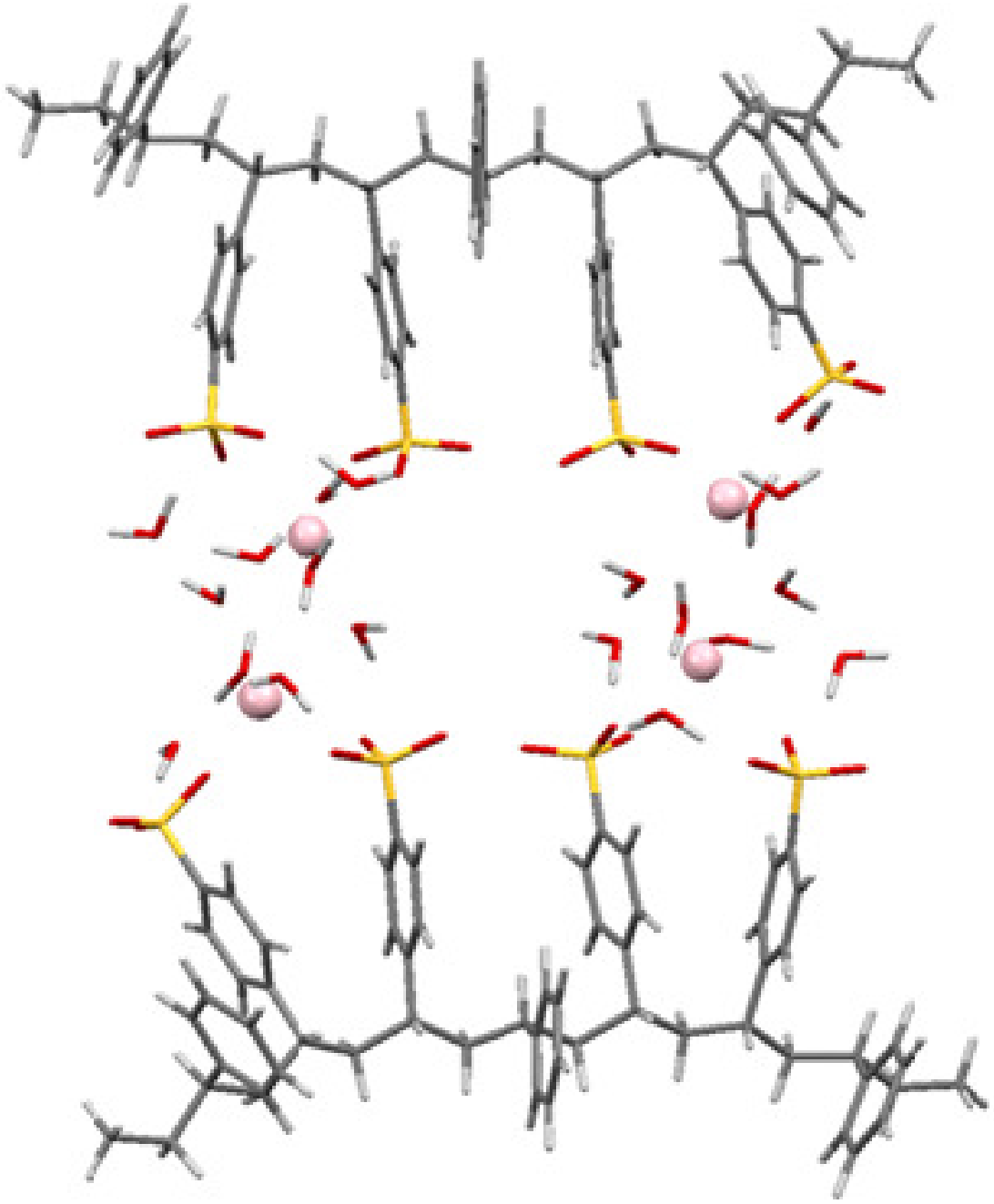

Figure IV.12: Optimized geometry of macromolecular model formed by two polymer fragments equilibrated by Ca^{2+}.

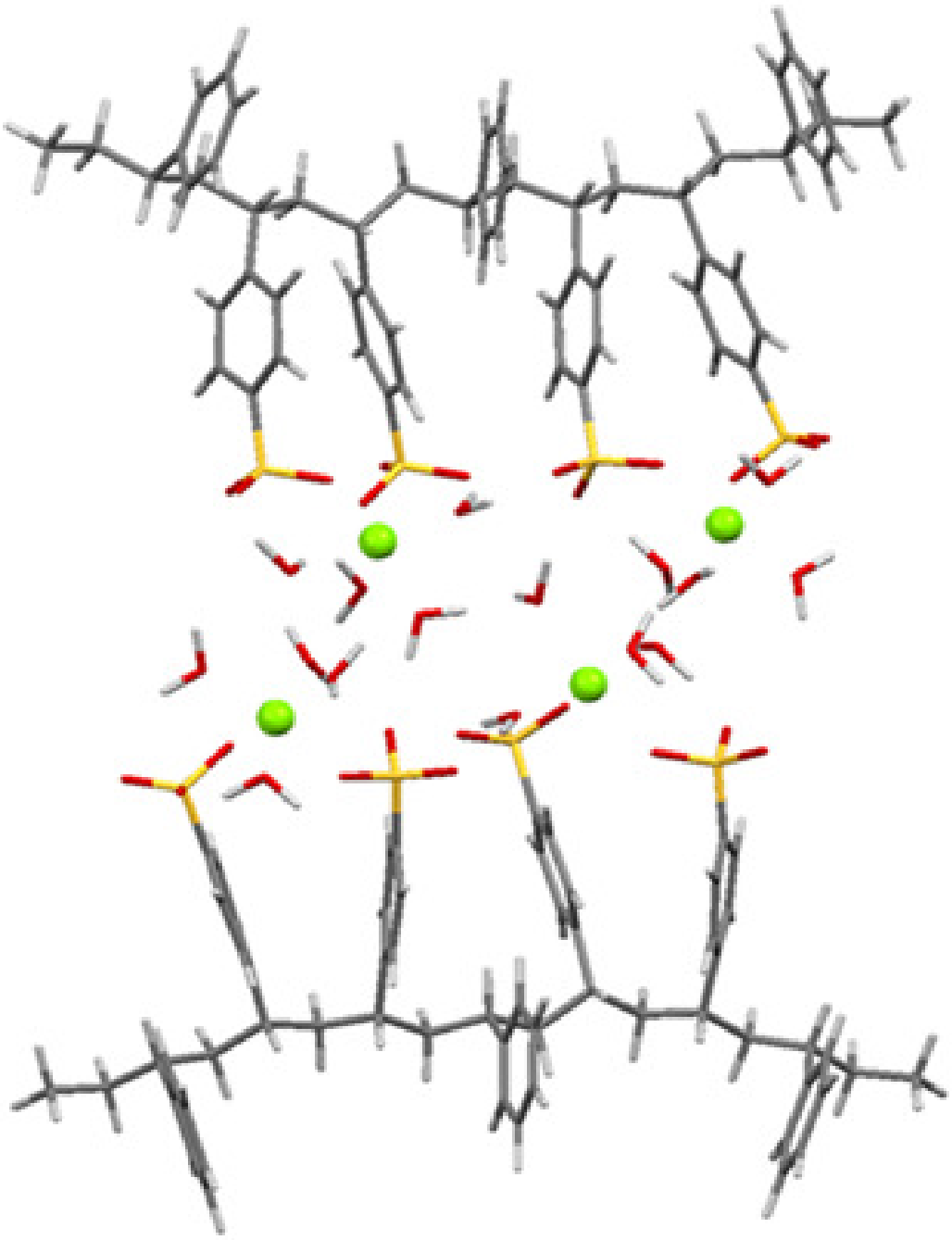

Figure IV.13: Optimized geometry of macromolecular model formed by two polymer fragments equilibrated by Mg^{2+}.

IV.2 Key interactions: sugar-polymer or polymer-polymer?

IV.2.1 Polymer-Sugar Interactions

As explained earlier, the influence of the membrane counter-ion on the transfer of glucose can have different origins. One can be the variation of the sugar solubility in the membrane, directly related to the interactions between the sugar and the polymer chains constituting the membrane. The energies related to these interactions, evaluated using the various complexes described in previous section IV.1.4, are reported in Table IV.5. These values are the average values of the interaction energies obtained for the different glucose-monomers complexes, considering different arrangements of the monomers around the hydrated glucose.

Counter-ions	$\Delta E_{sugar\text{-}mons}$ *(Kcal/mol)*	$\Delta E_{sugar\text{-}water}$ *(Kcal/mol)*
Na^+	*-78.01*	*-92.44*
Ca^{2+}	*-85.03*	*-88.06*
Mg^{2+}	*-85.15*	*-88.34*

Table IV.5: Average energies, related to glucose and polymer fragments interactions ($\Delta E_{sugar\text{-}mons}$), evaluated by using various hydrated glucose complexes. In the last column, the average energies associated to the glucose and its hydration shell interactions ($\Delta E_{sugar\text{-}water}$).

One can state that the values obtained for the different membrane counter-ions are almost similar. Indeed, the energy gap among the complexes containing sodium and those containing divalent cations does not exceed 7 Kcal/mol. The sign and absolute values of these energies indicate that the glucose is stabilized in the polymeric matrix equilibrated with these counter-ions, i.e. the negative sign of $\Delta E_{sugar\text{-}mons}$ means that the sugar is soluble in the membrane. The small differences found as function of the ion nature for the interactions between glucose and the polymer matrix are too small to explain the observed influence of the ion on the sugar flux. Thus the phenomenon is not fixed by such interactions. Indeed, the experimental results (see Table IV.7 next paragraph) show a significant change in the membrane transport properties due to the presence of Mg^{2+} and, to a lesser extent, to the presence of Ca^{2+}. In fact, the sugar flux in the membrane equilibrated with Na^+ is more than 2 times higher with respect to that in the same membrane equilibrated by Mg^{2+} and 1.5 times if Ca^{2+} is used as counter-ion. Instead, especially in the case of these two divalent cations, the sugar-polymer interaction energy is almost the same, so that it cannot be responsible for the counter-ion impact on the sugar flux.

Another important aspect to be considered is the change of the hydration shell of glucose

depending on the cation. Glucose-water adducts interacting with the functionalized monomers can be extracted from the optimized complexes. They can be compared to the hydrated sugar, obtained without considering the influence of the monomers in section IV.1.2 (Fig. IV.4). In the last column of Table IV.5, the average energies, associated to the interaction between glucose and its hydration shell, are reported ($\Delta E_{sugar\text{-}water}$). Again one can see that these values do not change significantly according to the counter-ions. However, it is interesting to note that these interaction energies are different from the interaction energies calculated in the previous section between glucose and water in the sugar solution, i.e. without the monomers presence (-101.5 Kcal/mol, see section IV.1.2). A change in the interaction between glucose and the water molecules is thus pointed out due to the presence of monomers equilibrated with different counter-ions. In any case, this change does not depend strongly on the type of counter-ion attached to the polymer backbone. Looking more closely to the interaction points, one can observe that only the water molecules near the cations and the monomers are affected by their presence. An example is illustrated in Fig. IV.10, for the complex containing Mg^{2+}. In Fig IV.10 (right), representing the initial geometry of the complex, the H-bond between the hydrogen C and the oxygen D, in the glucose hydration shell, is broken while a noncovalent interaction between the hydrogen A of the same molecules and oxygen B of SO_3^- group is formed, as can be seen in the optimized complex shown Fig IV.10 (center). Thus, the energy loss, that is found passing from the hydrated sugar in solution to the glucose linked to the functional monomers, is probably caused by a rearrangement of the noncovalent interactions. In particular, the break of an hydrogen bond between one water molecule and one glucose hydroxyl group is accompanied by the formation of a noncovalent electrostatic interaction between the water molecule and the monomers-cation adduct.

Summarizing, the analysis of the noncovalent interactions performed on various glucose-functionalized monomers complexes reveals that these interactions are only slightly affected by the nature of the considered counter-ions. Finally, the energies of the interactions between the sugar and monomers, equilibrated with different cations, are too similar to explain the variations of the glucose flux through the membrane observed for different membrane counter-ions, as previously measured [9].

IV.2.2 Chain-chain interactions

A modification of the membrane properties themselves according to the membrane counter-ion is another possibility to explain the influence of the ions on the sugar flux. On the basis of the finding concerning the interactions of the hydrated glucose with the cation-polymer adduct discussed above, the interactions between two fragments of the polymer chain were evaluated.

First, the average distances between the cations (counter-ions) and the $-SO_3^-$ groups along the polymer fragment representing the CMX membrane at the molecular level, as defined in section IV.1.4, were evaluated. Indeed, according to Karpenko-Jereb *et al.* [23], this distance can be related, somehow, to the solute transfer in the membrane. A value of 3.09 Å is obtained for the fragment containing Na^+ while smaller values of 2.42 Å and 2.08 Å are found in systems with Ca^{2+} and Mg^{2+}respectively. The average distances between an oxygen atom of a fragment and the nearest oxygen atom of the other were also estimated. Values of 8.57 Å, 7.56 Å, and 6.46 Å are obtained for the macromolecular models equilibrated with Na^+, Ca^{2+} and Mg^{2+}, respectively. Then, one can observe that the average distance between two neighbor oxygen atoms in two polymer fragments varies according to the cation. Moreover, these distances, as well as those previously calculated between the cations and the $-SO_3^-$ groups, along the same polymer chain, can be correlated to the experimental flux of sugar measured by Galier *et al*. [1]. Indeed, an increasing distance gives a higher sugar flux. These average distances are of the same range of magnitude as the values of the minimum molecular size d_{min} of the glucose at different hydration levels, as shown above in Table IV.3. On the other hand, they are smaller than the values of the effective diameter d_{eff} of the hydrated sugar. The model used in this Chapter to compute the distances between the polymer fragments has to be considered as an approximation. Indeed, one can expect that longer polymer fragments could be necessary to represent the whole membrane polymer structure and to obtain more accurate average chain-chain distances. But from this dimensional comparison, which nevertheless correlates with the experimental trend of the sugar flux, one can suggest that a stretch of the polymer chains, i.e. an increase of the chain-chain average distance, should take place in order to permit the diffusion of the hydrated sugar into the polymer matrix. Also the change of the sugar fluxes as function of the counter-ion could be linked more likely to a dynamic change in the chain-chain distance than to the average chain-chain distance in a static equilibrium. In other words, since the noncovalent interactions can be responsible of the polymer breath, thus of the dynamic chain-chain distances, one can imagine that these interactions could vary according to the cation used as counter-ion, so, the dynamic chain-chain distance may change.

To check this assumption, the enlargement of the chain-chain distance was considered. It is correlated with the interaction energies between the polymer chains, $\Delta E^{x}_{chain-chain}$, which were evaluated for the fragments equilibrated with the investigated counter-ions. The values are reported in the first column of Table IV.6. In the same Table, the ratios between $\Delta E^{x}_{chain-chain}$ and the number of water molecules trapped in the two polymer fragments (N_{H2O}), as defined in equation (IV.2), were also reported:

$$\overline{\Delta E}^{x}_{H_2O} = \frac{\Delta E^{x}_{chain-chain}}{N_{H_2O}} \qquad \text{(IV.2)}$$

From this equation, one can get $\overline{\Delta E}^{X}_{H_2O}$, which is the interaction energy *per* water molecule trapped in two polymer filaments for a given counter-ion, *x*, (i.e. Na^+, Ca^{2+} and Mg^{2+}). In other terms, the total cohesion energy between two polymer fragments is distributed among the water molecules embedded between these fragments. Thus, $\overline{\Delta E}^{x}_{H_2O}$ is the average energy associated to the electrostatic interactions that each water molecule, belonging to one polymer fragment, exerts on the other hydrated fragment. According to its definition, given in equation (IV.1), $\overline{\Delta E}^{X}_{H_2O}$ does not take into account the interactions between the water molecules belonging to the same fragment. It is very important to emphasize that the number of water molecules, N_{H2O}, used to calculate $\overline{\Delta E}^{x}_{H_2O}$ is not arbitrarily chosen, but that it corresponds to the number of water molecules in the first hydration shell of the investigated counter-ions interacting with the polymer backbone. The values are presented in Table IV.2 and they are found by means a high level of quantum theory as described in section IV.1.1. Not only the number of water molecules but also their arrangements inside the polymer fragments were the result of accurate QM/MM optimizations. Thus, both the number as well as the arrangements of the water molecules trapped in the polymer filaments are crucial aspects for the correct interpretation of the experimental measurements.

Cation	***ΔE chain-chain (Kcal/mol)***	***N° trapped H_2O***	***N° H-bond wire***	***ΔE^{x}_{H2O} (Kcal/mol)***	***ΔE^{x}_{Hwire} (Kcal/mol)***
Na^+	*-200.62*	*36*	*7*	*-5.57*	*-28.66*
Ca^{2+}	*-166.70*	*20*	*3*	*-8.33*	*-55.57*
Mg^{2+}	*-232.29*	*16*	*3*	*-14.52*	*-77.43*

Table IV.6: *Energies, $\Delta E_{chain-chain}$, of the interactions between polymer fragments (evaluated using macromolecular models); number of H_2O molecules and H-Bond wires trapped in the polymer fragments; interaction energies* per *trapped H_2O molecule and H-Bond wire.*

For further analysis on the cohesion energy among polymer fragments, wires or paths (H-bond wire), formed by water molecules linked one to the other by hydrogen bonds, were identified in the optimized macromolecular models. As shown in Fig. IV.14, an H-bond wire is defined as the shortest path, i.e. the path with the least number of hydrogen bonds, connecting two oxygen atoms of two SO_3^- groups located in two different chain fragments. The dead-end paths, shown Fig. IV.14, were not counted in the total number of wires and the O···H bonds with lengths up to 2.1 Å and a cutoff value angle of 120° were considered as hydrogen-bonding interactions[4].

As for $\overline{\Delta E}^x_{H_2O}$, the ratio between the total interaction energies, $\Delta E_{chain\text{-}chain}$, and the number of H-bond wires, found in the optimized macromolecular structures, N_{Hwire}, was calculated:

$$\overline{\Delta E}^x_{wire} = \frac{\Delta E^x_{chain-chain}}{N_{wire}} \qquad \text{(IV.3)}$$

$\overline{\Delta E}^x_{wire}$ is then the electrostatic interaction energy *per* H-bond wire. This time, the total interaction energy between two fragments was distributed among the water molecular wires (paths) connecting them. Thus, the contributions, taken into account by $\overline{\Delta E}^x_{H_2O}$, are the same as those considered by $\overline{\Delta E}^x_{wire}$. However, the quantities reveal two different behaviors since $\overline{\Delta E}^x_{H_2O}$ underlines the crucial role of the water in the supramolecular structure in a wet CMX membrane, while $\overline{\Delta E}^x_{wire}$ emphasizes the function of the H-bonds paths as “cohesion bridge” between two polymer chains into the membrane structure.

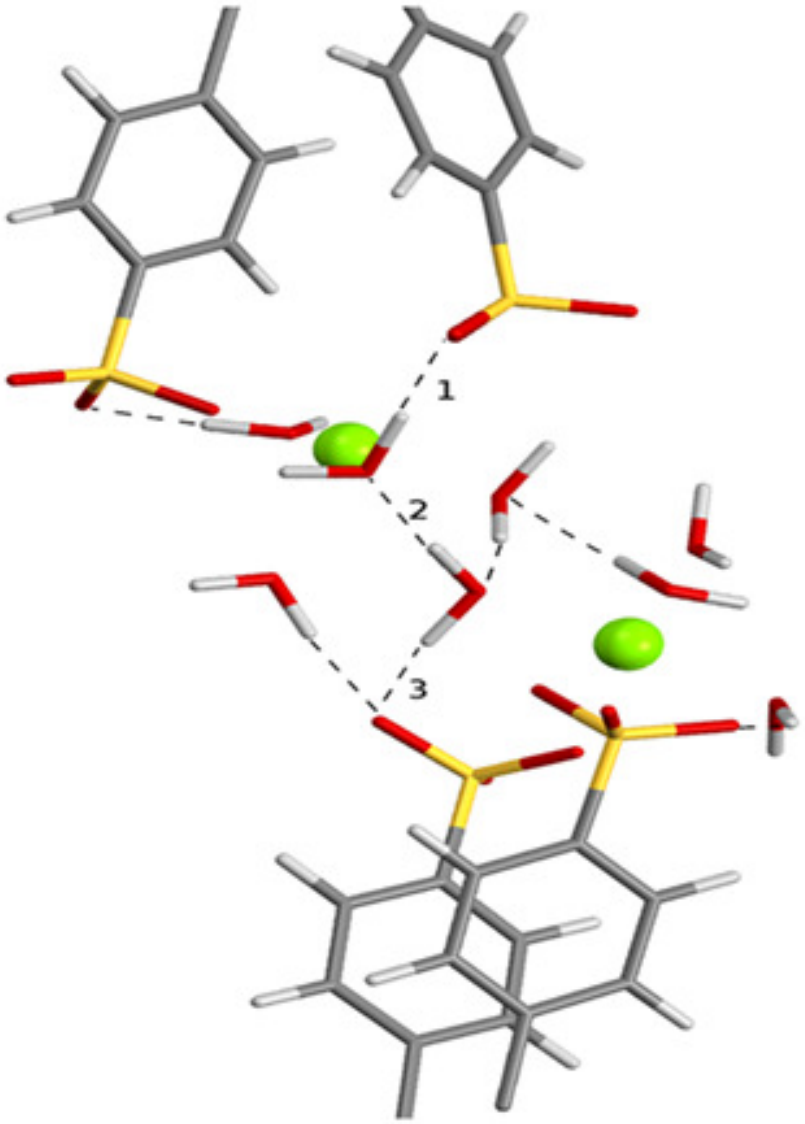

Figure IV.14: H-bond path indicated by 1, 2 and 3 numbers and connecting one oxygen of the $-SO_3^-$ group with one oxygen of sulfonic group located on other chain fragment. Dead end paths were not counted in the total number of wires.

A correlation between the experimental sugar fluxes and the values of $\overline{\Delta E}^{x}_{H_2O}$ as well as $\overline{\Delta E}^{X}_{wire}$, reported in the last two columns of Table IV.6, can be drawn. Indeed, increasing values of these energies are correlated to lower values of the sugar flux through the CMX membrane equilibrated by Na^+, Ca^{2+} and Mg^{2+}. This can be expressed by the following relationships:

$$J_a \propto \frac{1}{\overline{\Delta E}^{X}_{H_2O}} \qquad \text{(IV.4)}$$

and

$$J_a \propto \frac{1}{\overline{\Delta E}^{X}_{wire}} \qquad \text{(IV.5)}$$

This result is physically consistent since the increase of the cohesion between two polymer chains of the membrane, carried out *via* the embedded water molecules, requires a higher energy

for the sugar to diffuse through the membrane. To check further this assumption, the ratios between the experimental sugar fluxes and the corresponding computed values of $\overline{\Delta E}^{x}_{H_2O}$ and $\overline{\Delta E}^{x}_{wire}$ were evaluated. Using equation (IV.2) and (IV.4) or (IV.3) and (IV.5), respectively, the following two relationships can be derived, considering the system equilibrated with Na^+ as reference:

$$\frac{J_{Na}}{J_a} = \frac{\overline{\Delta E}^{x}_{H_2O}}{\overline{\Delta E}^{Na}_{H_2O}} \qquad \text{(IV.6)}$$

and

$$\frac{J_{Na}}{J_a} = \frac{\overline{\Delta E}^{x}_{wire}}{\overline{\Delta E}^{Na}_{wire}} \qquad \text{(IV.7)}$$

In Table IV.7, the values of the normalized experimental fluxes [9], obtained for xylose, glucose and sucrose, were compared with the corresponding theoretical ratios defined in equation (IV.6) and (IV.7). One can observe that, for a given sugar, the theoretical ratios are in the same range as the mean values of the normalized flux, obtained with the two investigated cations.

Counter-ion	$\frac{J_{Na}}{J_b}$ **(xylose)**	$\frac{J_{Na}}{J_b}$ ***(glucose)***	$\frac{J_{Na}}{J_b}$ ***(sucrose)***	$\frac{\overline{\Delta E}^{x}_{H_2O}}{\overline{\Delta E}^{Na}_{H_2O}}$	$\frac{\overline{\Delta E}^{x}_{wire}}{\overline{\Delta E}^{Na}_{wire}}$
Ca^{2+}	*1.33*	*1.45*	*1.66*	*1.49*	*1.94*
Mg^{2+}	*2.22*	*2.28*	*2.50*	*2.61*	*2.70*

Table IV.7: Ratios between xylose, glucose and sucrose normalized experimental fluxes and theoretical ratios between the corresponding $\overline{\Delta E}^{x}_{H_2O}$ and $\overline{\Delta E}^{x}_{wire}$ energies.

It means that the polymer fragments cohesion energy *per* embedded water molecules or *per* H-Bond wire is the driving force determining the influence of the counter-ion on the sugar flux. Thus, it can be assumed that the fluxes of organic molecules are driven by the noncovalent interactions carried out via single connecting molecular path or water molecules trapped in the polymer filaments constituting the membrane. The intermolecular interaction, governing the transport of the sugar, comes from water clusters that by means of hydrogen-bonding interactions form connecting paths between the polymer fragments. In light of this finding and comparing the values of $\Delta E^{x}_{chain-chain}$ (Table IV.6) with the trend of the experimental sugar fluxes, one can clearly emphasize the role of water-cation interactions on the transfer of sugars. These interactions determine the number of water molecules entrapped in the polymer as well

as the arrangement of those water molecules between the polymer chains. Although of lesser impact, other mechanisms could also be involved, as indicated by the slight dependence of the normalized flux with respect to the kind of sugar. In particular the differences between the normalized fluxes can derive from structural diversity of the sugars (e. g. size, number of OH groups) that can also affect the transfer through the membrane, but probably independently of the counter-ion.

IV.3 Conclusions

In a previous work, the fluxes of sugars in aqueous solutions were measured through a CMX cation exchange membrane, composed by sulfonated polystyrene-divinylbenzene. It was shown that the flux is fixed according to the membrane counter-ion [1]. Higher fluxes were observed when the membrane is equilibrated with a less hydrated counter-ion. The purpose of this Chapter was to carry a computational investigation, at the molecular level, to determine the main interactions and related mechanisms responsible for the change of the sugar transfer according to the membrane counter-ion.

Noncovalent interactions between hydrated glucose and sulfonated styrene monomers as well as interactions between the membrane polymer fragments were investigated by using accurate QM and QM/MM approaches. Each building block, merged in macromolecular models, was studied by means of a high theory level. In turn, the macromolecular models were used to investigate the glucose solubility inside the polymer as well as the chain-chain interactions as function of the Na^+, Ca^{2+} or Mg^{2+} counter-ions.

Analyzing the hydration of the investigated counter-ions in the building blocks, it was shown that the number of water molecules in the first hydration shell decreases ($Na^+ > Ca^{2+} > Mg^{2+}$) as the experimental fluxes of the sugars. The interaction energies between the functional monomers and the hydrated glucose, related to the sugar solubility in the polymer matrix, were found to be almost independent from the cation. Meanwhile, the negative energy values showed that the sugar can be considered as dissolved in the matrix, even if its solubility is not affected by the nature of the cations. It was thus concluded that the interaction between the glucose and the monomers is not the main mechanisms involved in the sugar transfer through the membrane.

The interactions between the polymer fragments were also investigated using macromolecular models. Unlike sugar- polymer fragment interactions, it was found that chain-chain interactions are very sensitive to the membrane counter ion.

First, the average distances between the counter-ions and the oxygen of the sulfonic group

belonging to the same fragment as well as the distances between two optimized polymer fragments were found to vary according to the cation. Then, due to the decrease of the fragment-fragment distance, a lower sugar flux can be expected, as was observed during the previous experimental investigation. But from a comparison of these distances with the computed effective diameter of the hydrated glucose another mechanism was suggested to explain the experimental results.

Comparing the normalized experimental fluxes with the theoretical ratios, defined by the corresponding $\overline{\Delta E}^{x}_{H_2O}$ and $\overline{\Delta E}^{x}_{wire}$ interaction energies, a correlation was pointed out. Indeed, lower interaction energy between polymer fragments systematically corresponds to a higher solute flux. Thus, it seems that, in the conditions investigated, the fluxes of organic molecules are driven by the noncovalent interactions in which single connecting water paths or water molecules trapped in the polymer filaments are involved. This work has shown that these noncovalent interactions depend on the nature of the counter-ion. Moreover, it has highlighted the crucial role of the water molecules coordinating the counter-ions in the polymer network. If the aforementioned average distance between one oxygen atom of one fragment and the nearest oxygen of the other is linked to the necessity of a polymer chains enlargement, $\overline{\Delta E}^{x}_{H_2O}$ and $\overline{\Delta E}^{x}_{wire}$ can be correlated to the required energy to make this happen. More precisely, it is the energy of temporary break of the connections between the polymer chains, which depends on the membrane counter ion, allowing the solute diffusion through the membrane.

In dense membranes like that investigated here the transfer occurs in free volume elements, i.e. those accessible to the solute It was also suggested that in certain conditions the free volume can vary with the polymer breath, corresponding to the widening and narrowing of the polymeric chains, i.e. the breaking and formation of noncovalent bonds among the trapped water molecules in the polymer network. Then, the solute opens a path in the polymer matrix following the break of the connections between the polymers chains, these connections being formed again after its passage. From the theoretical finding reported in this Chapter, one can affirm that, in the conditions investigated, such a polymer breath, affected by the membrane counter-ions, is the main mechanism fixing the solute transfer as observed at the macroscopic level.

IV.4 References

[1] S. Galier, J. Savignac, and H. Roux-de Balmann, "Influence of the ionic composition on the diffusion mass transfer of saccharides through a cation-exchange membrane," *Sep. Purif. Technol.*, vol. 109, no. 0, pp. 1–8, 2013.

[2] G. De Luca, F. Bisignano, A. Figoli, F. Galiano, E. Furia, R. Mancuso, O. Saoncella, M. Carraro, M. Bonchio, B. Gabriele, "Bromide ion exchange with a Keggin polyoxometalate on functionalized polymeric membranes: a theoretical and experimental study", *J. Phys. Chem. B*, vol.118 pp. 2396–404. 2014

[3] G. De Luca, L. Donato, S. García Del Blanco, F. Tasselli, and E. Drioli, "On the cause of controlling affinity to small molecules of imprinted polymeric membranes prepared by noncovalent approach: a computational and experimental investigation.," *J. Phys. Chem. B*, vol. 115, no. 30, pp. 9345–51, 2011.

[4] G. De Luca, A. Gugliuzza, and E. Drioli, "Competitive Hydrogen-Bonding Interactions in Modified Polymer Membranes: A Density Functional Theory Investigation," *J. Phys. Chem. B*, vol. 113, pp. 5473–5477, 2009

[5] G. De Luca, F. Bisignano, F. Paone, and S. Curcio, "Multi-scale modeling of protein fouling in ultrafiltration process," *J. Memb. Sci.*, vol. 452, pp. 400–414, 2014

[6] M. Valiev, E. J. Bylaska, N. Govind, K. Kowalski, T. P. Straatsma, H. J. J. Van Dam, D. Wang, J. Nieplocha, E. Apra, T. L. Windus, and W. A. De Jong, "NWChem: A comprehensive and scalable open-source solution for large scale molecular simulations," *Comput. Phys. Commun.*, vol. 181, no. 9, pp. 1477–1489, 2010.

[7] T. P. Straatsma, E. Apra, T. L. Windus, M. E. Dupuis, J. Bylaska, W. de Jong, S. Hirata, D. M. Smith, A. M. Hackler, T. L. Pollack, R. J. Harrison, J. Nieplocha, V. Tipparaju, M. Krishnan, E. Brown, G. Cisneros, G. I. Fann, H. Fruchtl, J. Garza, K. Hirao, R. Kendall, J. A. Nichols, K. Tsemekhman, M. Valiev, K. Wolinski, J. Anchell, D. Bernholdt, P. Borowski, T. Clark, D. Clerc, H. Dachsel, M. Deegan, K. Dyall, D. Elwood, E. Glendening, M. Gutowski, A. Hess, J. Jaffe, B. Johnson, J. Ju, R. Kobayashi, R. Kutteh, Z. Lin, R. Littlefield, X. Long, B. Meng, T. Nakajima, S. Niu, M. Rosing, G. Sandrone, M. Stave, H. Taylor, G. Thomas, J. van Lenthe, A. Wong, Z. Zhang, "NWChem, A Computational Chemistry Package for Parallel Computers, version 6.1.1"; *Pacific Northwest National Laboratory: Richland, WA,* 2005.

[8] M. D. Hanwell, D. E. Curtis, D. C. Lonie, T. Vandermeersch, E. Zurek, G. R. Hutchison, "Avogadro: an advanced semantic chemical editor, visualization, and analysis platform," *J. Cheminform*, vol.4 pp. 17, 2012.

[9] A. K. Rappé, C.J. Casewit, K. S. Colwell, W. A. Goddard III, W. M. Skiff, "UFF, a Full Periodic Table Force Field for Molecular Mechanics and Molecular Dynamics Simulations," *J. Am. Chem. Soc.,* vol. 114 pp. 10024–10035, 1982.

[10] J. P. Perdew, W. Yue "Accurate and simple density functional for the electronic exchange energy: Generalized gradient approximation*," Phys. Rev. B,* vol. 33 pp. 12–14, 1982.

[11] X. Xu, Q. Zhang, R. P. Muller, W. A. Goddard III, "An extended hybrid density functional (X3LYP) with improved descriptions of nonbond interactions and thermodynamic properties of molecular systems", *J. Chem. Phys,* vol. 122 pp. 014105, 2005.

[12] J. V. Burda, M. Pavelka, M. Šimánek, "Theoretical model of copper Cu(I)/Cu(II) hydration. DFT and ab initio quantum chemical study," *J. Mol. Struct. Theochem.*, vol. 683 pp. 183–193, 2004.

[13] M. Pavlov, P. E. M. Siegbahn, and M. Sandstrom, "Hydration of Beryllium, Magnesium, Calcium, and Zinc Ions Using Density Functional Theory," *J. Phys. Chem. A*, vol. 102, pp. 219–228, 1998.

[14] S. Simon, M. Duran, J. J. Dannenberg, "How does basis set superposition error change the potential surfaces for hydrogen-bonded dimers?," *J. Chem. Phys.*, vol. 105 pp. 11024, 1996.

[15] A. Bondi, "van der Waals Volumes and Radii," *J. Phys. Chem.*, vol. 68, pp. 441, 1964.

[16] C. Molteni, M. Parrinello, "Glucose in Aqueous Solution by First Principles Molecular Dynamics," *J. Am. Chem. Soc.,* vol. 120, pp. 2168–2171, 1998.

[17] S. J. Grabowski, W. A. Sokalski, E. Dyguda, J. Leszczyn, "Quantitative Classification of Covalent and Noncovalent H-Bonds," *J. Phys. Chem. B* vol. 110 pp. 6444–6446, 2006.

[18] A. Buekenhoudt, F. Bisignano, G. De Luca, P. Vandezande, M. Wouters, K. Verhulst, "Unravelling the solvent flux behaviour of ceramic nanofiltration and ultrafiltration membranes," *J. Membr. Sci.* Vol. 439, pp. 36–47, 2013.

[19] F. Bisignano, "Modeling of nanostructured membranes for wastewater purification," Dottorato in Scienza e Tecnica Bernardino Telesio Curriculum M3, XXVI ciclo, Università della Calabria, Italy, 2014.

[20] W. D. Cornell, P. Cieplak, C. I. Bayly, I. R. Gould, K. M. Merz, D. M. Ferguson, D. C. Spellmeyer, T. Fox, J. W. Caldwell, P. A. Kollman, "A Second Generation Force Field for the Simulation of Proteins, Nucleic Acids, and Organic Molecules," *J. Am. Chem. Soc.*, vol. 117, pp. 5179–5197, 1995.

[21] C. L. Brooks III, A. D. Mackerell, L. Nilsson, R. J. Petrella, B. Roux, Y. Won, G. Archontis, C. Bartels, S. Boresch, A. Caflisch, L. Caves, Q. Cui, A. R. Dinner, M. Feig, S. Fischer, J. Gao, M. Hodoscek, W. Im, K. Kuczera, T. Lazaridis, V. Ovchinnikov, E. Paci, R. W. Pastor, C. B. Post, J. Z. Pu, M. Schaefer, B. Tidor, R. M. Venable, H. L. Woodcock, X. Wu, W. Yang, D. M. York, M. Karplus, N. Heart, A. Arbor, "CHARMM: The biomolecular simulation program.", *J. Comput. Chem.,* vol. 30 pp. 1545, 2009.

[22] D. Beglov, B. Roux, "Finite representation of an infinite bulk system: Solvent boundary potential for computer simulations," *J. Chem. Phys,* vol. 100, pp. 9050, 1994.

[23] L. V. Karpenko-Jereb, A.-M. Kelterer, N. P. Berezina, A. V. Pimenov, "Conductometric and computational study of cationic polymer membranes in H+ and Na+-forms at various hydration levels," *J. Membr. Sci.*, vol. 444, pp. 127–138, 2013.

Chapter V

Characterizations of CMX membranes soaked in various electrolyte solutions

The aim of this Chapter is to investigate the influence of ions in solution on the physical characteristics of CMX membrane-water systems using experimental and computational tools. Furthermore, the correlation of these data with the previous computed ones as well as with the already investigated transport properties of CMX membrane can confirm the computational results and validate the proposed molecular mechanisms.

On one hand, the infrared spectra of CMX membranes soaked in several electrolytes are analyzed in the framework of Quantum Mechanics and by experimental measurements to verify the consistency between computational and experimental results. Indeed, molecular vibrations are very sensitive to changes in the environmental conditions and shift of characteristic peaks according to the cation was demonstrated by Falk [1] with Nafion membranes.

The other two experimental methods used in this Chapter are contact angle and differential scanning calorimetry (DSC). Contact angle was chosen for its simplicity of use and because changes in the contact angle are related to modifications in the surface properties. Thus it is a way to characterize the solution - membrane interface in the working environment. Additionally, DSC was employed since it allows the investigation of the state of the water embedded in the membrane, which is known to be influenced by the cation [2] [3].

V.1 Computational and experimental Infra-Red Spectroscopy

V.1.1 Computational details on *ab-initio* calculations of infrared frequencies

The IR spectra were computed in the frame Density Functional Theory (DFT) by using the hybrid functional X3LYP [4]. The structural models used to describe the noncovalent interactions between cation functional groups and water molecule were optimized to a minimum of energy after which the vibrational analysis was performed. During the computation of IR spectra by QM, the minimization of the energy with high level of theory is a crucial step. In fact, only the structure with a minimized energy is stable, thus physically representative of the real sample. But, imaginary frequencies can be found if the vibrational analysis is performed on non-optimized structures, revealing the unreliability of the modeling. All calculations refer to a structure composed by one cation, one or two functionalized monomers and one water molecule. Two initial configurations are taken into account for Mg^{2+} and Ca^{2+} calculations due to the different possible water arrangement in the structures with divalent cations, e. g. one in a central position with respect to the two SO_3^- groups and the other more external. The initial

geometries were selected from the structures computed in Chapter 4 for the evaluation of the polymer-cation systems hydration.

Considering that the vibrational shifts are affected by the local chemical environment around the reference chemical bonds, the molecular models used in this Chapter to evaluate the Infrared frequencies, are adequate for this purpose. For a quantitative comparison among the computed and the experimental spectra, a multi-factor scaling procedure would be necessary to adapt the theoretical data to the experimental ones [5]. However, the scaling procedure needs the use of empirical coefficients, individually set for each cation and calculation, which could affect the reliability of the data. For these reasons and since the objective is to check if there is a shift of some characteristic peaks according to the electrolyte, the results are compared on a qualitative basis only.

Triple-ζ basis sets were used during the geometry optimization and the vibrational analysis. "6-311G*" basis sets were applied on C, H, S and O atoms while the "6-311+G*" set was employed on the cations. The accuracy of basis sets and functional on these systems was tested in the previous Chapter. In order to have very reliable structures for a subsequent vibrational analysis, the convergence criteria based on Cartesian displacement and gradient thresholds were set as tight [6], the energy convergence threshold was imposed to 10^{-8} a.u. for the self-consistent field procedure and the root-mean-square of the electron density to 10^{-6} a.u.. All the calculations were performed by NWChem 6.1 [7], an open source *ab initio* computational chemistry software package with extensive capabilities for large scale simulations of chemical systems. Finally, the vibrational analysis was carried out using the Avogadro code [8].

V.1.2 Geometrical features of the optimized cation-monomers models.

Fundamental geometrical features, obtained from the optimized geometries of cation-monomers models, are reported in Figures V.1 to V.5 and then discussed since they are important for the further assignment of the absorption bands.

First, Fig. V.2 and V.4 show that different structures were obtained after the quantum optimizations of the aforementioned models in which the water molecule is interacting with both functional groups. In particular, in the structure with Mg^{2+} reported in Fig. V.4, one can observe that the water molecule shifts in a more external position, losing the interaction with one functional group and converging in geometry similar to the other optimized structure with Mg^{2+} shown in Fig V.5. On the other hand, the water molecule coordinating the Ca^{2+} (Fig. V.2)

maintains the interactions with both the functional groups, whereas the other optimized structure with the Ca^{2+} (external position) converges to a different and more open geometry as shown in Fig. V.3. Moreover, the last structure is more stable with respect to the equilibrium geometry of the water molecule in double interaction with the counter-ion since the difference between their formation energies is 9.8 Kcal/mol. However, by considering this energy gap, both structures are possible in a real system. Thus, the properties of both will be discussed. It is worth noting that in the case of Na^+ it was not possible to have a structure with a water molecule interacting with two functional groups without having a negatively charged polymer fragment or introducing another Na^+ in the system. Since the scope of this calculation was to investigate the influence of one cation on one water molecule, only structures with one functional group were taken into account for Na^+.

Computed significant bond lengths of the structures with Na^+, Ca^{2+} and Mg^{2+} respectively are reported in Tables V.1, V.2 and V.3. In these Tables, the key point is the cation-functional group distance evaluated as the distance between the centers of the target cation and of the nearest oxygen of the functional group. These distances are 2.3 Å for Na^+, 2.1 Å for Ca^{2+} and 1.9 Å for Mg^{2+}. It is important to emphasize that the smaller distance is an indication of a stronger interaction between the functional group and the counter-ions. This interaction, which is an attraction force between the functional group and the cations, modifies the electron density of the near environment, thus changing the noncovalent interactions investigated in the previous Chapter.

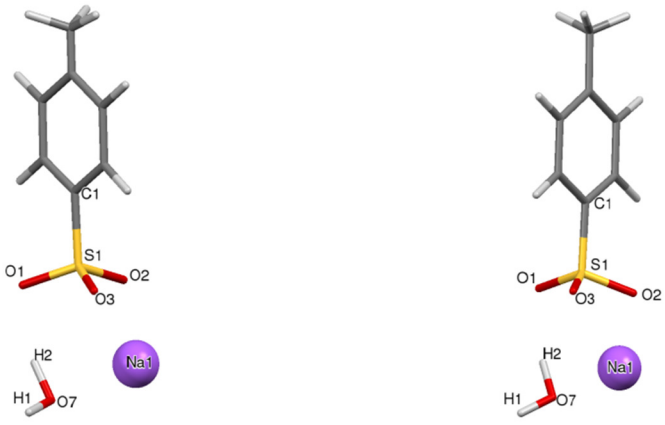

Figure V.1: Initial (left) and quantum optimized (right) geometries of functionalized styrene equilibrated by Na^+ in presence of a water molecule.

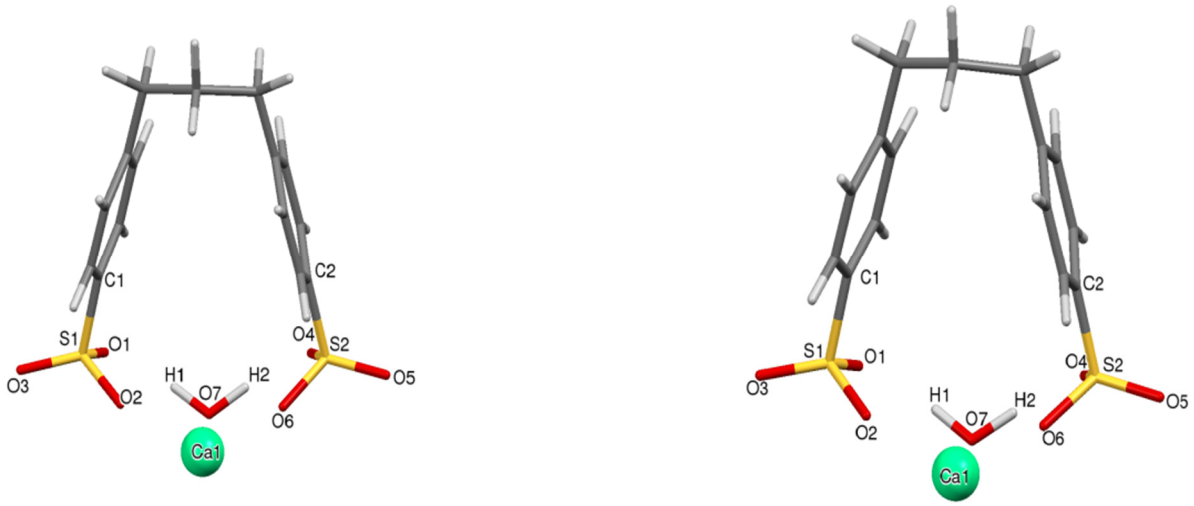

Figure V.2: Initial (left) and optimized (right) geometries of functionalized styrene monomer equilibrated by Ca^{2+} with water molecule in central position in the initial and optimized geometry.

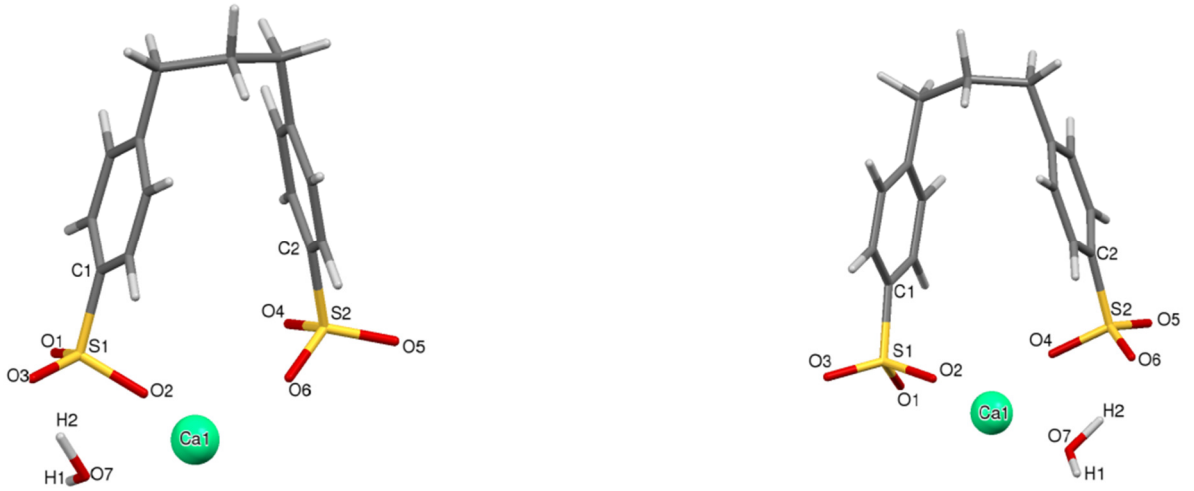

Figure V.3: Initial (left) and optimized (right) geometries of functionalized styrene monomer equilibrated by Ca^{2+} with water molecule in external position in the initial and optimized geometry.

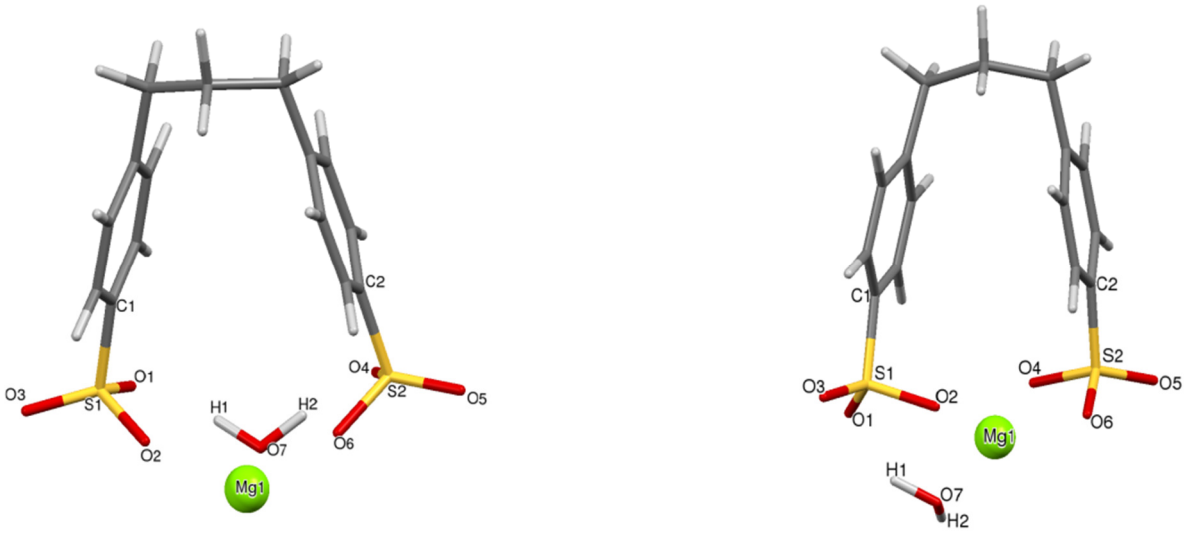

Figure V.4: Initial (left) and optimized (right) geometries of two functionalized styrene monomers equilibrated by Mg^{2+} with a water molecule in central position in the initial geometry.

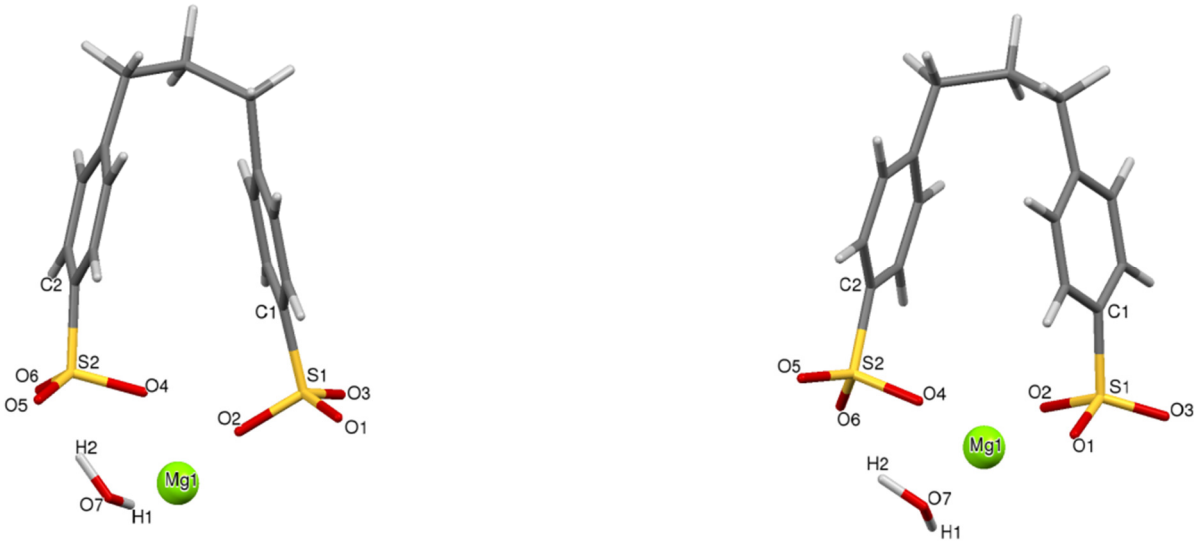

Figure V.5: Initial (left) and optimized (right) geometries of two functionalized styrene monomers equilibrated by Mg^{2+} with a water molecule in external position in the initial and optimized geometries.

Bond	Bond length (Å) Fig. V.1
C1-S1	1.789
S1-O1	1.487
S1-O2	1.499
S1-O3	1.498
Na1-O1	3.361
Na1-O2	2.309
Na1-O3	2.357
Na1-O7	2.264
H2-O1	1.889
H2-O2	2.944
H2-O3	2.999
Water molecule	
O7-H1	0.961
O7-H2	0.982
H1-O7-H2 (Angle)	106.12 (°)

Table V.1: Summary of the Bond Lengths in the Energy-Optimized Structures containing Na^+

Bond	Bond length (Å) Fig. V.2	Bond length (Å) Fig. V.3
C1-S1	1.794	1.791
C2-S2	1.795	1.793
S1-O1	1.484	1.519
S1-O2	1.542	1.524
S1-O3	1.454	1.451
S2-O4	1.485	1.531
S2-O5	1.455	1.455
S2-O6	1.542	1.492
Ca1-O1	3.510	2.324
Ca1-O2	2.153	2.285
Ca1-O3	4.495	4.128
Ca1-O4	3.509	2.181
Ca1-O5	4.495	4.548
Ca1-O6	2.155	3.580
Ca1-O7	2.248	2.308
H1-O1	1.829	5.266
H1-O2	3.001	4.030
H1-O3	4.116	6.297
H2-O4	1.827	2.731
H2-O5	4.104	3.719
H2-O6	3.003	1.683
Water molecule		
O7-H1	0.981	0.960
O7-H2	0.981	0.996
H1-O7-H2 (Angle)	111.14 (°)	109.19 (°)

Table V.2: Summary of the Bond Lengths in the Energy-Optimized Structures containing Ca^{2+}

Bond	Bond length (Å) Fig. V.4	Bond length (Å) Fig. V.5
C1-S1	1.792	1.787
C2-S2	1.788	1.793
S1-O1	1.493	1.529
S1-O2	1.540	1.532
S1-O3	1.452	1.448
S2-O4	1.531	1.539
S2-O5	1.448	1.452
S2-O6	1.530	1.493
Mg1-O1	3.117	2.042
Mg1-O2	1.927	2.033
Mg1-O3	4.256	3.850
Mg1-O4	2.038	1.927
Mg1-O5	3.836	4.252
Mg1-O6	2.041	3.157
Mg1-O7	2.005	2.002
H1-O1	1.722	5.340
H1-O2	2.735	3.338
H1-O3	3.696	4.388
H2-O4	3.296	2.729
H2-O5	5.213	3.674
H2-O6	4.342	1.713
Water molecule		
O7-H1	0.995	0.961
O7-H2	0.961	0.996
H1-O7-H2 (Angle)	109.73 (°)	109.94 (°)

Table V.3: Summary of the Bond Lengths in the Energy-Optimized Structures containing Mg^{2+}

The analysis of the computed bond lengths shows interesting effect of the cations-SO_3^- distances on the structural properties of the functional group. In every structure, the S-O bond closer to the cation is longer that the other bonds. In addition, the lengths of the other S-O bonds present in the same structure decreases when the distance between the inquired S-O bond and the cation increases. The length of these bonds depends on the nature of the specific cation, since the S-O distances are longer for Mg^{2+} (1.540 Å) with respect to Ca^{2+} (1.531 Å) and Na^+ (1.499 Å). The same behavior is also observed for the C-S distances. However, in this case, the difference is significant only between monovalent (1.789 Å) and divalent cations (1.791-1.794 Å), i.e. no significant differences are found in the structures with Ca^{2+} and Mg^{2+}. However, the modification of the S-O and C-S bonds according to the cation comes from the attraction between the partial negative charge distributed on the functional groups and the positive ions that reduce the nearest oxygen - cation distance. On the other hand, the S-O and C-S distances are stretched to allow the oxygen - cation approach. Moreover, the negligible variation between the C-S distances in the structures with Ca^{2+} and Mg^{2+}, as well as the non-dependence of the other bond lengths with respect to the cation, is a sign of the local effect of the cation on the polymeric structure. In fact, the effect on the farer bonds is shielded by the presence of the atoms forming the previous one, e. g. the cation influence on the C-S bond is screened by the closer oxygen atoms to the cation.

The optimized structures of the models show changes also in the water molecule geometries. For comparison, the structure of one water molecule was optimized in *vacuum* by the same level of quantum theory used in this Chapter. Even if several computational studies are available on the water molecules, the geometry was optimized with the same criteria to avoid possible issues due to the use of different basis sets or functionals. The optimized water molecule has both the bond lengths of 0.962 Å and the angle of 105.9°.

The corresponding bond lengths and angles of the water molecules influenced by cations in the investigated molecular models are reported at the bottom of Tables V.1, V.2, V.3 for Na^+, Ca^{2+} and Mg^{2+} respectively. Concerning the water, embedded in the monomer-cation systems, the differences between the calculated bond lengths (O7-H1 and O7-H2 for Na^+, Ca^{2+} and Mg^{2+}) reveal a loss of symmetry in 4 cases over 5, due to the stretching of the O-H bonds, caused by the hydrogen bonding of the O-H with the oxygen of the functional group. The change in the O-H length (e.g. 0.961 Å and 0.996 Å in the system with Mg^{2+}) discloses that the attractive interaction between the hydrogen of water and functional group is strong. Bearing in mind the structure of Fig. V.2, in which no loss in symmetry is detected, the water molecule interacts

with both SO_3^- (see distances H1-O1 and H2-O4 in Table V.2), thus there is a stretching of both the O-H bonds due to the symmetrical geometry of the total complex. In fact, both the O-H bonds have an identical length of 0.981 Å, which it is longer than the water in vacuum.

The H-O-H angle is also influenced by the different cations, in the optimized geometries. The stronger variation, with respect to the value of 105.9° which is the bond angle in *vacuum*, is observed in the structure with the water in a central position and the Ca^{2+} (Fig. V.2). In this case, the angle increases of about 5°, while variations of 3° and 4° are found for the other structures containing Ca^{2+} and Mg^{2+}, respectively. Otherwise a very small influence is observed on H-O-H angle by the Na^+.

Finally, it should be remembered that only one water molecule is considered in the models for each cation, while in the experimental samples, even if they are dried, the number of water molecules per functional group could be more. This could lead to some deviation with respect to the real values since the effect of the other hydrogen bonds (i.e. H-bonds involving the O and H non-interacting with the functional group) in which the investigated water molecule is involved are not considered. More precisely, an overestimation of the cations influence on the structural changes is possible, resulting in shorter distances, about 0.1 Å (section IV.1.1), than the ones computed with a proper hydration shell in the previous Chapter. However, the use of one water molecule was driven by the need to have highly stable structures for the vibrational analysis. Moreover, since the deviations are comparable and present in all the structures, they do not imply differences in the comparison among the computed values.

V.1.3 Vibrational properties: Quantum Mechanics and experiments

Infrared Spectroscopy is a very effective tool to investigate changes in bonds or interactions as function of the chemical environment since it is directly connected to the atoms involved in the vibrational mode and to the strength of bonds connecting them. Thus, a change in the aforementioned variables (i.e. elements and bond features) produces a shift in the absorption wavenumber. For this reason, the vibrational spectra were calculated in the frame of DFT using the molecular models described in the previous section (Fig. V.1-V.5).

The calculated infrared spectra, relative to the optimized models taken into account, are reported in Figures V.6 - V.10. The assignment of the wavenumbers are reported in Tables V.4 to V.8, while the complete list of assignments is reported in the supporting information for each model (Tables AII.1-AII.5)

In addition, assuming that the water mobility is governed by noncovalent interactions and considering the amorphous structure of the CMX membrane polymer matrix, no multi-factor scaling correction was applied to perform a quantitative IR analysis but a qualitative comparison between theoretical and experimental data was carried out. Since in his experimental studies on Nafion membrane, Falk [1] has pointed out that the effect of the cation is highly identifiable in the water and SO_3^- vibrational modes properties, we will focus on the characteristic absorption regions of those chemical groups interacting with the different cations and water (over 3000cm^{-1}).

First the O-H stretching of bound water molecules by H-bonds with the functional group was analyzed. A shift of the related bands was observed according to the nature of the counter-ion. Cations with higher interaction energy (Mg^{2+} > Ca^{2+} > Na^+) affect the structure of the water molecule and the functional groups, and this leads to a rearrangement of their electron density. Consequently, the hydrogen bonds between the water and the functional group are influenced by the cation and their nature. Based on the above discussion, in presence of a cation with higher interaction energy with water (see Chapter III), the hydrogen bond is stronger and the peak is shifted to lower wavenumbers.

The Quantum Mechanics calculations give a shift of the characteristic wavenumber of the stretching of O-H, forming hydrogen bonding with the oxygen of the aforementioned SO_3^-, at 3461 cm^{-1} for Na^+ (Table V.4) and lower values of 3234 cm^{-1} and 3217cm^{-1} in the case of Mg^{2+} (Table V.7 and V.8). The structures, containing Ca^{2+} as counter-ion show a different behavior depending on the position of the water molecule. More precisely, the structure with the water

in an external position (Fig. V.3) shows a stretching similar in wavenumber to the both structures containing Mg^{2+}. On the other hand, the optimized structure with the water in central position shows two vibrational modes for the O-H in interaction with the sulfonic groups: symmetrical and asymmetrical stretching (3469 cm^{-1} and 3530 cm^{-1}). The computed wavenumber of symmetrical vibrational mode is similar to the O-H stretching of the water in the structure with the Na^{+}, while the asymmetrical mode is obtained at a slightly higher wavenumber. It is worth noting that the stretching of the O-H groups that do not form hydrogen bonds with the oxygen of the sulfonic groups are very similar in the structures containing Na^{+}, Mg^{2+} and in the adduct with Ca^{2+} having the optimized water molecules in the external position (3865 cm^{-1}, 3875 cm^{-1}, 3878 cm^{-1} and 3891 cm^{-1}, respectively). On the other hand, the structure with Ca^{2+} with the water in a central position does not have this vibrational mode since both the O-H interact with the sulfonic groups. Nevertheless, considering that both structures containing Ca^{2+}, i.e. with water in central or external place, are possible, it is reasonable to suppose that a resulting peak associated to the stretching of the O-H groups forming hydrogen bonding with the sulfonic oxygen should be found in an intermediate frequency between that computed for the structure with the water in central position and 3182 cm^{-1}.

The scissoring vibrational modes, a particular kind of bending in which the movement of the molecule looks like a scissor, of water molecules show, in addition to the O-H stretching, a cation dependence. As in the previous case a shift to lower wavenumber is observed with values of 1772 cm^{-1}, 1761 cm^{-1} and 1741 cm^{-1} for similar structure, i.e. with the optimized water in the external position, containing Na^{+}, Ca^{2+} (Fig. V.3) and Mg^{2+}, respectively. Considering the adduct with the Ca^{2+} in central position, an associated wavenumber of 1716 cm^{-1} is found for the water scissoring vibrational mode. Thus, as in the case of the O-H stretching, an average wavenumber between this value and the one computed with the water in an external position should be taken. From a qualitative point of view, the decreasing in wavenumber reflects a decrease of the energy of this vibrational mode which traduces a stronger interaction of the water molecules with the cation-polymer.

The S-O vibrational modes of a SO_3^- group can be influenced by the environment *via* electrostatic interactions, according to the nature of cations present in the system. Consequently, also the CMX membrane vibrational properties should be affected by the nature of its counter-ions. In fact, the characteristic absorption peaks of this chemical group are shifted to lower wavenumbers following the interaction energy trend $Na^{+} < Ca^{2+} < Mg^{2+}$. This cation-dependent

shift shows a weakening of the S-O bond strength due to a modification in the electron density. In fact, it is possible to assume that the electrons are displaced on the oxygen due to the attractive forces of the cation coming from its positive charge. Moreover, the capability of the cation to attract the electrons depends on its interaction energy. The one having higher interaction energy can attract more the electrons producing the observed shift depending on the nature of the counter-ion. This hypothesis is also confirmed by the variation of the S-O length in function of the counter-ion as discussed above.

In addition, the QM computed S-O stretching modes can be divided in 3 different sets: the S-O close to the water (i.e. forming H-bond with the hydrogen of water) and the asymmetric and symmetric SO_3^- stretching of the entire chemical group. The absorption at 1155 cm^{-1} in the Na^+ spectrum as well as 1069 cm^{-1}, 1075cm^{-1} and 1087cm^{-1} for the two models containing Ca^{2+} and 1067cm^{-1} in both Mg^{2+} structures can be assigned to the S-O stretching in interaction with the water molecule (i.e. the first set). This specific vibrational mode that involves the oxygen in interaction with the water molecule is a symptom of the strong local interactions existing between the water and the functionalized polymer. Furthermore, as already discussed, the shift to lower energy in presence of Ca^{2+} and especially of Mg^{2+} shows a great modification of the electron density due to the attraction forces of these cations on the environment in the equilibrated membranes. The same trend is also observed from the values reported in Tables V.5 – V.8 for the asymmetrical and symmetrical stretching of the total functional groups starting from 1115 cm^{-1} down to 979 cm^{-1} for the optimized structures with Na^+ and at a lower wavenumber for Ca^{2+} and Mg^{2+}. The presence, in the computed spectra, of multiple frequencies related to the symmetrical stretching, (e. g. 996 cm^{-1} and 934 cm^{-1} in the case of Mg^{2+}), proves that the cation-functional group distance plays an important role on their interactions since farer functional groups are less influenced. Moreover, the presence of a cation-dependent shift in all the computed vibrational mode sets of the SO_3^- groups is a good evidence of the influence of the cation on the functional group and on their capability to interact with the water entrapped in the membrane.

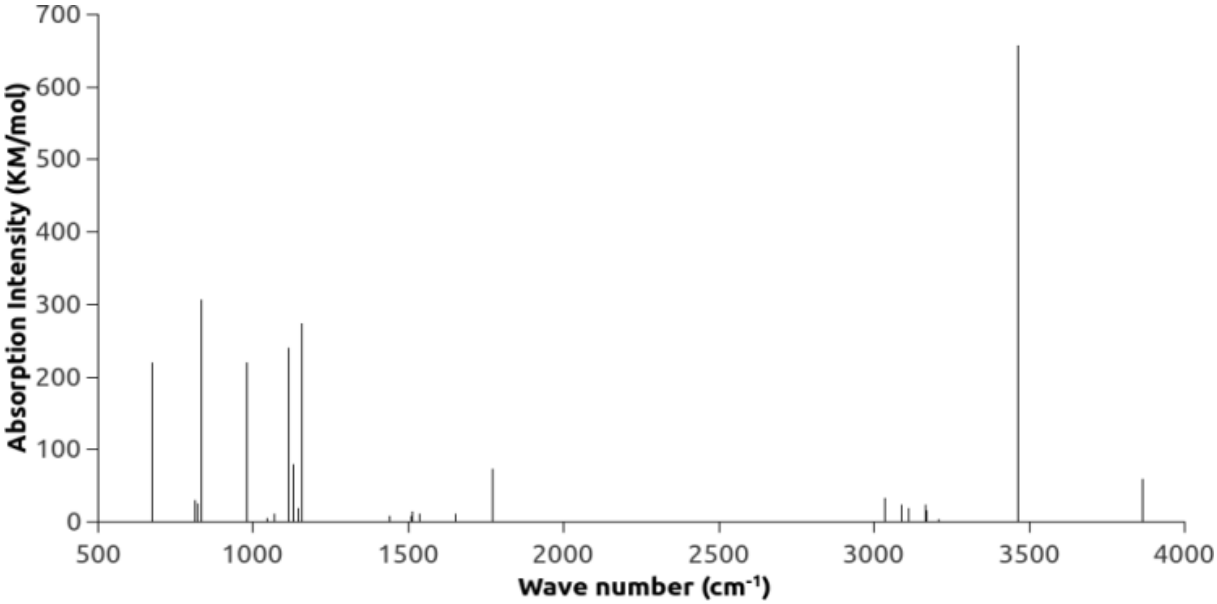

Figure V.6: QM computed IR spectra of functionalized styrene-Na^+…H_2O adduct (Fig. V.1)

Absorption wavenumber (cm^{-1})	**Intensity (KM/mol)**	**Assignment**
978	219	SO3 ST(S)
1115	239	SOST(S)(S1-O2), CHRR
1155	273	SO ST(S) (S1-O1),
1772	73	H2O SC
3462	657	OH ST (O7-H2)
3866	59	OH $_{ST}$ (O7-H1)

Table V.4: Relevant computed absorption wavenumber, intensities and assignments for the optimized structure containing Na^+(optimized geometry Fig. V.1, computed spectra Fig. V.6)

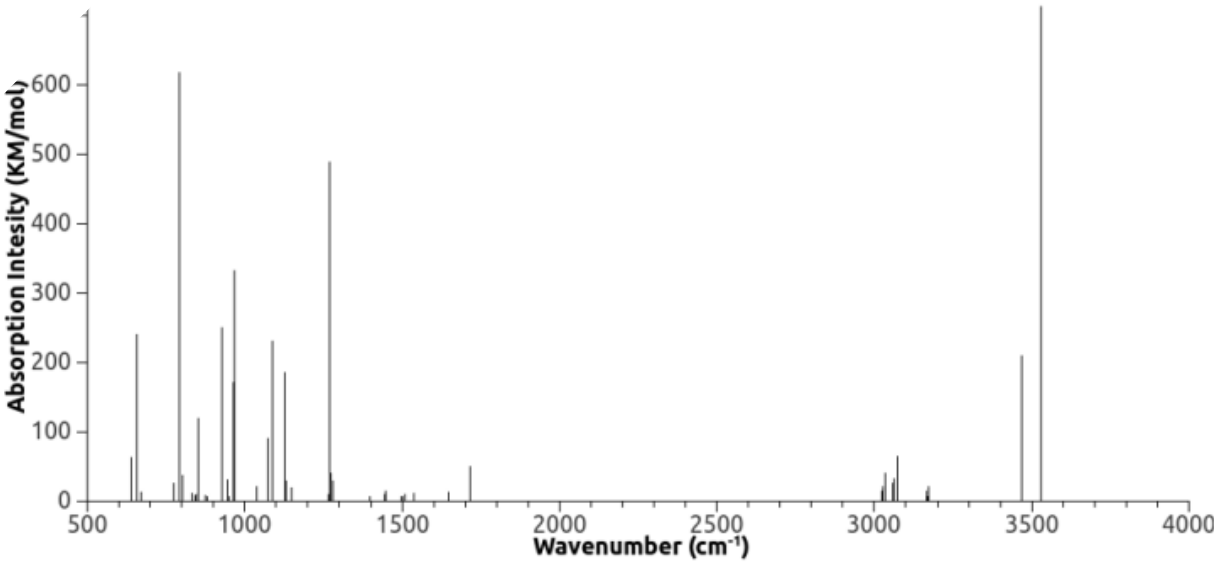

Figure V.7: QM computed IR spectra of functionalized styrene-Ca^{2+}…H_2O adduct (Fig. V.2)

Absorption wavenumber (cm^{-1})	**Intensity (KM/mol)**	**Assignment**
928	250	SO $_{ST(AS)}$ (S1-O2, S2-O6), CH $^{C}_{B}$
965	333	$SO_{3\ ST(S)}$
1075	90	SO $_{ST}$ (S1-O1, S2-O4)
1087	230	SO $_{ST}$(S1-O2, S1-O3, S2-O5, S2-O6)
1270	489	SO $_{ST}$ (S1-O3, S2-O5)
1273	40	SO $_{ST}$ +CH $^{C}_{S}$
1279	30	SO $_{ST}$ +CH$^{C}_{S}$
1716	50	H_2O $_{SC}$
3469	210	H_20 $_{ST(S)}$
3530	712	H_20 $_{ST(AS)}$

Table V.5: Relevant computed absorption wavenumber, intensities and assignments for the optimized structure containing Ca^{2+}(optimized geometry Fig. V.2, computed spectra Fig. V.7)

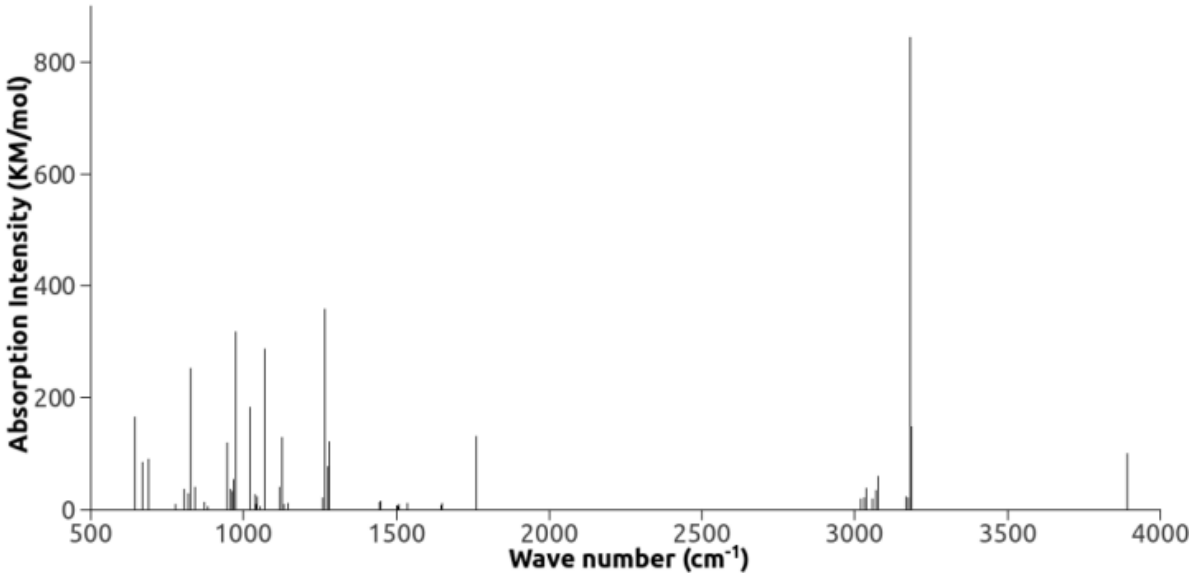

Figure V.8: QM computed IR spectra of functionalized styrene-Ca^{2+}…H_2O adduct (Fig. V.3)

Absorption wavenumber (cm^{-1})	**Intensity (KM/mol)**	**Assignment**
947	120	$SO_{3\ ST(S)}$
973	319	$SO_{3\ STsym}$ CH $^{R}_{TO}$
1022	183	SO $_{ST}$ (S1-O1)
1069	288	SO $_{ST}$ (S2-O6) CH $^{R}_{B}$
1267	358	SO $_{ST}$ (S2-O5) , CH^{C}_{SC}
1278	76	SO $_{ST}$ (S1-O3) , CH^{C}_{SC}
1281	121	SO $_{ST}$ (S1-O3) , CH^{C}_{SC}
1761	131	H_2O $_{SC}$
3183	844	OH $_{ST}$ (O7-H2)
3891	99	OH $_{ST}$ (O7-H1)

Table V.6: Relevant computed absorption wavenumber, intensities and assignments for the optimized structure containing Ca^{2+}(optimized geometry Fig. V.3, computed spectra Fig. V.8)

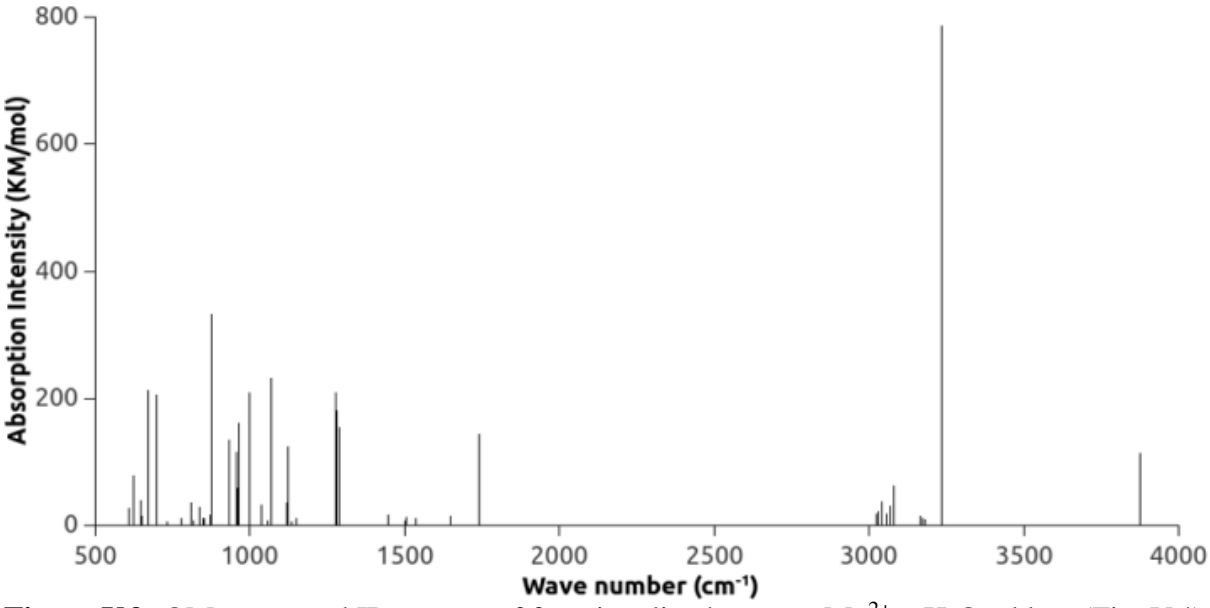

Figure V.9: QM computed IR spectra of functionalized styrene-Mg^{2+}…H_2O adduct (Fig. V.4)

Absorption wavenumber (cm^{-1})	**Intensity (KM/mol)**	**Assignment**
934	134	$SO_{3\ ST(S)}$ (far)
999	209	SO $_{ST}$ (S2-O6)
1067	230	SO $_{ST}$ (S1O3)
1276	209	SO $_{ST}$ (S1-O3) CH^{C}_{TW}
1288	153	SO $_{ST}$ (S2-O5)
1742	142	H_20 $_{SC}$
3234	786	OH $_{ST}$ (O7-H1)
3875	113	OH $_{ST}$ (O7-H2)

Table V.7: Relevant computed absorption wavenumber, intensities and assignments for the optimized structure containing. Mg^{2+}(optimized geometry Fig. V.4, computed spectra Fig. V.9)

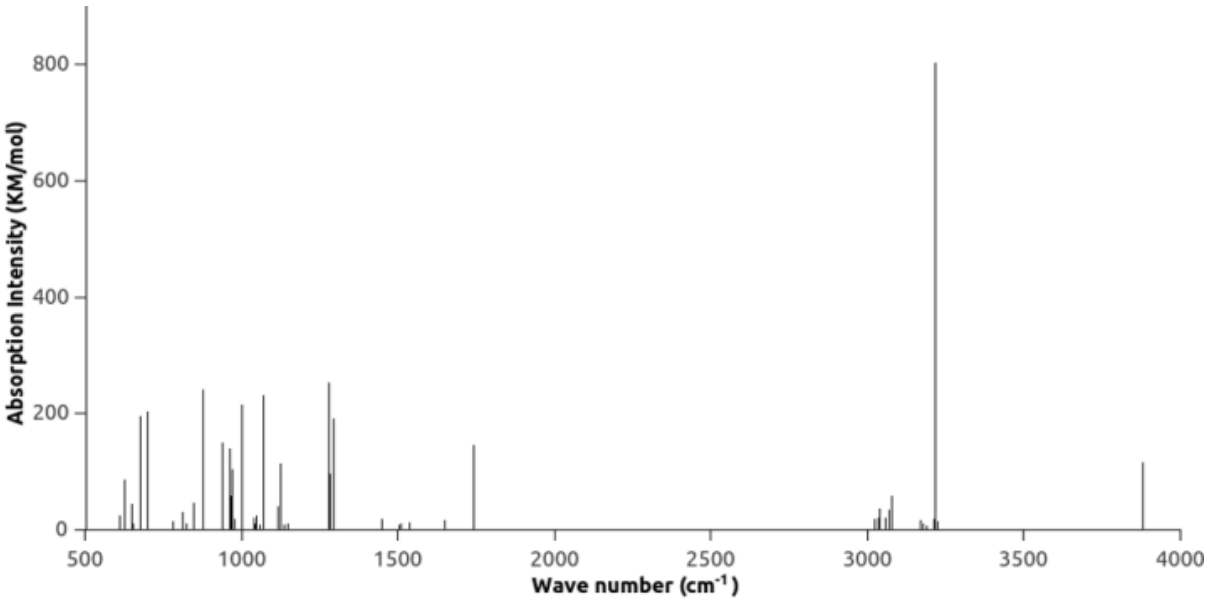

Figure V.10: QM computed IR spectra of functionalized styrene-Mg^{2+}…H_2O adduct (Fig. V.5)

Absorption wavenumber (cm^{-1})	**Intensity (KM/mol)**	**Assignment**
934	149	$SO_{3\ ST(S)}$
997	215	SO $_{ST}$ (S2-O4, S2-O6)
1068	231	SO $_{ST}$ (S1-O1)
1276	253	SO $_{ST}$ (S1-O3) CH^{C}_{TW}
1290	191	SO $_{ST}$ (S2-O5)
1741	144	H_20 $_{SC}$
3218	802	OH $_{ST}$ (O7-H2)
3878	116	OH $_{ST}$ (O7-H1)

Table V.8: Relevant computed absorption wavenumber, intensities and assignments for the optimized structure containing Mg^{2+}(optimized geometry Fig. V.5, computed spectra Fig. V.10)

For comparison, the experimental infrared spectra of the CMX membrane soaked in NH_4^+, Na^+, Ca^{2+} and Mg^{2+} are reported in the Figures V.11 – V.14 and discussed below.

In the experimental spectra, the presence of wide absorption over 3000 cm^{-1} reveals a non-negligible presence of water molecules even if the samples were dried for 48h at 50°C.

In the experimental spectrum of the membrane equilibrated with Ca^{2+} (Fig. V.13), the presence of water in several configurations does not allow the separation of the symmetrical or asymmetrical O-H stretching. Indeed, a broad peak resulting from the overlaps of the different O-H stretching is detected for the whole experimental spectrum. However, the influence of the different chemical environments produces a shift in these resulting peaks. In fact, the experimental peaks obtained with Na^+, Ca^{2+} and Mg^{2+} are found at 3446 cm^{-1}, 3414 cm^{-1} and 3387 cm^{-1} respectively. This is in agreement with the results of theoretical analysis described above showing the same trend for the shift according to the counter-ion. The shift to lower wavenumber for Ca^{2+} and Mg^{2+} show that the stretching modes of the O-H forming hydrogen bonding are energetically weaker with more hydrated (in solution) counter-ions [12]. This result is physically consistent since energetically weaker O-H bonds means that the hydrogen forms stronger hydrogen bonds with the SO_3^- Ca^{2+} or Mg^{2+} adducts than with Na^+. This finding helps to establish a relationship between the structural characteristics and the transport properties in this kind of membranes since stronger H-bonds between the water and the SO_3^- group, due to the presence of a different counter-ion, can be associated to lower sugar fluxes. Moreover, the peak of these broad bands can be assigned to the O-H stretching mode involved in O-H···O hydrogen bond, so that an elongation of the O-H bond is also found.

Unfortunately, the experimental peaks related to the scissoring modes of the water molecules cannot be discussed and a comparison among computational and experimental data of this particular vibrational mode was not feasible. This issue is due to the experimental limitations, namely the resolution of the instrument.

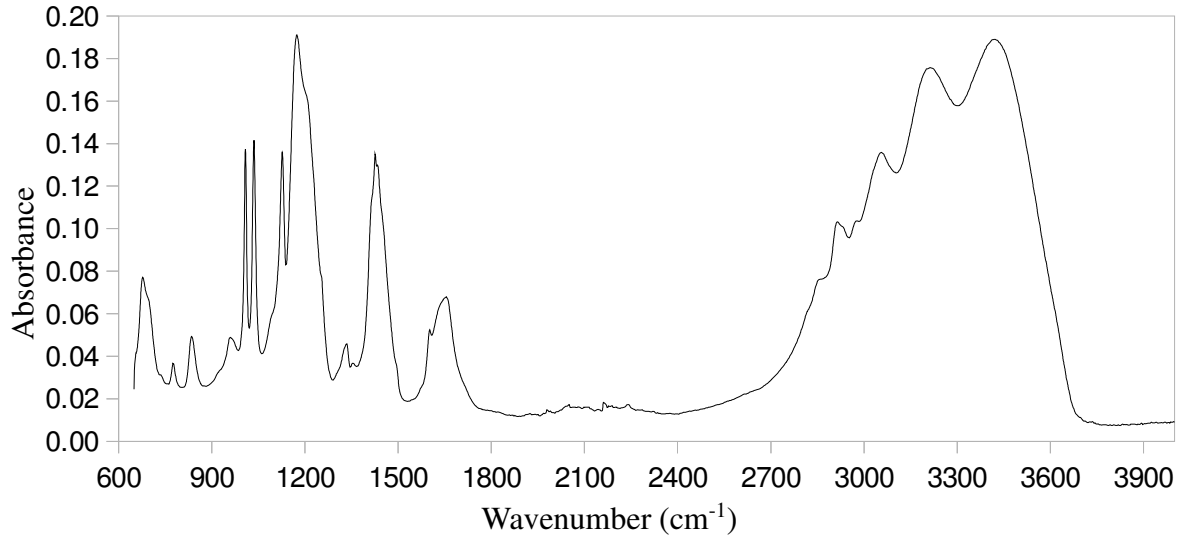

Figure V.11: IR spectra of CMX membrane equilibrated by NH_4^+ as counter-ion

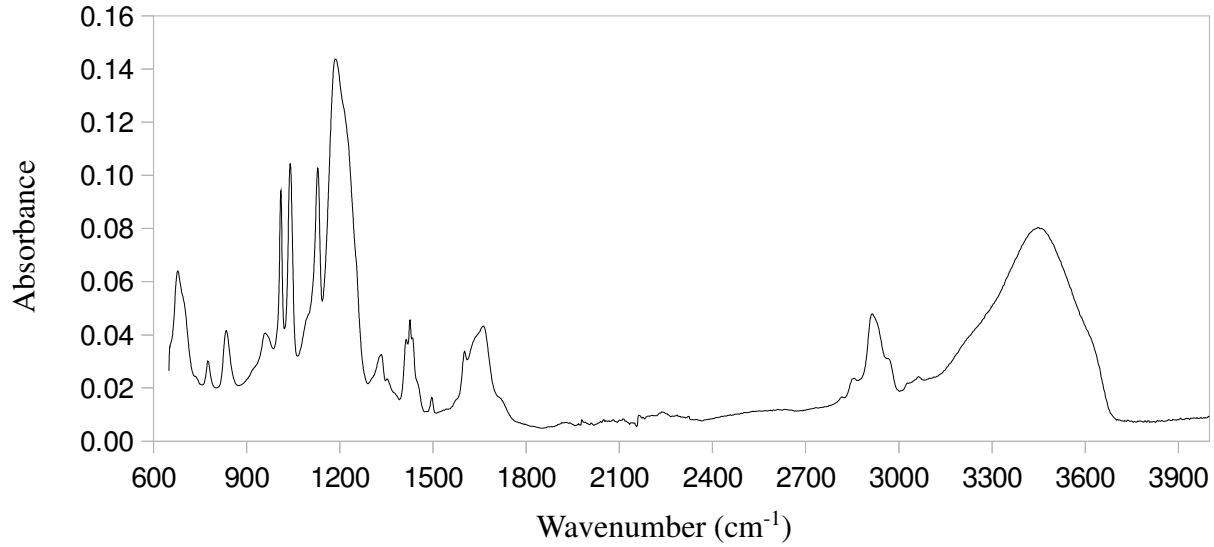

Figure V.12: IR spectra of CMX membrane equilibrated by Na^+ as counter-ion

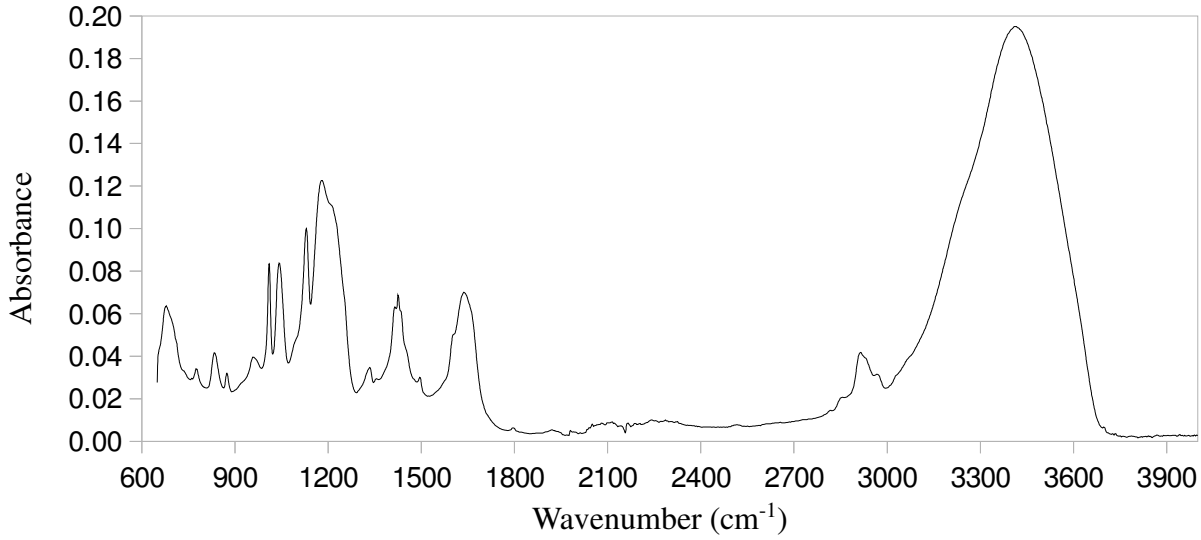

Figure V-13: IR spectra of CMX membrane equilibrated by Ca^{2+} as counter-ion

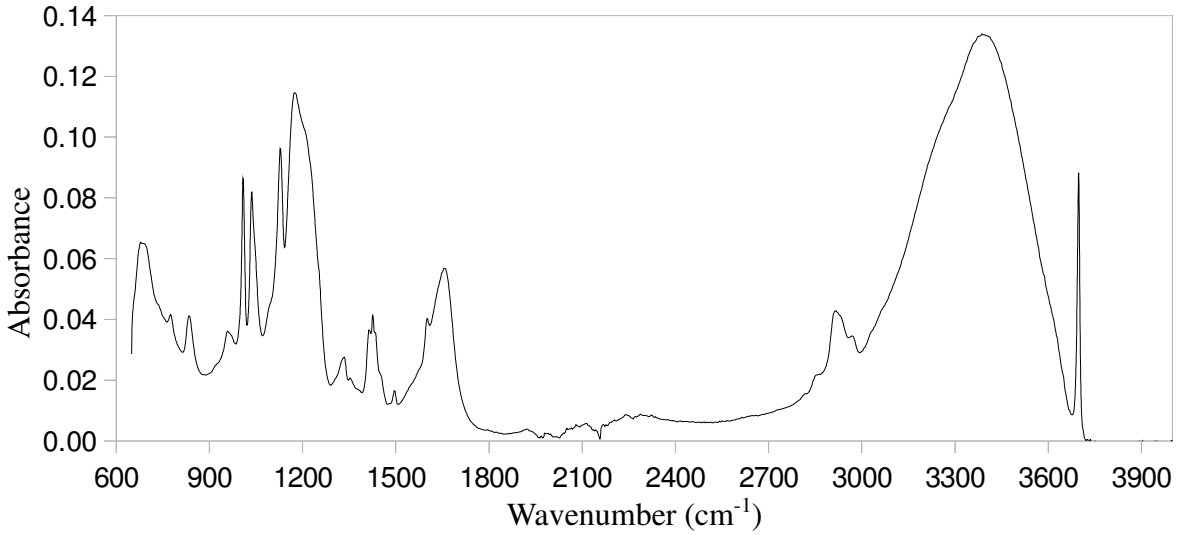

Figure V-14: IR spectra of CMX membrane equilibrated by Mg^{2+} as counter-ion

A shift based on the nature of the counter-ion is also detected in the experimental spectra in the characteristic zone of symmetric S-O stretching close to 1180 cm^{-1}. More precisely, intense absorption bands are detected at 1186 cm^{-1} for Na^+, 1179 cm^{-1} for Ca^{2+} and 1174 cm^{-1} for Mg^{2+}. According to literature data as well as to the computational spectra obtained in the previous section, these bands can be assigned to the S-O symmetric stretching. Thus, again, the divalent cations effect is visible in a shift of the S-O stretching band to lower wavenumber.

More complex is the assignment of the other computed and experimental peaks in the spectra. Due to their lower intensities, they are difficult to be tracked since they are in competition with the phenyls and aliphatic chain characteristic absorption bands. Nevertheless, from the analysis of both theoretical and experimental spectra in the characteristic regions of C-C and C-H vibrations (500-1200 cm^{-1} and 3000-3300cm^{-1}), it is possible to note the very local influence of the cations on the surrounding environment. In fact, no cation dependent variations are observed for all these peaks because they are shielded from the closer atoms and too far to be influenced.

A particular case is the IR spectra of CMX membrane equilibrated by NH_4^+. Indeed, the vibrational behavior of the N-H bonds, present in its molecular structure, is similar to the characteristic of O-H vibrational modes. In fact, from the corresponding experimental spectrum, in the called "water zone" (over 3000 cm^{-1}), a broad absorption zone is present in which three peaks are predominant at 3423 cm^{-1} , 3213 cm^{-1} and 3055 cm^{-1}. The last two peaks correspond to asymmetrical and symmetrical stretching of N-H bonds of the ammonium, while the peak at 3423 cm^{-1} is due to the overlap of the stretching modes of water molecules. Considering the sugar fluxes trend ($NH_4^+ > Na^+ > Ca^{2+} > Mg^{2+}$) obtained in a previous work and the IR data, the peak related to the stretching modes of water falls at an unexpected wavenumber, since it was supposed to be found at higher wavenumber for NH_4^+. Considering the trend of wavenumber for monoatomic ions ($Na^+ > Ca^{2+} > Mg^{2+}$), the H_2O vibrational modes in membranes equilibrated with NH_4^+ was expected to be at higher wavenumber than the peak for the same vibration but with Na^+ as counter-ion (3446 cm^{-1}), and not at 3423 cm^{-1} as experimentally measured. The same unexpected behavior of the membrane with NH_4^+ is the position of the peak related to the S-O stretching that is found at 1173 cm^{-1} while it was expected at values at least slightly more than 1186 cm^{-1} in order to respect the sugar fluxes trend ($J_{NH4+} > J_{Na+} > J_{Ca2+} > J_{Mg2+}$).

Possible explanations on these unexpected shifts can be due to the fact that NH_4^+ is a molecule and not a monoatomic cation (unlike other ions). At the same time, the presence of N-H bonds encourages the formation of H-bonds with the sulfonated group and/or the water molecules that

can affect the vibrational mode present in the structure. In fact, the establishment of a H-bond with the water molecule and/or the SO_3^- group can have a kind of "anchor" effect that decreases the wavenumber of absorption. These strong interactions can be emphasized in the preparation sample process, in particular during the drying step. With the extraction of the water molecules from the polymer matrix, the ammonium cations - SO_3^- interactions are encouraged since water molecules that could act as a shield are removed. Furthermore, some sort of weak acid-base interactions/effects could also play a role in the band shifts e. g. a partial protonation of the functional groups.

These differences in the vibrational spectra of the CMX membrane when equilibrated with various kinds of ions show that Infra-Red Spectroscopy is a powerful technique to investigate ion-membrane interactions, in particular if interaction spots are present in the polymeric network, i.e. the functional groups. In fact, vibrational properties are strictly related to the electron density and thus to the capability of the material to interact with the environment. In this specific case, shift at lower wavenumber of S-O as well as of O-H stretching modes can be related to stronger S-O ... O-H hydrogen bonds.

Further, the IR analysis made in this Chapter for monoatomic cations are in agreement with previous computational findings, showing that the long and short term interactions depend on the presence of the different monoatomic cations following a trend similar to the shift to lower wavenumber found in this Chapter.

V.1.4 Correlation with sugar fluxes

Reminding that the aim of this Thesis is to characterize physical changes in the water-membrane system as function of the counter-ion, some interesting correlations can be drawn.

Firstly, both the computed and experimental IR spectra of monoatomic ions show that a decrease in wavenumber of some specific vibration mode, i.e. water and SO_3^- characteristic stretching, can be correlated to a decrease in the sugar fluxes through CMX membrane. Unfortunately, the same correlation cannot be extended to polyatomic ions. Even if caution is needed if polyatomic ions are present, as in the case of NH_4^+ cation, the IR analysis could be an important tool to have a first evaluation of the transfer properties of CMX and Ion-Exchange membranes in general.

Secondly, the geometrical properties computed in the section can be also associated to the sugar fluxes through the CMX membrane. In particular, as observed in previous work by Karpenko-Jereb and colleagues [9], the counter-ion-functional group distance can be related to a change in the transport properties of the membranes. Here, as shown in Figure V.15, the same trend is observed since a smaller cations-SO_3^- distance, i.e. $Mg^{2+} < Ca^{2+} < Na^+$, corresponds to a lower measured flux of xylose, glucose and sucrose [10]. A linear trend describes the influence of the cation-functional group distance on the mass transfer for all the three sugars. Thus, the assumption of Karpenko-Jereb *et al* [9] concerning the transfer of ions through the ion exchange membrane can be extended to the transfer of neutral organic solutes. Furthermore, the same trend coincides with the increase of the Stokes radius of the sugars, 3.2 Å, 3.6 Å and 4.5 Å for xylose, glucose and sucrose respectively. Then, it is found that the transfer of a sugar also depends on its size as it is conventional for the transfer of neutral organic matter through ion exchange membranes [11].

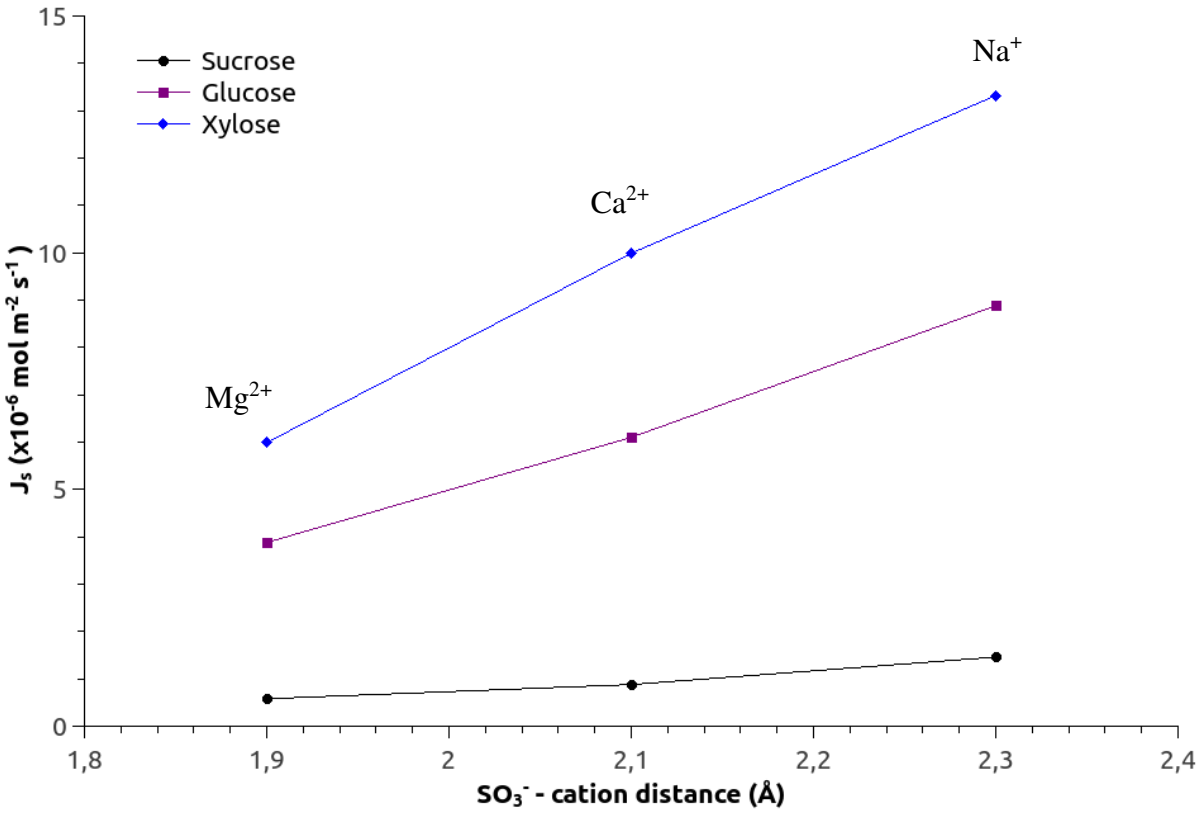

Figure V.15: SO_3^- - cation distances Vs Sugar fluxes measured in diffusion regime [Sugar] =1 mol L^{-1} [electrolyte]= 1equiv. L^{-1} [10].

V.2 Contact Angle measurements

Table V.9 gives the values of the contact angles obtained for the CMX membrane equilibrated with different cations. It should be remembered that a surface is "mostly hydrophilic" when $\theta < 90°$, and "mostly hydrophobic" when $\theta > 90°$. Since for all the conditions θ is lesser than 90° one can conclude that the CMX membrane is mainly hydrophilic. Moreover, contact angle measurements point out a remarkable influence of the counter-ion on the hydrophilic character of the membrane as shown from the different values of θ as function of the solution in which the membrane is soaked. The smaller contact angle is observed for the membrane soaked in NH_4Cl, while the higher is observed for the membrane equilibrated by $MgCl_2$. One can deduce that the CMX membrane hydrophilicity decreases for increasing counter-ion hydration:

$NH_4^+ > K^+ > Na^+ > Li^+ > Ca^{2+} > Mg^{2+}$

Aqueous solutions	$\theta \pm \sigma$ (°)	γ_l (mJ/m²) [14]	γ_s (mJ/m²)

(0.1M)			
NH_4Cl	23.2 ±0.3	72.12	66.40
KCl	23.6 ±1.2	72.15	66.24
NaCl	24.9 ±0.1	72.16	65.61
LiCl	25.9 ±0.3	N/A*	-
$CaCl_2$	32.6 ±1.4	72.39	61.43
$MgCl_2$	45.7 ±0.4	72.37	52.18

Table V.9: Measured contact angles, **θ**, solution surface free energy γ_l, and membrane surface free energy γ_s. *Li value not available by Dutcher-Wexler-Clegg method.

The role of ions can be imputable to a modification of the sulfonated group capability to interact with the external water molecule, or rather as a sort of screening effect of the ions on the hydrophilic sulfonated groups. In fact, polystyrene shows a contact angle of 40° [13] for water/air. Since CMX is a polystyrene-divinylbenzene membrane with hydrophilic sulfonic functional groups, a smaller contact angle is expected. The prevision is fully respected for the monovalent ions as well as for the Ca^{2+}. But on the contrary, the contact angle obtained with the membrane soaked in Mg^{2+} is higher than 40°. Variations in the contact angle reveal a change of the surface free energy of the membrane. In Table 6 the surface free energy values (γ_s) of the CMX membrane soaked in different electrolytes, calculated from measured contact angles and surface tension of the liquid (γ_l) using Dutcher - Wexler - Clegg method, are reported [14]. This method is a fitting procedure for the concentration dependent terms based upon available measurements of the surface tensions for the investigated salts at different temperatures. After the correction for the liquid properties, the trends of the impact of the electrolytes on the membrane surface also follow the hydration number trend. The fluxes of some saccharides measured in previous work through a CMX membrane are put in parallel with the surface free energies of the membrane soaked in different electrolytes (NH_4^+, Na^+, Ca^{2+}, Mg^{2+}) in Figure V.16.One can observe that a good correlation is obtained. More precisely, the mass transfer decreases for decreasing surface free energies.

The contact angle measurements can be also compared with the computational work carried out in the framework of Quantum Mechanics/Molecular Mechanics theory in Chapter IV. In the previous Chapter, the chain-chain interaction energies in the polymer network were computed in presence of 3 different cations (Na^+, Ca^{2+}, Mg^{2+}). The chain-chain interactions in presence

of Ca^{2+} were found 1.5 times stronger than the chain-chain interactions with Na^{+}. The chains in a CMX membrane equilibrated by Mg^{2+} has been found 2.5 time more cohesive compared to the membrane soaked in Na^{+} (see Table IV.7).

Moreover, considering that cations with higher hydration numbers have also higher hydration energies, one can suppose that they can induce stronger intra-systems interactions. Consequently, the probability that a functional group of the polymer network interacts with an external molecule is lower. The fact that divalent cations bind to two functional groups makes it more likely that a part of the functional groups is pulled away from the surface to associate with cations located inside the membrane. As such, it can be envisaged that the surface concentration of the sulfonic groups may be lower in presence of divalent cations as compared to monovalent ones. This kind of shielding effect could decrease the membrane wettability. Additionally, in the case of lower hydrated counter-ion, their ability to promote intra-surface interactions is weaker, thus the probability that an SO_3^- group interacts with the environment is higher.

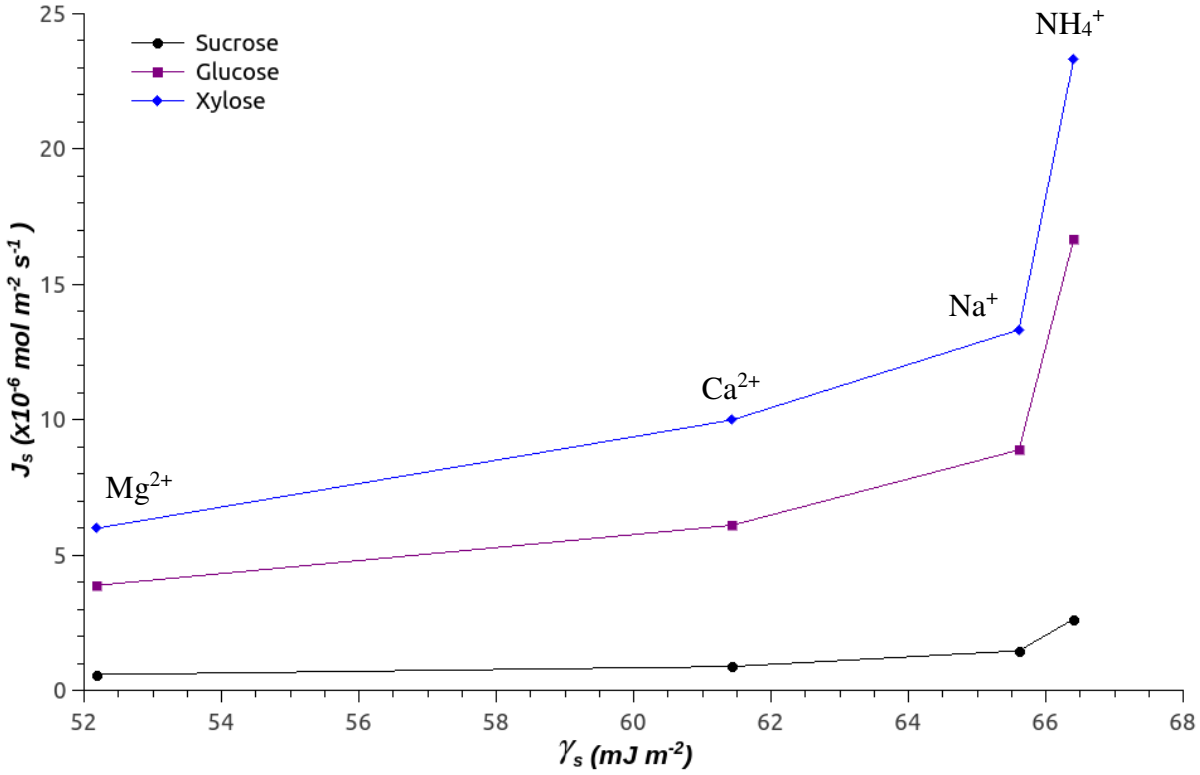

Figure V.16: Sugar fluxes vs surface energies of CMX membrane in several ionic forms (Mg^{2+}, Ca^{2+}, Na^{+} and NH_4^{+}). Sugar fluxes measured in diffusion regime [Sugar] =1 mol L^{-1} [electrolyte]= 1equiv. L^{-1} [10]

V.3 Thermal properties of CMX membrane

Water confined in membranes has different properties with respect to the water in the bulk. Due to the interactions with the membrane, the water can have three different states: free water, freezable water and non-freezable water [15]. The free water is involved only in water-water interactions and its properties are similar to the water in the bulk. Freezable water is the water that has both polymer-water and water-water interactions. It usually has a reduced crystallization temperature with respect to the free water. The non-freezable water has interactions only with the membrane, and it is not possible to observe phase transitions by DSC method.

DCS was used to characterize the CMX membrane soaked in electrolytes containing different cations.

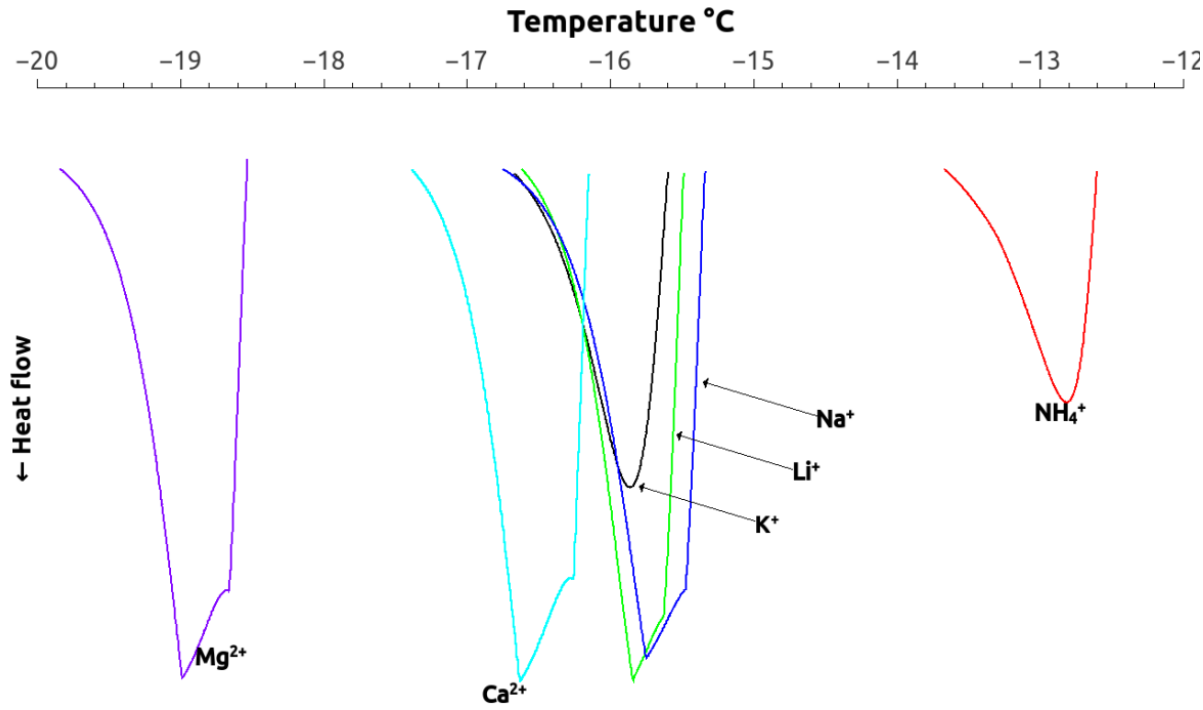

Figure V.17: DSC cooling peaks for CMX membrane equilibrated by different counter-ions.

In Figure V.17, the characteristic peaks of the freezable water in the membrane are reported for each counter-ion (NH_4^+, K^+, Na^+, Li^+, Ca^{2+} and Mg^{2+}). One can observe that the peak at 0 °C which would correspond to the free water is not detected. The absence of this peak gives the information that all the water enclosed in the membrane is affected by the polymer matrix. Supercooled freezing water peaks are detected in the temperature range between -12 and -20 °C depending on the counter-ion used to equilibrate the CMX membrane. More precisely, lower

supercooled freezing temperature ($NH_4^+ > Na^+ \approx K^+ \approx Li^+ > Ca^{2+} > Mg^{2+}$) are obtained for increasing counter ion hydration ($NH_4^+ < K^+ < Na^+ < Li^+ < Ca^{2+} < Mg^{2+}$). It is worth noting the overlap of the freezing peaks for three similar cations (Na^+, K^+, Li^+).

This membrane property is also put in parallel with the sugar fluxes measured in similar conditions, as reported in Fig. V.18. One can state that a good correlation is obtained between the sugar fluxes through the CMX membrane and the freezing temperature obtained from DSC measurements. More precisely, one can observe that lower freezing temperatures, observed for increasing counter-ion hydration, corresponds to lower sugar fluxes. This suggests that the freezing point of the water entrapped in the membrane is directly affected by a physical property of the membrane that influences also the transfer of sugar. This physical property can be associated to the noncovalent interactions investigated in the previous Chapter.

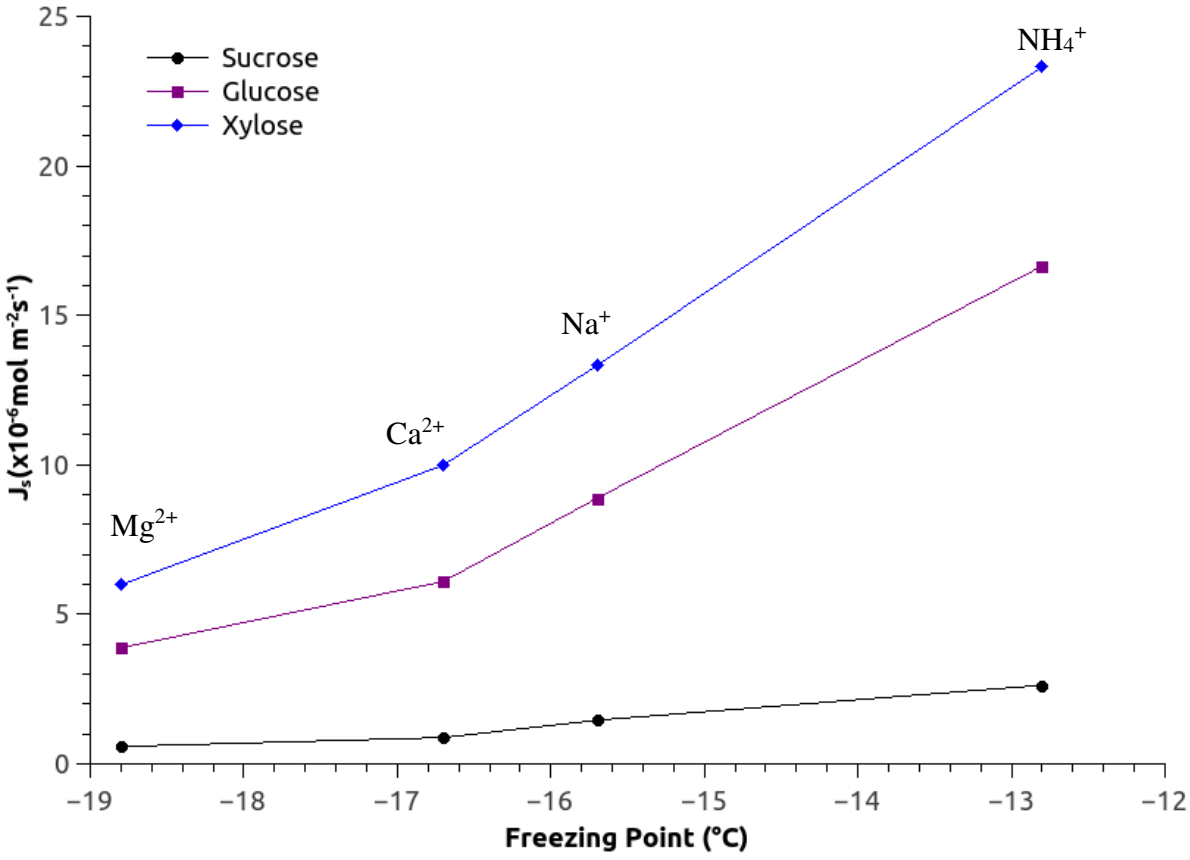

Figure V.18: Sugar fluxes in function of the freezing temperature of water entrapped in CMX membrane soaked in different electrolytes. Sugar fluxes measured in diffusion regime [Sugar] =1 mol L^{-1} [electrolyte]= 1equiv. L^{-1} [10].

The content and state of water are crucial for the transport of neutral solute through cation exchange membrane. The shift to lower temperatures of the freezing point of the freezable water according to the cation reveals a different state of the water due to the interactions with the polymer-counter-ion system. One can affirm that the state of water in CMX membrane depends on the cation used to equilibrate the membrane, and that the higher is the hydration number (and thus the interaction energy) of the cation, the higher is its impact on the water producing a change in the diffusion of matter through the membrane. The effect of the cation is clearer if these data are compared with the computational work presented in Chapter 4 and previous experimental works. Glucose, xylose and sucrose diffusional transport in CMX membranes soaked in Na^+, Ca^{2+}, Mg^{2+} and NH_4^+were studied and a clear decrease of sugar fluxes was observed in the presence of Ca^{2+} and Mg^{2+} [10]. Furthermore, in Chapter 4 it is shown that the cation has a strong influence on the long and short interactions that govern the cohesion between the polymer chains. In particular, it was found that the cohesion energy among the polymer chains constituting the membrane increases with the interaction energy of the ions used to equilibrate it, i.e. the membrane counter-ion. Moreover, it is shown that the interactions between the chains are established by "interactions path" with a polymer-water-water-polymer structure. The water molecules involved in these interaction paths could give rise to the supercooling effects represented by the peaks at temperatures below 0°C as shown in Figure V.17.

The temperature of the freezing peaks in the samples could give also information about the differences of free volume elements size inside the membrane. In fact, the lowering of the triple point temperature of a liquid probe due to the confinement in a porous material is the basic principle of thermoporometry [16] [17]. Even if it is an uncommon way to characterize the free volume elements size in the structure of dense membrane, thermoporometry technique is applied to a large number of different porous materials especially when classical methods cannot be adapted. Using the Gibbs–Thomson equation[18] it is possible to affirm that the equilibrium temperature of liquid-solid phase transitions is determined by the radius of curvature at the liquid-solid interface. This radius of curvature is directly correlated to the available space. Smaller is this space, lower is the freezing temperature of the freezable liquid. In this work, the liquid phase can be always considered as water since one can assume the cations to be part of the solid phase due to their strong interactions with SO_3^- groups. Thus, the shift to lower temperature for divalent cations such as Ca^{2+} and Mg^{2+} support the hypothesis that the interstitial volume in the membrane decreases with increasing cation hydration number. Unfortunately a quantitative analysis of the average free volume elements size is not possible since the developed mathematical relationships are adapted for materials with well-defined

pores and in the range 2-150nm [19] [20] rather than a swollen network. Considering the decreasing sugar fluxes with decreasing freezing temperature, it is possible to affirm that the two physical phenomena are correlated. Furthermore, this correlation is supported by the output of the computational modeling shown in the previous Chapter that evidences a decreasing average distances between polymer chain fragments representative of CMX membranes equilibrated by Na^+, Ca^{2+} and Mg^{2+}.

V.4 Conclusion

A complete vibrational analysis was performed on CMX membrane in presence of different cations by experimental and Quantum Mechanics methods in the framework of DFT on a qualitative basis only. Both experimental and computational spectra present a shift to lower wavenumber of particular peaks following the hydration scale of cations in solution as found in literature. These peaks are assigned to the O-H stretching of the water molecules vibrations and S-O stretching as part on the polymeric system in contact with the cations. The shift to lower wavenumber reflects a decrease of the energy of this vibrational mode which means a stronger interaction of the water molecules with the cation-polymer system. Energetically weaker S-O or O-H bonds in the models containing Ca^{2+} or Mg^{2+} means that the oxygen of sulfonic groups or the hydrogen of water form stronger hydrogen bonds in the $Ph\text{-}SO_3^{-}\cdots Ca^{2+}$ or Mg^{2+} adducts compared to Na^+, showing how the divalent counter-ions bind stronger with the water molecule, near cations, as for sodium ions. Thus, the trend found for the monoatomic cations is in agreement with previous computational findings, in which the long and short term interactions follow a trend similar to the IR shifts found in this Chapter.

Contact angle measurements carried out with the CMX membrane equilibrated with different electrolytes (LiCl, KCl, NaCl, NH_4Cl, $CaCl_2$ and $MgCl_2$) and the correlated surface energy properties have confirmed that the presence of different electrolytes changes the water affinity of the polymer matrix following the hydration shell scale of the ions in solution. The experimental data indicate that a membrane soaked by a more hydrated cation loses part of its water affinity, even if its properties are always in the range of hydrophilic membrane. This behavior can be attributed to a decrease of the accessibility of the sulfonated functional groups due to a higher attraction with the cations.

Particular is the case of the influence made by the presence of NH_4^+. The unexpected behavior

of the IR measurements and the non-linear correlation in the contact angle analysis for membrane soaked in NH_4^+ suggest that this ion affects the CMX membrane properties with an additional (or a different) way compared to the other ions. One explanation could be the multiatomic structure of the ion and its possibility to interact by hydrogen binding. DSC data provided the experimental proof that the state of water inside the CMX membrane changes according to the membrane counter-ion. Moving from less to more hydrated cations causes a decrease in the freezing point of the water trapped in the membrane polymer network. This trend points out that higher interactions occur between polymer, cation and water in presence of more hydrated cations. Furthermore, according the thermoporometry theory, a lower freezing point of the liquid trapped in the membrane corresponds to a smaller free volume. Thus, in our case the decreasing of the freezing point could also be associated to a decreasing of the volume accessible to water which is directly related to the membrane permeability for water and small neutral components.

Experimental and theoretical approaches suggest that cations used as counter-ion in CMX membrane have a strong impact on the state of the water present in the system. In particular, the noncovalent interactions between the different components of the system are more influenced by highly hydrated cations as found in solution.

V.5 References

[1] M. Falk, "An infrared study of water in perfluorosulfonate (Nafion) membranes," *Can. J. Chem.*, vol. 58, pp. 1495–1501, 1980.

[2] K. Asaka, N. Fujiwara, K. Oguro, K. Onishi, and S. Sewa, "State of water and ionic conductivity of solid polymer electrolyte membranes in relation to polymer actuators," vol. 505, pp. 24–32, 2001.

[3] T. Okada, G. Xie, O. Gorseth, S. Kjelstrup, N. Nakamura, and T. Arimura, "Ion and water transport characteristics of Na®on membranes as electrolytes," vol. 43, no. 24, pp. 3741–3747, 1998.

[4] J. Cerny and P. Hobza, "The X3LYP extended density functional accurately describes H-bonding but fails completely for stacking," *Phys. Chem. Chem. Phys.*, vol. 7, pp. 1624–1626, 2005.

[5] W. Koch and M. C. Holthausen, *A Chemist's Guide to Density Functional Theory*, II., vol. 3. 2001.

[6] "http://www.nwchem-sw.org/index.php/Geometry_Optimization visited on 11-sept-2014." .

[7] M. Valiev, E. J. Bylaska, N. Govind, K. Kowalski, T. P. Straatsma, H. J. J. Van Dam, D. Wang, J. Nieplocha, E. Apra, T. L. Windus, and W. A. De Jong, "NWChem: A comprehensive and scalable open-source solution for large scale molecular simulations," *Comput. Phys. Commun.*, vol. 181, no. 9, pp. 1477–1489, 2010.

[8] M. D. Hanwell, D. E. Curtis, D. C. Lonie, T. Vandermeersch, E. Zurek, and G. R. Hutchison, "Avogadro: an advanced semantic chemical editor, visualization, and analysis platform.," *J. Cheminform.*, vol. 4, no. 1, pp. 17,. 2012.

[9] L. V. Karpenko-Jereb, A.-M. Kelterer, N. P. Berezina, and A. V. Pimenov, "Conductometric and computational study of cationic polymer membranes in H+ and Na+-forms at various hydration levels," *J. Memb. Sci.*, vol. 444, pp. 127–138, 2013.

[10] S. Galier, J. Savignac, and H. Roux-de Balmann, "Influence of the ionic composition on the diffusion mass transfer of saccharides through a cation-exchange membrane," *Sep. Purif. Technol.*, vol. 109, no. 0, pp. 1–8, 013.

[11] N. Mogi, E. Sugai, Y. Fuse, and T. Funazukuri, “Infinite dilution binary diffusion coefficients for six sugar at 0.1 MPa and temperature from 273.2 to 353.2) K,” *J. Chem. Eng. Data*, vol. 52, pp. 40–43, 2007.

[12] *Y. Marcus*, *Ion Properties*, Marcel Dekker, New York, *1999*.

[13] R. Jayasekara, I. Harding, I. Bowater, G. B. Y. Christie, and G. T. Lonergan, “Biodegradation by Composting of Surface Modified Starch and PVA Blended Films,” vol. 11, no. 2, 2003.

[14] C. S. Dutcher, A. S. Wexler, and S. L. Clegg, “Surface tensions of inorganic multicomponent aqueous electrolyte solutions and melts.,” *J. Phys. Chem. A*, vol. 114, no. 46, pp. 12216–30, 2010.

[15] Y. S. Kim, L. Dong, A. H. Michael, E. G. Thomas, V. Webb, and J. E. McGrath, “State of Water in Disulfonated Poly(arylene ether sulfone) Copolymers and a Perfluorosulfonic Acid Copolymer (Nafion) and Its Effect on Physical and Electrochemical Properties,” *Macromolecules*, vol. 36, no. 17, pp. 17–21, 2003.

[16] M. Iza, S. Woerly, C. Danumah, S. Kaliaguine, and M. Bousmina, “Determination of pore size distribution for mesoporous materials and polymeric gels by means of DSC measurements: thermoporometry,” *Polymer (Guildf).*, vol. 41, pp. 5885–5893, 2000.

[17] M. R. Landry, “Thermoporometry by differential scanning calorimetry: experimental considerations and applications,” *Thermochim. Acta*, vol. 433, no. 1–2, pp. 27–50, 2005.

[18] J. B. W. Webber, “Studies of nano-structured liquids in confined geometries and at surfaces.,” *Prog. Nucl. Magn. Reson. Spectrosc.*, vol. 56, no. 1, pp. 78–93, 2010.

[19] Torben Smith Sorenson, *Surface Chemistry and Electrochemistry of Membranes Torben Smith Sorenson*, 1st ed. Press, CRC, 1999.

[20] S. Escribano, P. Aldebert, and M. Pineri, “Volumic electrodes of fuel cells with polymer electrolyte membranes: electrochemical performances and structural analysis by thermoporometry,” *Electrochim. Acta*, vol. 43, no. 14–15, pp. 2195–2202, 1998.

Chapter VI

Conclusion

Different studies carried out these last years pointed out that the performances of the membrane processes, especially Nanofiltration or Electrodialysis, can be significantly affected when applied to solutions containing significant amount of salts. Indeed, it was reported, with NF membranes as well as with ion-exchange ones used in electrodialysis, that the transfer of an organic solute changes according to the nature and concentration of the ions. Dealing with nanofiltration, it was shown that the mass transfer modification is mainly fixed by the influence of the electrolyte on the solute properties. An increasing transfer was observed with ions of increasing hydration number. On the contrary, for ion-exchange membranes, it was reported that the mass transfer variation is mainly governed by the modification of the membrane properties which are fixed by the ionic composition. In this case, decreasing mass transfer was obtained when the membrane is equilibrated with increasing hydrated counter-ion. Then, whilst different mechanisms are involved depending on the membrane and solute properties, in any case, the mass transfer modification has been correlated to the hydration state of the ions

The effects observed at the macroscopic scale, i.e. the modification of the organic solute transfer according to the ionic composition, result from mechanisms taking place at the molecular scale. Consequently, the knowledge of the multiple noncovalent interactions, taking place at the nano-scale, between the polymer, the water and the solutes (ions, organic compounds) is a bottleneck regarding the improvement of the membrane processes. Thus, the development of new complementary approaches to characterize these systems at the microscopic scale is necessary.

This was the objective of this Thesis. A fundamental multi-scale approach was proposed, combining experimental and theoretical tools in order to get microscopic and macroscopic parameters characterizing the investigated interactions for different ionic compositions.

In a first part, the properties of the ions were investigated, since it was shown that they affect the separation process of organic solute through membranes. It was based on previous experimental correlations between the hydration properties of ions and the modification of the transfer of organic solutes through different kinds of membranes used in nanofiltration and electrodialysis. Thus, water-ion clusters were modeled in the frame of Density Functional Theory (Quantum Modeling) at various hydration levels to investigate the solvation properties of ions in solution by computational methods. Specifically, the coordination and hydration numbers of ions were computed as well as the water-ion distances and the interaction energy between the investigated ions and the water molecules inside their hydration shell. The results were compared to those found in the literature showing a good agreement. Then, the computed properties were correlated with experimental data obtained in previous works dealing with the

sugar diffusion fluxes through nanofiltration and ion-exchange membranes for different ionic compositions. Except for the coordination number, good correlations between computed ions hydration properties in solution and sugar fluxes were found. It was thus concluded that the coordination number is not the appropriate parameter to consider probably because it only takes short rang interactions into account, on the contrary to the hydration number. The correlations pointed out between the hydration number and the interaction energy of the ions and the corresponding sugar flux show the link between mechanisms taking place at the molecular scale and macroscopic parameters that was previously pointed out from the qualitative point of view.

Secondly, the study was focused on the case of the transfer of a sugar (glucose) through a cation exchange membrane. Noncovalent interactions taking place at the molecular scale, between the solute and a membrane polymer fragment as well as between the polymer fragments inside the membrane were investigated using a combined Quantum Mechanics/Molecular Mechanics approach. Due to the complexity of the investigated system, the QM/MM study was carried out in two steps. In the first step, the system was separated in small building blocks and independently studied by Quantum Mechanics. The glucose hydration shell as well as the hydration of polymer fragments was thus investigated. Then, the optimized building blocks were merged in bigger systems in order to get the interaction energies between the sugar-polymer and the chain-chain in polymer network.

The results have shown that the presence of the membrane monomer changes the glucose-water interaction energy compared to that in solution. Negative values were obtained for the glucose-monomer interaction energy showing that the glucose is solubilized in the polymer. But no significant variation was found according to the cation. It means that in the conditions investigated, the interaction between the glucose and the monomers that is linked to the solubility of glucose inside the membrane is not the main mechanisms controlling the sugar transfer through the membrane according to the cation.

The most significant results were obtained during the evaluation of the chain-chain interaction energies. Indeed, it was found that the average distance between the counter-ion and the oxygen of the sulfonic group belonging to the same fragment as well as the distance between two polymer fragments changes according to the cation. Then, due to the decrease of the fragment-fragment distance observed with increasingly hydrated cation, a lower sugar flux can be expected, as was observed during the previous experimental investigation. Moreover, a relation between the interaction energy and the water embedded in the polymeric structure, forming hydrogen bonding wire between the chains, has been pointed out. An inverse trend between these interaction energies and the sugar fluxes was observed. Indeed, the chain mobility is

expected to decrease for increasing interaction energies transferred by these wire, what is the case for a membrane equilibrated with more hydrated cations such as divalent ones. Thus, it was demonstrated that the cohesion energy among the polymeric chains constituting the CMX membrane is governed by the hydration of the membrane counter-ion. Then the sugar flux was found to be fixed according to the value of the cohesion energy and then to the hydration of the membrane counter-ion.

In the last chapter, the CMX membrane was characterized in various electrolytes using both computational and experimental methods.

A complete vibrational analysis was performed in presence of different cations by experimental and Quantum Mechanics methods on a qualitative basis only. Both experimental and computational spectra have pointed out a shift to lower wavenumber of some particular peaks (O-H stretching of water molecules and S-O stretching) following the hydration of the cations in solution. The shift to lower wavenumber for increasing cation hydration, linked to the decrease of the energy of this vibrational mode, has been related to stronger interactions between the water molecules and the cation-polymer.

Contact angle measurements and the correlated surface energy properties have confirmed that the presence of different electrolytes changes the water affinity of the polymer matrix following the hydration scale of the ions in solution. The experimental results have shown that a membrane soaked with a more hydrated cation loses part of its water affinity. This behavior has been attributed to a decrease of the accessibility of the sulfonated functional groups due to a higher attraction with the cations.

Differential Scanning Calorimetry experiments have provided an experimental proof concerning the change of the state of the water contained in the CMX membrane according to the electrolyte. Decreasing values of the freezing point of the water trapped in the membrane polymer network were obtained for a CMX membrane soaked with more hydrated cations. This trend pointed out that higher interaction occurs between polymer, cation and water for more hydrated cation. According to the thermoporometry theory, the decreasing of the freezing point could also be associated to a decrease of the volume accessible to water, a parameter which is directly related to the membrane permeability for small neutral solutes.

Experimental and theoretical approaches at the molecular scale suggest that the cation used as counter-ion to equilibrate the CMX membrane has a strong impact on the state of the water embedded in the membrane. In particular, the noncovalent interactions between the different components of the system are more influenced by highly hydrated cations as found in solution. Finally, it was shown that the influence of the counter-ion hydration on the noncovalent

interactions and the sugar fluxes can be correlated by both qualitative and a quantitative analysis.

As further developments of this Thesis, several are the possibilities concerning both computational and experimental approaches.
Concerning the computational methods, a big question mark is still pending on the interaction among the sugars and the electrolytes. This work is of fundamental importance to understand the influence of the ionic composition on the transfer of solute in Nanofiltration systems since it was concluded from previous study that it is mainly fixed by ion/solute interactions taking place in the solution. Focused calculations could be performed in order to investigate if ions affect only the hydration shell of the sugars, or if their structure can also be changed according to the ions (different conformer/isomer).
Dealing with CMX membranes, the computational approach carried out in this work could be continued considering the optimized structure obtained in the present work as starting point to investigate the effect of the electric field on the polymeric structure or on the involved noncovalent interactions. Moreover, the information obtained by means of Quantum Mechanics could be exploited to customize the Force Fields and to perform Molecular Dynamics calculations with *ad hoc* parameters. This would permit to enlarge the dimensions of the model and to model the diffusion of the organic matter through the membrane.
The experimental characterization of the membrane under different environments is also an important point. Different methods could be considered to investigate the mechanical properties of the membrane polymer at the molecular-scale. Innovative techniques, able to measure the Young's modulus and other mechanical properties of the membrane by Atomic Force Microscope could be interesting to evaluate. The water sorption uptake could be another relevant technique since it could be compared with the computational data. Another output of these measurements is the diffusion coefficient of the water in the membrane equilibrated by different counter-ion. It can be also compared with the computational data, since the chain-chain interaction energy should affect also the diffusion coefficient of the water.

At the end of this manuscript, it could be affirmed that this Thesis paves the way for the understanding of the mechanisms by which membrane processes are affected by the presence of ions in the system. Thus, this study can be used as reference for further developments in process intensification for treatment of complex fluids.

Summaries in French/Résumés en français

Chapitre 1

Introduction

L'expansion de la population mondiale conduit à une pression de plus en plus forte sur les ressources naturelles. A l'heure actuelle, cette demande excède la capacité de notre écosystème à se régénérer. L'impact de l'activité humaine sur l'environnement est perceptible à travers la désertification, la déforestation, le changement climatique, la perte de biodiversité, la raréfaction des ressources en eau,… Une des possibilités pour faire face à cette demande et supporter une croissance industrielle durable réside dans l'intensification des procédés.

Les technologies membranaires peuvent jouer un rôle de première importance dans ce contexte. En effet, les systèmes membranaires ont divers atouts: une faible consommation énergétique, comparés aux procédés traditionnels, une capacité à transporter efficacement et sélectivement des composés spécifiques (recyclage de l'eau, des produits chimiques ou des matières premières, «zéro rejet»), un potentiel à catalyser des réactions. Leur modularité permet également de réduire significativement la taille des installations. Durant ces dernières décennies, le génie des procédés membranaires a déjà offert des solutions intéressantes pour accroitre les performances de diverses opérations de transformations dans de nombreux secteurs de l'industrie (agroalimentaire, pharmacie, industries textiles par exemple).

Les procédés membranaires sont d'ores et déjà utilisés pour traiter des fluides complexes, contenant des acides aminés issus de procédés biotechnologiques, des acides carboxyliques issus de bioraffineries. Un autre domaine d'application d'importance est celui du traitement des eaux usées, saumures, lixiviats ou autre type d'eaux (civil, pharmacie, nucléaire,..). Ici encore, l'objectif est de séparer et recycler les composés valorisables contenus dans ces eaux tout en assurant une épuration performante de celles-ci. Tous ces liquides ont en commun la présence de sels, parfois à des concentrations élevées. Au cours des dix-quinze dernières années, différentes études ont mis en évidence que la présence de sels peut modifier significativement les performances des procédés membranaires, en particulier leur capacité à éliminer ou concentrer des espèces organiques. La plupart des résultats disponibles dans la littérature concernent le cas de la nanofiltration, bien que des phénomènes identiques aient été également

observés avec des membranes échangeuses d'ions utilisées en électrodialyse.

Pour des molécules neutres, le transfert à travers la membrane est principalement gouverné par des effets stériques, liés à la taille des espèces. Il dépend donc de la taille relative des solutés et des dimensions des pores ou de la fraction de volume libre de la membrane. Ainsi, une augmentation du transfert peut être attribuée à une augmentation des dimensions caractéristiques de la membrane, à une diminution de la taille du soluté transférant ou, plus probablement, à un couplage des deux.

La principale difficulté pour étudier les mécanismes de transfert dans de telles situations réside dans le fait que les deux contributions peuvent changer en fonction de la composition de l'électrolyte et des propriétés structurales de la membrane. Une approche expérimentale originale a été développée récemment afin de distinguer les effets de chacune des contributions. D'une part, l'impact de l'électrolyte sur les propriétés structurales de la membrane est évalué à partir de la mesure du flux de sucre dans un système sucre/eau en ayant préalablement conditionnée la membrane dans l'électrolyte. D'autre part, l'impact de l'électrolyte sur les propriétés du soluté est déterminé à partir de la mesure du flux de sucre dans un système sucre/électrolyte comparé à celui mesuré pour les systèmes sucres/eau.

En utilisant cette procédure spécifique, Boy et al. [22] ont montré que le flux de diffusion de sucres (xylose, glucose et saccharose) à travers une membrane de NF en présence de divers électrolytes (NaCl, Na_2SO_4, $CaCl_2$, $MgCl_2$) est principalement fixé par l'influence de l'électrolyte sur les propriétés du soluté. En d'autres termes, dans les conditions considérées, les modifications de la membrane en fonction de l'électrolyte sont négligeables. Ces travaux ont également confirmé que des électrolytes plus hydratés ou à des concentrations plus élevées conduisent à une augmentation plus importante du transfert de soluté (Table I.1).

	J_s ($x10^{-7}$ mol m^{-2} s^{-1})		
Electrolyte	Xylose	Glucose	Sucrose
Na2SO4	15.3	12.1	6.3
NaCl	7.5	4.6	0.7
CaCl2	11.6	12.1	22.8
MgCl2	13.2	14.4	18.3

Table I.3: Flux de diffusion de sucres à travers une membrane de Nanofiltration en présence de différents électrolytes. [Sucre] =1 mol L^{-1} [Electrolyte]= 1equiv. L^{-1}[22].

Cet effet a été quantifié en déterminant le volume molaire apparent (AMV) et plus précisément sa variation, ΔV, un paramètre macroscopique qui caractérise l'état d'hydratation des espèces dans les systèmes soluté/électrolyte. Une relation a ainsi été établie entre le volume molaire apparent des sucres et leur transfert à travers une membrane de NF en régime de diffusion pour différents électrolytes. Dans les conditions où les propriétés de la membrane ne changent pas selon l'électrolyte, il a été confirmé que l'augmentation du transfert de soluté en présence d'électrolyte provient de la déshydratation qui en résulte.

Cette procédure développée afin de dissocier la contribution de chaque phénomène a aussi été utilisée par Savignac et al. [25], [26] pour étudier le transfert de sucres à travers des membranes échangeuses d'ions. Le transfert de différents sucres (xylose, glucose et saccharose) a été étudié en régime de diffusion dans des solutions d'électrolytes (NaCl, NH_4Cl, $CaCl_2$, et $MgCl_2$). Il a été démontré que l'influence de la composition de l'électrolyte sur le transfert de sucre est due principalement aux modifications des propriétés de la membrane, fixées par le conditionnement de celle-ci. Une corrélation quantitative a été établie entre le transfert de sucre et le nombre d'hydratation du contre ion de la membrane. En effet, il a été montré que le transfert de sucre à travers une membrane échangeuses d'ions diminue lorsque la membrane est équilibrée avec un contre-ion plus hydraté, calcium versus sodium par exemple dans le cas d'une membrane CMX

(Table I.2).

Ainsi, dans le cas de membrane de NF, la modification du transfert de sucre en fonction de l'électrolyte est principalement fixée par les modifications du soluté. A contrario, dans le cas de membranes échangeuses d'ions, la modification du transfert de soluté avec l'électrolyte provient des modifications des propriétés de la membrane.

	J_s ($x10^{-6}$ mol m^{-2} s^{-1})		
Electrolyte	Xylose	Glucose	Sucrose
NH4Cl	23.31	16.65	2.63
NaCl	13.32	8.88	1.46
CaCl2	9.99	6.11	0.88
MgCl2	5.99	3.88	0.55

Table I.4: Flux de diffusion de sucres à travers une membrane de CMX conditionnée avec différents électrolytes. [Sucre] =1 mol L^{-1} [Electrolyte]= 1equiv. L^{-1} [25].

Ces phénomènes observés à l'échelle macroscopique résultent de mécanismes siégeant à l'échelle moléculaire. Ainsi, la connaissance des interactions multiples à l'échelle nanométrique, entre le polymère, l'eau et les solutés (ions, espèces organiques) constituent un verrou pour l'amélioration des procédés mettant en œuvre ces membranes. De nouvelles approches permettant de caractériser ces systèmes à l'échelle moléculaire sont donc nécessaires.

A cette échelle, les interactions faibles non covalentes semblent pouvoir expliquer les phénomènes observés à partir de mesures macroscopiques. C'est la raison pour laquelle, l'étude de ces interactions fait l'objet de cette thèse. On s'intéresse plus particulièrement au transfert d'une espèce organique neutre, le glucose, à travers une membrane échangeuse de cations.

L'objectif est d'étudier le comportement d'une membrane CMX en combinant des approches

expérimentales et numériques. Plus précisément, il s'agit de comprendre les mécanismes et les interactions selon lesquels les contre ions utilisés pour conditionner la membrane affectent le transfert du soluté organique.

Des méthodes expérimentales seront aussi mises en œuvre afin d'obtenir une représentation des propriétés des membranes à l'échelle moléculaire. La spectroscopie infrarouge (IR), la calorimétrie différentielle (DSC) et des mesures d'angle de contact seront utilisées pour caractériser les propriétés physiques des membranes et leur variation avec la composition ionique. Les résultats expérimentaux et calculés seront comparés afin d'identifier les mécanismes moléculaires mis en jeu. Ces résultats seront également corrélés à ceux obtenus à l'échelle macroscopique (mesures de flux à travers la membrane).

Le manuscrit se décompose de la façon suivante.

Dans le chapitre 2, les approches expérimentales et numériques seront détaillées. Les bases théoriques des approches numériques seront présentées et discutées. Les diverses méthodologies expérimentales seront décrites.

Le chapitre 3 concerne l'étude des propriétés des ions en solution en utilisant une approche de modélisation moléculaire. Les valeurs calculées seront également corrélées aux valeurs expérimentales de flux de sucres à travers des membranes de NF et échangeuses d'ions obtenues dans des travaux antérieurs.

Le cœur de l'étude de modélisation fera l'objet du chapitre 4. Dans une première partie, les aspects théoriques de deux méthodes, mécanique quantique et mécanique moléculaire, seront détaillés, ainsi que la méthode hybride QM/MM utilisée par la suite. La construction des blocs élémentaires « building blocks » sera présentée. Dans une deuxième partie, l'étude théorique des interactions polymère-sucre d'une part et polymère-polymère d'autre part sera présentée et discutée.

Le chapitre 5 sera consacré à la caractérisation de la membrane CMX en utilisant diverses méthodes expérimentales. Les spectres infrarouges seront également modélisés en utilisant la

mécanique quantique et les résultats seront comparés à ceux obtenus expérimentalement. Les résultats obtenus par DSC et mesure d'angle de contact seront présentés et discutés.

Les conclusions et perspectives de ce travail seront détaillées dans le chapitre 6.

Chapitre 2

Approches expérimentales et modélisation

Méthodes numériques - modélisation

Le lien entre méthodes numériques et expérimentation est de plus en plus important. Les outils de simulation et modélisation peuvent constituer par exemple des «yeux» pour les expérimentateurs afin d'observer des mécanismes à l'échelle nanométrique. Elles peuvent également permettre d'obtenir de grandes quantités d'informations et des connaissances impossibles ou très difficiles à obtenir par des méthodes expérimentales.

Les méthodes numériques peuvent être divisées en 3 grandes catégories selon l'échelle de simulation, de l'échelle moléculaire à l'échelle macroscopique.

La première catégorie est celle des modèles nano et sub-nano. Dans les calculs de mécanique quantique *ab initio*, les propriétés électroniques sont prises en compte afin de déterminer les énergies d'interaction (formation et rupture de liaisons), les propriétés spectrales et les interactions non covalentes. Cette approche a également l'avantage de ne requérir aucun paramètre ajustable [4], [5]. Malheureusement les modèles quantiques ne sont pas utilisables pour des systèmes au-delà d'une centaine d'atomes, les ressources nécessaires devenant trop importantes. La mécanique moléculaire requiert quant à elle des ressources moindre et permet de traiter des systèmes comprenant jusqu'à 10^9 atomes. En outre, on peut calculer les propriétés dynamiques ainsi que les trajectoires, déterminer les différents conformères et les énergies d'empilement. A contrario, étant donné que l'information sur les électrons est perdue, il est impossible d'étudier la formation/rupture des liaisons, y compris les liaisons non covalentes.

La deuxième catégorie est celle des modèles mésoscopiques, dans lesquels une composition discrète des matériaux est considérée. Les entités représentant les matériaux ne sont plus les atomes mais des complexes supra moléculaires dans lesquels les propriétés atomiques sont moyennées. Ces méthodes peuvent être utilisées pour l'étude de la stabilité thermique, de la morphologie, des conditions de la formation de domaines et les propriétés qui en découlent.

La dernière catégorie est celle des modèles macroscopiques dans lesquels l'objet d'étude est décrit comme une cellule unitaire continue. Les détails concernant les interactions moléculaires

ne sont pas pris en compte. Ces modèles permettent d'étudier par exemple des propagations de fracture, des transferts de chaleur ou de matière ainsi que le comportement des structures à l'échelle macroscopique.

L'objectif de cette thèse est d'étudier les phénomènes, à l'échelle moléculaire, qui contrôlent le transfert d'espèces organiques neutres à travers une membrane polymère. C'est la raison pour laquelle la mécanique quantique et la mécanique moléculaire, ainsi qu'une approche combinant les deux, sont utilisées.

Méthodes expérimentales

La membrane utilisée dans ce travail est une membrane échangeuse de cations CMX (Neosepta) en polystyrène-divinylbenzène sulfoné. Les membranes sont conditionnées selon la norme NF X 45-2000 avant toute caractérisation. Ce traitement consiste en un lavage acide (HCl) suivi d'un lavage basique (NaOH) et d'un trempage dans la solution d'électrolyte considérée. Il permet de nettoyer la membrane d'éventuelles impuretés résiduelles dues au processus de fabrication et de l'équilibrer avec l'électrolyte. Les membranes sont ensuite conservées dans le même électrolyte. Elles sont lavées à l'eau ultrapure avant les analyses de spectroscopie Infrarouge (IR) ou de calorimétrie différentielle à balayage (DSC) afin d'éliminer l'excès de sels.

Les solutions d'électrolyte utilisées contiennent un anion commun, Cl^-, afin d'étudier la seule influence du cation, contre-ion de la membrane: LiCl, KCl, NH_4Cl, NaCl, $CaCl_2$, $MgCl_2$.

Trois méthodes sont utilisées afin de caractériser les membranes en fonction du cation présent dans l'électrolyte.

La première méthode est la spectroscopie infrarouge, méthode non destructive utilisée pour étudier les propriétés des matériaux grâce à l'interaction entre la matière et la lumière dans le domaine infrarouge (longueurs d'onde entre 10 et 13000 cm^{-1}). Elle repose sur le fait que les liaisons chimiques sont susceptibles de vibrer lorsqu'elles sont irradiées à des longueurs d'onde

spécifiques. La radiation doit avoir une énergie spécifique, qui correspond à celle permettant la transition d'une liaison covalente de son niveau vibrationnel fondamental à un niveau excité. Ce changement de niveau énergétique provoque un mouvement de rotation ou une vibration des atomes mis en jeu ce qui conduit à une modification du moment dipolaire de la molécule. Les modes vibratoires prépondérants sont l'élongation (variation de la distance entre atomes) et la déformation (variations des angles de liaison), qui peuvent être couplés.

La deuxième méthode est la mesure de l'angle de contact. C'est un paramètre intéressant puisqu'il permet de caractériser les propriétés de surface des membranes, comme leur caractère hydrophile/hydrophobe, ou d'obtenir par extrapolation les énergies libres de surface.

Dans cette étude, les angles de contact des membranes CMX équilibrées avec différents électrolytes ont été déterminés en utilisant la technique de la bulle captive.

La dernière méthode est la DSC, couramment utilisée pour étudier les propriétés thermiques de matériaux. Le principe repose sur le fait que lors d'une transition de phase, une certaine quantité d'énergie est échangée avec l'environnement. L'analyse thermique d'un matériau soumis à un cycle de chauffage-refroidissement connu est effectuée, en parallèle avec un matériau de référence soumis aux mêmes conditions. Lorsque la température de transition de phase est atteinte, le matériau absorbe ou dégage de l'énergie. En comparant les flux thermiques avec le matériau de référence, on peut déterminer la quantité d'énergie nécessaire au changement de phase.

Chapitre 3

Propriétés des ions en solution et corrélation avec le transfert de soluté à travers des membranes de nanofiltration et échangeuses d'ions

L'objectif de ce chapitre est de comprendre quelles sont les propriétés des ions susceptibles d'affecter le transfert de la matière organique à travers des membranes. Il se repose sur des corrélations expérimentales mises en évidence précédemment entre les propriétés d'hydratation des ions et la modification du transfert de solutés organiques à travers des membranes utilisées en nanofiltration et en électrodialyse. Ainsi, les clusters formés par l'eau et les cations sont modélisés à différents niveaux d'hydratation afin d'étudier l'effet des interactions entre les molécules d'eau sur les propriétés de solvatation.

L'étude des solutions électrolytiques est un vaste domaine. Dans la plupart des cas, les résultats concernant les propriétés de ces solutions dépendent en outre des méthodes utilisées. L'évaluation du nombre de coordination par des techniques expérimentales fournit des informations sur le sel mais pas sur les ions considérés individuellement. Avec le développement des technologies numériques, la mécanique quantique ou la mécanique moléculaire ont également été utilisées pour étudier les propriétés des ions en solution. Plusieurs travaux sont disponibles dans la littérature, mais dans ce cas également, les résultats dépendent des méthodes mises en œuvre ou des hypothèses.

L'étude des propriétés d'hydratation des ions a été réalisée dans ce travail dans le cadre de la DFT (Density of Functionnal Theory, Théorie de la Fonctionnelle de la Densité) en utilisant la fonctionnelle d'échange-corrélation X3LYP. Cette fonctionnelle est reconnue pour sa capacité à décrire les liaisons hydrogène dans des clusters impliquant des ions. Trois cations (Na^+, Ca^{2+}, et Mg^{2+}) et 2 anions (Cl^- et SO_4^{2-}) interagissant avec un nombre croissant de molécules d'eau ont été étudiés.

Dans la première partie du chapitre, une approche de modélisation est proposée pour calculer les propriétés des ions en interaction avec l'eau. Les nombres de coordination et d'hydratation sont calculés ainsi que les distances entre les molécules d'eau et les ions et les énergies d'interactions entre les molécules d'eau et les ions dans leur couche d'hydratation. Cette approche est tout d'abord validée en comparant les résultats avec ceux de la littérature et les

structures géométriques des couches de coordination sont étudiées.

Dans un deuxième temps, des corrélations sont recherchées entre les énergies d'interaction des ions avec les clusters d'eau et le transfert de sucres à travers des membranes de nanofiltration ou échangeuses d'ions.

Dans le cas de la nanofiltration, des travaux antérieurs ont montré que l'influence des ions sur le transfert des sucres est due principalement à la modification de leur couche d'hydratation.

Dans le cas des membranes échangeuse d'ions, des travaux antérieurs ont montré que les ions modifient les propriétés des membranes à l'échelle macroscopique. Dans cette thèse, une corrélation est établie entre les propriétés des ions et les flux de sucres dans le cas d'une membrane CMX. Cette corrélation relie les flux de sucres à travers la membrane, au sein de laquelle les contre ions équilibrent les charges négatives portées par les chaines du polymère, et les énergies d'interaction de ces contre ions en solution aqueuse. Bien que l'énergie d'interaction entre les ions et l'eau dépende des interactions au sein de la matrice polymère, une bonne prévision des flux est obtenue, ceux-ci étant d'autant plus faibles que l'énergie d'interaction ion-eau est élevée. Evidemment, une telle corrélation doit être considérée avec prudence eu égard à la complexité des mécanismes moléculaires gouvernant le transfert.

La compréhension des mécanismes mis en jeu, en particulier l'influence des ions sur le transfert, est un sujet ambitieux. Les résultats obtenus dans ce chapitre montrent que l'on peut corréler les propriétés des ions en solution et les flux de sucres, ce qui confirme le rôle déterminant des ions. Cette modélisation *ab initio* de l'hydratation des ions est importante car elle fournit un support pour des études ultérieures concernant les mécanismes moléculaires mis en jeu dans l'influence des ions sur le transfert de solutés organiques à travers des membranes. Dans le cas de la nanofiltration la déshydratation des sucres en fonction de la nature des ions doit être étudiée puisqu'il a été montré que c'est le facteur clé. Dans le cas des membranes échangeuses d'ions, c'est la modification structurale du réseau de polymère constituant la membrane qui doit être étudiée en fonction des ions. Cette étude fait l'objet du chapitre suivant.

Chapitre 4

Rôle des interactions non covalentes sur le transfert de sucres à travers une membrane CMX: approche couplant mécanique quantique et mécanique moléculaire

Dans ce chapitre, une approche théorique est effectuée en utilisant une modélisation moléculaire combinée exempte de paramètres ajustables. Des approches antérieures *ab initio* (quantiques) ont mis en évidence le rôle des interactions non covalentes et en particulier des liaisons hydrogène, sur les propriétés des membranes polymères, comme la capacité d'échange d'ions, l'affinité moléculaire, ainsi que l'augmentation non linéaire de la sorption de l'eau en fonction du taux d'additif par exemple. Plus précisément, nous nous intéressons dans ce chapitre aux interactions non covalentes et aux mécanismes par lesquels les ions affectent le transfert des sucres caractérisés par leur flux. Les blocs élémentaires «building blocks» tels que les groupements phényl sulfonates, les monomères de styrène hydratés neutralisés par les différents cations, Na^+, Ca^{2+} et Mg^{2+}, et le glucose hydratés sont assemblés dans des structures supramoléculaires, i.e. complexes glucose-polymère et fragment double de chaine polymère, afin de représenter le différentes parties du système macroscopique.

Afin de représenter avec précision et de manière satisfaisante les interactions mises en jeu, la mécanique quantique est nécessaire. Cependant, étant donné la taille des systèmes étudiés par mécanique quantique, l'approche combinée QM/MM présentée dans le chapitre 2 est utilisée. Les blocs élémentaires sont étudiés au niveau quantique. Lorsque la taille des systèmes excède 100-150 atomes, une approche combinée est adoptée. Les calculs sont réalisés avec le logiciel NWChem.

La modélisation *ab initio* de systèmes polymères est difficile étant donnée le nombre élevé d'atomes mis en jeu et la présence de nombreux conformères ou l'enroulement des chaines. Cette complexité est encore renforcée par la présence des cations. Une analyse conformationnelle des fragments de polymère a donc été nécessaire pour déterminer les conformères les plus stables. Cette recherche a été réalisée par une approche de mécanique moléculaire en utilisant le code Avogadro et le champ de force universel. Les conformères les plus probables ont été déterminés par mécanique quantique puis optimisés par mécanique moléculaire. L'analyse de l'hydratation des contre ions dans les blocs élémentaires de polymère

a montré que le nombre de molécules d'eau présentes dans la 1ère couche d'hydratation décroit (Na^+>Ca^{2+}>Mg^{2+}) comme le flux de sucre observé expérimentalement. Les énergies d'interaction entre le glucose hydraté et les monomères fonctionnels, qui caractérisent la solubilité du glucose dans la matrice, se sont avérées très peu dépendantes du cation. Les valeurs négatives obtenues ont montré cependant que le glucose est solubilisé dans la matrice polymère. Les interactions entre les fragments de polymère ont également été étudiées en utilisant des modèles macromoléculaires. Contrairement aux interactions entre le sucre et le polymère, nous avons montré que les interactions chaine-chaine varient de façon très sensible selon le contre ion de la membrane. Cette dépendance a été mise en évidence en calculant la distance entre les contre ions et l'atome d'oxygène du groupement sulfonique d'un même fragment ou la distance entre deux fragments. Par ailleurs, les résultats ont montré qu'une diminution de cette distance est corrélée à une diminution du flux de sucre montrant ainsi le lien étroit entre des grandeurs à l'échelle moléculaire et des grandeurs macroscopiques. Cependant, la comparaison des distances avec le diamètre effectif calculé pour le glucose suggère l'existence d'un mécanisme additionnel contribuant au transfert de soluté.

Deux valeurs théoriques ont été définies. La première, $\overline{\Delta E}_{H_2O}^{X}$représente pour un contre ion donné, *x*, l'énergie d'interaction par molécule d'eau piégée entre deux fragments de polymère. En d'autres termes, on considère que l'énergie totale de cohésion entre 2 fragments est répartie sur les molécules d'eau piégées entre ces deux fragments. La deuxième grandeur, $\overline{\Delta E}_{wire}^{x}$, est pour un contre ion donné, x, l'énergie due aux interactions électrostatiques par liaison hydrogène. On considère donc que l'énergie totale est répartie sur les connections entre les molécules d'eau.

En comparant les flux expérimentaux normalisés et les valeurs de $\overline{\Delta E}_{H_2O}^{X}$ et $\overline{\Delta E}_{wire}^{x}$ une corrélation a été mise en évidence. En effet, nous avons montré qu'une énergie d'interaction plus faible correspond systématiquement à un flux de sucre plus élevé. Ainsi il semble que dans les conditions étudiées, le flux de sucre soit contrôlé par les interactions non covalentes

impliquant les molécules d'eau piégées dans les fragments. Ce travail a démontré également que ces interactions non covalentes dépendent de la nature du contre ion et souligné le rôle crucial des molécules d'eau de coordination des contre ions dans le réseau polymère.

Chapitre 5

Caractérisation de la membrane CMX conditionnée par différents électrolytes

L’objectif ce chapitre est d'étudier l'influence des ions en solution sur les caractéristiques physiques de la membrane CMX à l'aide de méthodes expérimentales et numériques. En outre, ces données sont mises en parallèle avec les grandeurs calculées précédemment ainsi qu'avec les grandeurs de transport afin de confirmer les résultats des calculs et de valider les mécanismes moléculaires proposés.

Les propriétés géométriques calculées peuvent être également associées aux flux de sucres à travers la membrane CMX. En particulier, la distance entre les contre ions et le groupement sulfonique peut être liée à un changement des propriétés de transport des membranes comme cela a été précédemment observé par Karpenko-Jareb et al.. Plus précisément, les distances les plus faibles, i.e. $Mg^{2+} < Ca^{2+} < Na^{+}$, correspondent aux flux les plus faibles pour le xylose, le glucose et le saccharose. L'influence de la distance entre les contre ions et le groupement sulfonique sur le transfert pour les trois sucres considérés est décrite par une variation linéaire. Ainsi, l'hypothèse de Karpenko-Jereb et al. concernant le transfert des ions à travers la membrane échangeuse d'ions peut être étendue au transfert de solutés organiques neutres.

Une analyse vibrationnelle complète a été réalisée sur la membrane CMX en présence de différents cations par des méthodes expérimentales et numériques (mécanique quantique, DFT). Les spectres expérimentaux et calculés présentent une diminution du nombre d'onde des pics caractérisant les vibrations d'élongation des liaisons O-H des molécules d’eau ou les vibrations de déformation S-O en contact avec les cations. Nous avons observé que cette diminution est d’autant plus forte que le cation est hydraté. Le déplacement vers des nombres d'onde plus faibles traduit une diminution de l'énergie du mode de vibration considéré qui signifie une plus forte interaction entre les molécules d'eau et le site cationique. Les énergies de liaisons S-O et O-H plus faibles observées dans les systèmes contenant Ca^{2+} et Mg^{2+} signifient que l'oxygène des groupes sulfoniques ou l'hydrogène de l'eau forment des liaisons hydrogène plus fortes dans les systèmes $Ph\text{-}SO3^{-}$... Ca^{2+} ou Mg^{2+} par rapport à Na^{+}. Ainsi, la tendance observée pour les cations monoatomiques est en accord avec les résultats de modélisation obtenus précédemment,

pour lesquels les interactions suivent une tendance similaire aux déplacements des nombres d'ondes observés dans ce chapitre.

Des mesures d'angle de contact ont été effectuées avec la membrane CMX équilibrée avec différents électrolytes (LiCl, KCl, NaCl, NH_4Cl, $CaCl_2$ et $MgCl_2$). Les énergies de surface déduites de ces mesures ont montré que l'affinité du polymère pour l'eau dépend de l'hydratation du contre-ion de la membrane. En effet, nous avons observé qu'une membrane conditionnée avec un cation plus hydraté perd une partie de son affinité avec l'eau, même si elle reste hydrophile. Ce comportement peut être attribué à une diminution de l'accessibilité des groupes fonctionnels sulfonés suite à une attraction plus élevée avec les cations.

L'analyse des résultats obtenus en utilisant la DSC a montré que l'état de l'eau à l'intérieur de la membrane CMX change selon le contre-ion de celle-ci. En effet, il a été observé que la diminution du point de solidification de l'eau contenue dans le polymère est d'autant plus prononcée que le contre-ion de la membrane est hydraté. Ainsi, les interactions polymère/cation/eau sont d'autant plus importantes que le contre-ion de la membrane est hydraté. En outre, une diminution du point de solidification de l'eau piégée dans la membrane correspond à un volume libre plus faible. Ainsi, dans notre cas, la baisse du point de solidification peut également être associée à une diminution du volume accessible à l'eau qui est directement lié à la perméabilité de la membrane à l'eau ainsi qu'aux solutés.

Les approches théoriques et expérimentales utilisées dans ce travail suggèrent que le cation constituant le contre-ion de la membrane CMX a un fort impact sur l'état de l'eau présente dans le système. En particulier, les interactions non covalentes entre les différents constituants du système sont plus influencées par des cations fortement hydratées.

Chapitre 6

Conclusion

Différentes études menées ces dernières années ont montré que les performances des procédés membranaires, en particulier la Nanofiltration ou l'Electrodialyse, peuvent être significativement affectées lorsqu'ils sont utilisés pour traiter des solutions contenant une quantité importante de sels. En effet, il a été observé, avec des membranes de NF, ainsi qu'avec celles utilisées dans l'électrodialyse, que le transfert d'un soluté organique change selon la nature et la concentration des ions. Concernant la nanofiltration, il a été montré que la modification du transfert est principalement fixée par l'influence de l'électrolyte sur les propriétés de soluté. Il a été également confirmé que des ions plus hydratés ou des concentrations plus élevées conduisent à une augmentation plus importante du transfert de soluté. A contrario, dans le cas de membranes échangeuses d'ions, la modification du transfert de soluté avec l'électrolyte est principalement fixée par la modification des propriétés de la membrane. Dans ce cas, contrairement à la Nanofiltration, une diminution du transfert a été observée avec l'augmentation de l'hydratation du contre-ion de la membrane. Ainsi, bien que différents mécanismes soient impliqués en fonction des propriétés de la membrane ou du soluté, dans tous les cas, la modification du transfert a été corrélée à l'état d'hydratation des ions.

Les phénomènes observés à l'échelle macroscopique, c'est-à-dire la modification du transfert soluté organique selon la composition ionique, résultent de mécanismes siégeant à l'échelle moléculaire. Ainsi, la connaissance des interactions non covalentes multiples à l'échelle nanométrique, entre le polymère, l'eau et les solutés (ions, espèces organiques) constitue un verrou pour l'amélioration des procédés membranaires. De nouvelles approches permettant de caractériser ces systèmes à l'échelle microscopique sont donc nécessaires.

C'est ce que nous avons entrepris de faire dans ces travaux. Une approche multi-échelle fondamentale a été proposée, combinant des outils théoriques et expérimentaux afin d'obtenir les paramètres microscopiques et macroscopiques caractérisant les interactions concernées pour différentes compositions ioniques.

Dans un premier temps, les propriétés des ions ont été étudiées, puisqu'il a été démontré qu'ils

affectent les performances du procédé lors de la séparation de solutés organiques à travers des membranes. Les propriétés calculées ont été corrélées avec des données expérimentales obtenues dans des travaux antérieurs étudiant le transfert de sucres par diffusion à travers des membranes de Nanofiltration et échangeuses d'ions en fonction de la composition ionique. Des corrélations satisfaisantes ont été obtenues entre les propriétés calculées caractérisant l'hydratation des ions et les grandeurs de transfert de sucres.

Dans un second temps, le transfert d'une espèce neutre, le glucose, à travers une membrane échangeuse de cations (CMX) a été considéré. Les interactions non covalentes qui siègent à l'échelle moléculaire, entre le soluté et un fragment de polymère ainsi qu'entre deux fragments de polymère ont été étudiées en utilisant une approche combinée Mécanique Quantique/ Mécanique Moléculaire. Les résultats les plus significatifs ont été obtenus au cours de l'évaluation des énergies d'interaction polymère-polymère. En effet, il a été observé que la distance moyenne entre le contre-ion et l'oxygène du groupe sulfonique appartenant au même fragment ainsi que la distance entre deux fragments de polymère sont modifiées en fonction de la nature du contre-ion de la membrane. Les résultats ont montré qu'une diminution de cette distance est corrélée à une diminution du flux de sucre mettant ainsi en évidence le lien étroit entre des grandeurs à l'échelle moléculaire et des grandeurs macroscopiques. En outre, une relation entre l'énergie d'interaction et l'eau contenue dans la structure polymérique, formant des liaisons hydrogènes entre les chaînes, a été soulignée. Plus précisément, nous avons montré qu'une énergie d'interaction plus faible correspond systématiquement à un flux de sucre plus élevé. Ainsi il semble que dans les conditions étudiées, le flux de sucre soit contrôlé par les interactions non covalentes impliquant les molécules d'eau piégées dans les fragments. Ce travail a démontré également que ces interactions non covalentes dépendent de la nature du contre ion et souligné le rôle crucial des molécules d'eau de coordination des contre ions dans le réseau polymère.

Dans le dernier chapitre, la membrane CMX a été caractérisée dans différents électrolytes à

l'aide de méthodes numériques et expérimentales (IR, DSC et angle de contact). Les résultats issus des approches expérimentales et théoriques à l'échelle moléculaire ont montré que le cation utilisé comme contre-ion pour équilibrer la membrane CMX a un fort impact sur l'état de l'eau contenue dans la membrane. En particulier, les interactions non covalentes entre les différents constituants du système sont plus influencées par des cations fortement hydratées. Enfin, il a été démontré que l'influence de l'hydratation du contre-ion sur les interactions non covalentes et les flux de sucre peut être corrélée à la fois au niveau qualitatif que quantitatif.

Les perspectives de ce travail sont nombreuses, tant sur le plan expérimental que théorique.

Concernant les méthodes numériques, la modélisation des interactions sucre/électrolyte reste un verrou à lever pour améliorer la compréhension du transfert d'un soluté neutre à travers une membrane de Nanofiltration, ce transfert étant principalement fixé par l'influence de la composition ionique sur les propriétés du soluté. A titre d'exemple, des calculs pourraient être envisagés afin de déterminer si les ions affectent uniquement la couche d'hydratation des sucres, ou s'ils sont susceptibles de modifier également leur structure.

Pour les membranes CMX, l'approche numérique conduite dans ce travail pourra être utilisée comme point de départ afin d'étudier l'effet du champ électrique sur la structure polymérique ou sur les interactions non covalentes impliquées. Par ailleurs, les informations obtenues par le biais de la mécanique quantique pourraient être exploitées pour ajuster les champs de Force afin d'effectuer des calculs de dynamique moléculaire avec des paramètres ad hoc. Cela permettrait d'élargir les dimensions du système et de modéliser la diffusion de la matière organique à travers la membrane.

La caractérisation expérimentale de la membrane sous différents environnements est également un point important. Différentes méthodes sont envisageables pour étudier les propriétés mécaniques d'une membrane polymérique à l'échelle moléculaire. Des techniques innovantes, capables de mesurer le module de Young et autres propriétés mécaniques de la membrane par microscopie à force atomique (AFM) pourraient être intéressantes. La détermination de la

teneur en eau absorbée pourrait également être intéressante, non seulement pour caractériser la membrane mais également pour comparer les résultats avec ceux issus de la modélisation. Une autre exploitation des données consiste à déterminer le coefficient de diffusion de l'eau dans la membrane équilibrée par différents contre-ions. Ce coefficient peut également être comparé avec les données issues de la modélisation comme l'énergie d'interaction de chaîne-chaîne.

Pour conclure, cette thèse ouvre la voie à la compréhension des mécanismes qui gouvernent le transfert d'espèce neutre à travers des membranes en présence de sels. Ainsi, cette étude peut servir de référence pour de nouveaux développements dans l'intensification des procédés pour le traitement des fluides complexes.

Nomenclature

Abbreviations

AEM	Anion Exchange Membrane
AMV	apparent molar volume
CEM	Cation Exchange-Membrane
CN	Coordination Number
DFT	Density Functional Theory
DSC	Differential Scanning Calorimetry
ED	ElectroDialysis
F_{HK}	external potential for a quantum system
g	scaling factor for QM/MM
H	Hamiltonian operator
HF	Hartree-Fock
IEM	Ion-Exchange Membrane
IR	Infra-Red
KET	N-ethyl-o,p-toluensulfonamide,
MM	Molecular Mechanics
NF	NanoFiltration
N_H	Hydration Number
PEG	Polyethylene glycol
PES	potential energy surface
QM	Quantum Mechanics
QM/MM	Quantum Mechanics/Molecular Mechanics
STO	Slater-type orbitals
T_{el}	electron kinetic energy
V_{coul}	Coulomb potential
$V_{el\text{-}el}$	Electron-electron force

$V_{exc-corr}$	exchange - correlation energy
V_{ext}	External potential
V_{nu-el}	nucleus-electron force

Symbols

c	Speed of light	(m s^{-1})
d	distance	(Å)
E	energy of a generic system	(a.u)
$E_{complex}$	energy of a ion-water structure	(a.u)
E_{ion}	energy of an isolated ion in vacuum	(a.u)
$E_{Hyd.shell}$	energy of a water cluster	(a.u)
$\Delta E^{x}_{chain-chain}$	cohesion energy between two polymer fragments	(Kcal mol^{-1})
$\overline{\Delta E}^{X}_{H_2O}$	Interaction energy per water	(Kcal mol^{-1})
ΔE_i^w	ion-water cluster interaction energy	(Kcal mol^{-1})
$\overline{\Delta E}^{x}_{wire}$	Interaction energy per wire	(Kcal mol^{-1})
ΔH	hydration enthalpy	(Kcal mol^{-1})
I	IR intensity	(KM mol^{-1})
J_s, J_b	Sugar Flux	(mol m^{-2} s^{-1})
M_x, M_y	atomic mass	(g)
k,	force constants of the vibrational modes	(dyne cm^{-1})
ΔV	variation of AMV	-
z_a, z_b	valence number of ion	e

Greek Symbols

γ_l	solution surface free energy
γ_s	membrane surface free energy
Θ	contact angle
μ	reduced mass of the atoms,
ν	vibrational frequency
π	Pi
(ρ_{el})	electron density
σ	standard deviation
Φ	interaction parameter for contact angle
ϕ	atomic orbital
Ψ	wave function
ψ	molecular orbital

Annexes

Annex I

Used .par file for Amber calculation

```
Electrostatic 1-4 scaling factor     0.833333
Relative dielectric constant     1.000000
Parameters epsilon R*
Atoms
CA     12.01000 3.59824E-01 1.90800E-01                    1 1111111111
           6 1.79912E-01 1.90800E-01
CT     12.01000 4.57730E-01 1.90800E-01                    1 1111111111
           6 2.28865E-01 1.90800E-01
HA      1.00800 6.27600E-02 1.45900E-01                    1 1111111111
           1 3.13800E-02 1.45900E-01
HC      1.00800 6.56888E-02 1.48700E-01                    1 1111111111
           1 3.28444E-02 1.48700E-01
HWS     1.00800 6.56887E-02 6.00000E-02                    1 1111111111
     Q       1 3.28444E-02 6.00000E-02
Na     22.99000 1.15897E-02 1.86800E-01                    1 1111111111
          11 5.79485E-03 1.86800E-01
O2     16.00000 8.78640E-01 1.66120E-01                    1 1111111111
           8 4.39320E-01 1.66120E-01
OWS    15.99940 7.11280E-01 1.68370E-01                    1 1111111111
     Q       8 3.55640E-01 1.68370E-01
S      32.06000 1.04600E+00 2.00000E-01                    1 1111111111
          16 5.23000E-01 2.00000E-01
Mg     24.30500 4.30952E-02 1.36000E-01                    1 1111111111
          12 2.15476E-02 1.36000E-01
Ca     40.08000 3.78520E-02 1.74000E-01                    1 1111111111
          20 1.89260E-02 1.74000E-01
Bonds
CA   -CA      0.14000 3.92459E+05
CA   -CT      0.15100 2.65266E+05
CA   -HA      0.10800 3.07106E+05   -0.050000
CT   -CT      0.15260 2.59408E+05
CT   -HC      0.10900 2.84512E+05   -0.050000
CA   -S       0.17590 2.20979E+05
Angles
HC   -CT   -HC      1.91114 2.92880E+02
CT   -CT   -HC      1.91114 4.18400E+02
CT   -CT   -CT      1.91114 3.34720E+02
CA   -CT   -CT      1.98968 5.27184E+02
CA   -CT   -HC      1.91114 4.18400E+02
CA   -CA   -CT      2.09440 5.85760E+02
CA   -CA   -CA      2.09440 5.27184E+02
CA   -CA   -HA      2.09440 4.18400E+02
CA   -CA   -S       2.07885 5.23350E+02
CA   -S    -O2      1.87605 5.63543E+02
Proper dihedrals
    -CT   -CT   -        0.00000 6.50844E-01    3
```

HC -CT -CT -CT 0.00000 6.69440E-01 3
HC -CT -CT -HC 0.00000 6.27600E-01 3
CT -CT -CT -CT 3.14159 8.36800E-01 1
-CA -CT - 0.00000 0.00000E+00 2
-CA -CA - 3.14159 1.51670E+01 2
-CA -S - 3.14159 3.26570E+01 6
Improper dihedrals
CA -CA -CA -CT 3.14159 4.60240E+00 2
- -CA -HA 3.14159 4.60240E+00 2
S -CA -CA -CA 3.14159 4.60548E+00 2

Used .par file for Charmm calculation

Electrostatic 1-4 scaling factor 1.000000
Relative dielectric constant 1.000000
Parameters epsilon R*
Atoms
CA 12.01100 2.92880E-01 1.99240E-01 1 1111111111
6 2.92880E-01 1.99240E-01
CT1 12.01100 8.36800E-02 2.27500E-01 1 1111111111
6 4.18400E-02 1.90000E-01
CT2 12.01100 2.30120E-01 2.17500E-01 1 1111111111
6 4.18400E-02 1.90000E-01
CT3 12.01100 3.34720E-01 2.06000E-01 1 1111111111
6 4.18400E-02 1.90000E-01
HA 1.00800 9.20480E-02 1.32000E-01 1 1111111111
1 9.20480E-02 1.32000E-01
HP 1.00800 1.25520E-01 1.35820E-01 1 1111111111
1 1.25520E-01 1.35820E-01
HWS 1.00800 1.92464E-01 2.24500E-02 1 1111111111
1 1.92464E-01 2.24500E-02
O 15.99900 5.02080E-01 1.70000E-01 1 1111111111
8 5.02080E-01 1.40000E-01
OWS 15.99940 6.36386E-01 1.76820E-01 1 1111111111
8 6.36386E-01 1.76820E-01
S 32.06000 1.88280E+00 2.00000E-01 1 1111111111
16 1.88280E+00 2.00000E-01
Na 22.99000 4.69000E-02 1.36375E-01 1 1111111111
11 2.34500E-02 1.36375E-01
Cross
Bonds
CA -CA 0.13750 2.55224E+05
CT1 -CT1 0.15000 1.86188E+05
CT2 -CA 0.14900 1.92464E+05
CT2 -CT1 0.15380 1.86188E+05
CT2 -CT2 0.15300 1.86188E+05
CT3 -CA 0.14900 1.92464E+05
CT3 -CT1 0.15380 1.86188E+05
CT3 -CT2 0.15280 1.86188E+05
CT3 -CT3 0.15300 1.86188E+05
HA -CA 0.10830 2.84512E+05
HA -CT1 0.11110 2.58571E+05
HA -CT2 0.11110 2.58571E+05
HA -CT3 0.11110 2.69450E+05
HP -CA 0.10800 2.84512E+05
CA -S 0.11110 2.58744E+05
S -O 0.14480 4.52174E+05
Angles
CA -CA -CA 2.09440 3.34720E+02 0.24162 2.92880E+02
CT1 -CT2 -CA 1.87623 4.33462E+02 0.00000 0.00000E+00
CT1 -CT2 -CT1 1.98095 4.88273E+02 0.25610 9.33869E+01
CT2 -CA -CA 2.13454 3.83254E+02 0.00000 0.00000E+00
CT2 -CT1 -CT1 1.93732 4.46433E+02 0.25610 6.69440E+01

CT2 -CT2 -CA 1.88496 4.35136E+02 0.00000 0.00000E+00
CT2 -CT2 -CT1 1.98095 4.88273E+02 0.25610 9.33869E+01
CT2 -CT2 -CT2 1.98269 4.88273E+02 0.25610 9.33869E+01
CT2 -CT3 -CT1 1.98095 4.88273E+02 0.25610 9.33869E+01
CT3 -CA -CA 2.13454 3.83254E+02 0.00000 0.00000E+00
CT3 -CT1 -CT1 1.89368 4.46433E+02 0.25610 6.69440E+01
CT3 -CT1 -CT2 1.98968 4.46433E+02 0.25610 6.69440E+01
CT3 -CT1 -CT3 1.98968 4.46433E+02 0.25610 6.69440E+01
CT3 -CT2 -CA 1.87623 4.33462E+02 0.00000 0.00000E+00
CT3 -CT2 -CT1 1.98095 4.88273E+02 0.25610 9.33869E+01
CT3 -CT2 -CT2 2.00713 4.85344E+02 0.25610 6.69440E+01
CT3 -CT2 -CT3 1.98968 4.46433E+02 0.25610 6.69440E+01
HA -CA -CA 2.09440 2.42672E+02 0.21525 2.09200E+02
HA -CT1 -CT1 1.92161 2.88696E+02 0.21790 1.88531E+02
HA -CT1 -CT2 1.92161 2.88696E+02 0.21790 1.88531E+02
HA -CT1 -CT3 1.92161 2.88696E+02 0.21790 1.88531E+02
HA -CT1 -HA 1.90241 2.97064E+02 0.18020 4.51872E+01
HA -CT2 -CA 1.87623 4.12542E+02 0.00000 0.00000E+00
HA -CT2 -CT1 1.92161 2.79742E+02 0.21790 1.88531E+02
HA -CT2 -CT2 1.92161 2.21752E+02 0.21790 1.88531E+02
HA -CT2 -CT3 1.92161 2.89533E+02 0.21790 1.88531E+02
HA -CT2 -HA 1.90241 2.97064E+02 0.18020 4.51872E+01
HA -CT3 -CA 1.87623 4.12542E+02 0.00000 0.00000E+00
HA -CT3 -CT1 1.92161 2.79742E+02 0.21790 1.88531E+02
HA -CT3 -CT2 1.92161 2.89533E+02 0.21790 1.88531E+02
HA -CT3 -CT3 1.92161 3.13800E+02 0.21790 1.88531E+02
HA -CT3 -HA 1.89194 2.97064E+02 0.18020 4.51872E+01
HP -CA -CA 2.09440 2.51040E+02 0.21525 1.84096E+02
CA -CA -S 2.16000 4.60548E+02
CA -S -O 2.12000 7.11756E+02
O -S -O 2.18940 1.08857E+03
Proper dihedrals
CA -CA -CA -CA 3.14159 1.29704E+01 2
CT1 -CT2 -CA -CA 3.14159 9.62320E-01 2
CT2 -CA -CA -CA 3.14159 1.29704E+01 2
CT2 -CT2 -CT2 -CT2 0.00000 6.27600E-01 1
CT3 -CA -CA -CA 3.14159 1.29704E+01 2
CT3 -CT2 -CA -CA 3.14159 9.62320E-01 2
CT3 -CT2 -CT2 -CT2 0.00000 6.27600E-01 1
CT3 -CT2 -CT2 -CT3 0.00000 6.27600E-01 1
HA -CA -CA -CA 3.14159 1.46440E+01 2
HA -CA -CA -HA 3.14159 1.04600E+01 2
HA -CT1 -CT2 -CA 0.00000 1.67360E-01 3
HA -CT3 -CT2 -CA 0.00000 1.67360E-01 3
HP -CA -CA -CA 3.14159 1.75728E+01 2
HP -CA -CA -CT2 3.14159 1.75728E+01 2
HP -CA -CA -CT3 3.14159 1.75728E+01 2
HP -CA -CA -HP 3.14159 1.00416E+01 2
-CT1 -CT1 - 0.00000 8.36800E-01 3
-CT1 -CT2 - 0.00000 8.36800E-01 3
-CT1 -CT3 - 0.00000 8.36800E-01 3

```
    -CT2  -CA   -       0.00000 0.00000E+00    6
    -CT2  -CT2  -       0.00000 8.15880E-01    3
    -CT2  -CT3  -       0.00000 6.69440E-01    3
    -CT3  -CA   -       0.00000 0.00000E+00    6
CA   -CA   -CA   -S      0.00000 8.37360E-01    3
HP   -CA   -CA   -S      0.00000 8.37360E-01    3
CA   -CA   -S    -O      0.00000 0.00000E+00    3
Improper dihedrals
CA   -    -    -CA     0.00000 7.53120E+02
```

Annex II

Complete assignment of computed IR bands

Absorption wavenumber (cm-1)	Intensity (KM/mol)	Assignment
675.716	219.584	H2O R, CH CSC, SO3 ST(S)
813.793	29.946	H2O TW, CHRB,CH3 ST
820.745	25.061	CH RW
834.179	306.346	H2OTW, OHST, CH RR
979.939	219.3	SO3 ST(S)
1044.41	5.074	CCC RSC
1068.861	10.612	CH CSC
1115.051	239.575	SOST(S)(S1-O2), CHRR
1128.33	79.275	CH RB
1146.661	18.883	CH RSC(Kekule)
1155.66	273.311	SO ST(S) (S1-O1),
1438.418	7.974	CC RST(Kekule)
1509.245	8.036	CH3 SC
1510.584	14.197	CH3 SC
1536.476	11.198	CH RTW
1650.472	10.718	CC RST
1771.899	73.216	H2O SC
3033.68	32.169	CH CST

3086.871	23.431	CH CST
3112.215	19.015	CH CST
3166.553	23.805	CH RST
3167.663	16.004	CH RST
3209.341	3.793	CH RST
3461.97	656.977	OH ST (O7-H2)
3865.956	59.059	OH ST (O7-H1)

Table AII.1: Calculated Infrared Spectrum of structure with Na^+ (Fig. V.1) and Assignments

Absorption wavenumber (cm^{-1})	Intensity (KM/mol)	Assignment
639.898	63.63	H_2O_R
656.375	239.788	CH^{C}_{R}
670.993	12.937	H_2O_R, CH^{R}_{B}, SO_3
774.062	25.253	H_2O_R, CH^{R}_{B}, SO_3
793.979	617.398	H_2O_R
804.2	37.037	CH^{R}_{W}
833.254	10.584	CH^{R}_{W}
841.166	7.505	CH^{R}_{TO}
847.442	9.845	CH^{R}_{TO}
852.762	119.833	H_2O_{TW}
873.074	8.444	CH^{C}_{R}, CH^{R}_{W}
880.435	6.069	CH^{C}_{R}, CH^{R}_{W}
928.181	250.091	$SO_{ST(AS)}$ (S1-O2, S2-O6), CH^{C}_{B}
946.99	30.183	CH^{R}_{TO}
950.589	5.648	CH^{R}_{TO}, $SO_{3\ ST(S)}$
963.454	171.392	CH^{R}_{TO}, $SO_{3\ ST(S)}$
965.473	332.935	$SO_{3\ ST(S)}$
1037.14	21.256	CH^{R}_{B}, CH^{C}_{R}
1038.924	20.38	$C\text{-}C\text{-}C^{R}_{SC}$
1075.193	89.963	SO_{ST} (S1-O1, S2-O4)

1087.647	230.486	SO_{ST}(S1-O2, S1-O3, S2-O5, S2-O6)
1126.474	9.778	CH^{R}_{B}
1128.95	186.237	CH^{R}_{B}
1132.475	28.969	CH^{R}_{SC}
1147.964	18.725	$CH^{R}_{SC(Kekule)}$
1267.659	9.364	CH^{C}_{SC}
1270.385	488.891	SO_{ST} (S1-O3, S2-O5)
1273.852	39.983	SO_{ST} +CH^{C}_{S}
1279.165	29.771	SO_{ST} +CH^{C}_{S}
1396.845	5.788	CH^{C}_{SC}
1444.404	9.868	$CC^{R}_{ST(Kekule)}$, CH^{C}_{ST},
1446.826	14.484	$CC^{R}_{ST(Kekule)}$, CH^{C}_{ST},
1499.633	6.109	CH^{C}_{SC}
1501.784	7.02	CH^{C}_{SC}
1507.84	9.334	CH^{C}_{SC}
1536.35	11.42	$CH^{R}_{TW,}$ $CH^{C}_{ST,}$
1647.95	5.54	C-C $^{R}_{ST}$
1649.153	12.659	C-C $^{R}_{ST}$
1715.853	49.92	H_2O_{SC}
3023.064	13.756	CH^{C}_{ST}
3027.692	20.739	CH^{C}_{ST}

3035.57	40.171	CH $^{C}_{ST}$
3059.857	25.529	CH $^{C}_{ST}$
3061.583	31.826	CH $^{C}_{ST}$
3074.828	64.16	CH $^{C}_{ST}$
3164.648	9.459	CH $^{R}_{ST}$
3166.313	15.223	CH $^{R}_{ST}$
3169.501	6.914	CH $^{R}_{ST}$
3173.202	20.417	CH $^{R}_{ST}$
3469.224	210.411	H_20 $_{ST(S)}$
3530.032	712.222	H_20 $_{ST(AS)}$

Table AII.2: Calculated Infrared Spectrum of structure with Ca^{2+} (Fig. V.2) and Assignments

Absorption wavenumber (cm^{-1})	Intensity (KM/mol)	Assignment
642.68	165.776	$H_2O\ _R$+ CH $^C_{SC}$
668.628	84.599	$H_2O\ _R$+ CH $^C_{SC}$
690.782	89.802	$H_2O\ _R$+ CH $^C_{SC}$
776.354	9.603	CH ^R_B, CH $^C_{SC}$
807.411	36.023	CH ^C_W
819.562	29.332	CH ^C_W
827.748	251.757	$H_2O\ _{TW}$
840.858	40.683	CH ^R_W, CH $^C_{TW}$
872.953	13.602	CH ^R_W, CH $^C_{TW}$
884.669	5.634	CH ^R_W, CH $^C_{TW}$
946.655	119.791	$SO_{3\ ST(S)}$
957.269	37.043	CH $^R_{TO}$ $SO_{3\ ST}$
964.579	33.31	CH $^R_{TO}$ $SO_{3\ ST}$
967.009	52.997	CH $^R_{TO}$ $SO_{3\ ST}$
973.335	318.651	$SO_{3\ STsym}$ CH $^R_{TO}$
1021.632	183.035	SO $_{ST}$ (S1-O1)
1036.661	26.66	CCC $^R_{SC}$
1040.816	10.289	CCC $^R_{SC}$
1043.568	22.858	CCC $^R_{SC}$
1056.544	6.389	C-C $^C_{ST}$

1069.348	287.871	SO $_{ST}$ (S2-O6) CH $^{R}_{B}$
1118.288	39.601	CH $^{R}_{B}$
1124.174	129.343	CH $^{R}_{B}$
1133.146	9.153	CH $^{R}_{S}$
1145.58	11.232	CH $^{R}_{SC\ (Kekule)}$
1259.281	21.657	CH $^{C}_{TW}$
1266.866	358.287	SO $_{ST}$ (S2-O5) , CH$^{C}_{SC}$
1278.145	76.276	SO $_{ST}$ (S1-O3) , CH$^{C}_{SC}$
1280.648	121.593	SO $_{ST}$ (S1-O3) , CH$^{C}_{SC}$
1447.024	13.024	CC$^{R}_{ST(Kekule)}$, CH $^{C}_{SC}$,
1447.398	16.161	CC$^{R}_{ST(Kekule)}$, CH $^{C}_{SC}$,
1500.121	7.673	CH $^{C}_{SC}$
1505.192	5.425	CH $^{C}_{SC}$
1508.173	10.046	CH $^{C}_{SC}$
1535.354	10.809	CH $^{R}_{TW}$
1646.858	7.577	CC $^{R}_{ST}$
1647.876	12.351	CC $^{R}_{ST}$
1761.435	131.397	H_2O $_{SC}$
3021.216	18.921	CH $^{C}_{ST}$
3031.409	21.223	CH $^{C}_{ST}$
3038.631	38.324	CH $^{C}_{ST}$

3056.857	19.718	CH $^{C}_{ST}$
3068.23	34.639	CH $^{C}_{ST}$
3076.742	60.597	CH $^{C}_{ST}$
3165.993	13.191	CH $^{R}_{ST}$
3167.479	23.947	CH $^{R}_{ST}$
3172.937	20.605	CH $^{R}_{ST}$
3182.997	844.037	OH $_{ST}$ (O7-H2)
3184.712	149.316	CH $^{R}_{ST}$
3891.443	99.34	OH $_{ST}$ (O7-H1)

Table AII.3: Calculated Infrared Spectrum of structure with Ca^{2+} (Fig. V.3) and Assignments

Absorption wavenumber (cm^{-1})	Intensity (KM/mol)	Assignment
609.518	26.171	$CH\ ^{C,R}{}_{R}$
623.355	78.5	$CH\ ^{C,R}{}_{R}$
647.794	38.526	$H_2O\ _{R}$, $CH\ ^{C,R}{}_{R}$
650.059	12.91	$H_2O\ _{R}$, $CH\ ^{C,R}{}_{R}$
651.129	13.542	$H_2O\ _{R}$, $CH\ ^{C,R}{}_{R}$
671.507	211.412	$H_2O\ _{R}$, $CH\ ^{R}{}_{R}$,
696.852	205.695	$H_2O\ _{R}$, $OH\ _{ST}$ (O7-H2) $CH\ ^{C,R}{}_{R}$
731.739	5.709	$CH\ ^{R}{}_{TO}$, $CH\ ^{C}{}_{SC}$
776.908	11.291	$CH\ ^{R}{}_{B}$, $CH\ ^{C}{}_{SC}$
807.491	34.896	$CH\ ^{R}{}_{B}$, $CH\ ^{C}{}_{SC}$
817.444	6.634	$CH\ ^{R}{}_{W}$, $CH\ ^{C}{}_{SC}$
835.675	28.229	$CH\ ^{R}{}_{W}$, $CH\ ^{C}{}_{SC}$
848.445	10.709	$CH\ ^{R}{}_{TO}$, $CH\ ^{C}{}_{SC}$
850.372	10.041	$CH\ ^{R}{}_{TO}$
872.471	16.591	$CH\ ^{C}{}_{R}$
873.533	331.647	$H_2O\ _{TW}$, $CH\ ^{C}{}_{R}$
934.502	134.632	$SO_3\ _{ST(S)}$ (far)
954.175	114.348	$CH\ ^{R}{}_{TO}$, $CH\ ^{C}{}_{R}$
959.612	57.543	$CH\ ^{R}{}_{TO}$, $CH\ ^{C}{}_{R}$
963.2	161.01	$CH\ ^{R}{}_{TO}$, $CH\ ^{C}{}_{R}$

998.601	208.918	SO $_{ST}$ (S2-O6)
1038.658	32.036	CCC $^{R}{}_{SC}$
1057.929	7.237	CH $^{C}{}_{R}$
1067.092	230.835	SO $_{ST}$ (S1O3)
1116.54	34.489	CH $^{R}{}_{B}$
1122.466	123.799	CH $^{R}{}_{B}$
1133.961	5.582	CH $^{C, R}{}_{SC}$
1147.8	9.8	CH $^{C,}{}_{SC(Kekule)}$
1276.311	209.081	SO $_{ST}$ (S1-O3) CH$^{C}{}_{TW}$
1282.037	179.298	CH $^{C}{}_{TW, SC}$
1288.14	153.528	SO $_{ST}$ (S2-O5)
1446.709	15.477	CC$^{R}{}_{ST(Kekule)}$,
1448.184	14.649	CC$^{R}{}_{ST(Kekule)}$,
1499.698	7.861	CH $^{C}{}_{SC}$
1506.213	12.374	CH $^{C}{}_{SC}$
1534.868	11.175	CH $^{R}{}_{TW}$, CH$^{C}{}_{SC}$
1645.564	9.07	CC$^{R}{}_{ST}$
1646.658	13.558	CC$^{R}{}_{ST}$
1741.791	142.398	H_20 $_{SC}$
3023.42	17.795	CH $^{C}{}_{ST}$
3031.843	21.04	CH $^{C}{}_{ST}$

3040.843	36.585	CH $^{C}_{ST}$
3058.909	17.577	CH $^{C}_{ST}$
3068.299	30.134	CH $^{C}_{ST}$
3078.855	61.514	CH $^{C}_{ST}$
3166.963	14.682	CH $^{R}_{ST}$
3172.811	11.392	CH $^{R}_{ST}$
3180.516	8.498	CH $^{R}_{ST}$
3182.08	8.689	CH $^{R}_{ST}$
3234.396	786.292	OH $_{ST}$ (O7-H1)
3875.553	113.246	OH $_{ST}$ (O7-H2)

Table AII.4: Calculated Infrared Spectrum of structure with Mg^{2+} (Fig. V.4) and Assignments

Absorption wavenumber (cm^{-1})	Intensity (KM/mol)	Assignment
607.791	24.262	$CH\ ^{C,R}{}_{R}$
623.513	85.57	$CH\ ^{C,R}{}_{R}$
648.007	43.852	$H_2O\ _{R}$, $CH\ ^{C,R}{}_{R}$
651.315	10.708	$H_2O\ _{R}$, $CH\ ^{C,R}{}_{R}$
674.165	194.744	$H_2O\ _{R}$, $CH\ ^{R}{}_{R}$, SO_3
698.073	201.909	$H_2O\ _{R}$, $OH\ _{ST}$ (O7-H2) $CH\ ^{C,R}{}_{R}$
776.665	13.711	$CH\ ^{R}{}_{B}$, $CH\ ^{C}{}_{SC}$
808.093	30.554	$CH\ ^{R}{}_{B}$, $CH\ ^{C}{}_{SC}$
819.814	10.523	$CH\ ^{R}{}_{W}$, $CH\ ^{C}{}_{SC}$
842.018	45.322	$CH\ ^{R}{}_{W}$, $CH\ ^{C}{}_{SC}$
844.151	5.761	$CH\ ^{R}{}_{TO}$, $CH\ ^{C}{}_{SC}$
873.853	96.193	$CH\ ^{C}{}_{R}$
875.475	240.927	$H_2O\ _{TW}$, $CH\ ^{C}{}_{R}$
934.68	148.718	$SO_{3\ ST(S)}$
958.271	139.554	$CH\ ^{R}{}_{TO}$, $CH\ ^{C}{}_{R}$
965.075	57.865	$CH\ ^{R}{}_{TO}$, $CH\ ^{C}{}_{R}$
966.725	104.158	$CH\ ^{R}{}_{TO}$, $CH\ ^{C}{}_{R}$
974.537	18.48	$CH\ ^{R}{}_{TO}$, $CH\ ^{C}{}_{R}$
996.727	215.004	$SO\ _{ST}$ (S2-O4, S2-O6)
1036.179	19.058	$CCC\ ^{R}{}_{SC}$

1039.843	10.038	CCC $^{R}_{SC}$
1042.954	24.165	CCC $^{R}_{SC}$
1056.024	7.619	CH $^{C}_{R}$
1067.696	231.193	SO $_{ST}$ (S1-O1)
1115.006	40.381	CH $^{R}_{B}$
1122.708	113.361	CH $^{R}_{B}$
1134.078	7.675	CH $^{C, R}_{SC}$
1147.077	10.07	CH $^{C, R}_{SC}$
1275.86	253.273	SO $_{ST}$ (S1-O3) CH$^{C}_{TW}$
1281.247	95.38	CH $^{C}_{TW, SC}$
1290.145	190.75	SO $_{ST}$ (S2-O5)
1447.335	12.84	CC$^{R}_{ST(Kekule)}$,
1448.259	17.987	CC$^{R}_{ST(Kekule)}$,
1499.484	8.571	CH $^{C}_{SC}$
1508.38	10.134	CH $^{C}_{SC}$
1534.728	11.739	CH $^{R}_{TW}$, CH$^{C}_{SC}$
1645.615	8.003	CC$^{R}_{ST}$
1646.63	14.916	CC$^{R}_{ST}$
1741.102	144.521	H_20 $_{SC}$
3022.416	18.386	CH $^{C}_{ST}$
3033.193	20.57	CH $^{C}_{ST}$

3039.941	36.142	CH $^{C}_{ST}$
3058.192	19.91	CH $^{C}_{ST}$
3070.23	33.191	CH $^{C}_{ST}$
3078.364	58.06	CH $^{C}_{ST}$
3169.239	12.159	CH $^{R}_{ST}$
3169.989	15.597	CH $^{R}_{ST}$
3175.84	9.958	CH $^{R}_{ST}$
3187.44	6.734	CH $^{R}_{ST}$
3211.232	16.953	CH $^{R}_{ST}$
3217.742	802.147	OH $_{ST}$ (O7-H1)
3222.05	13.973	CH $^{R}_{ST}$
3878.422	115.609	OH $_{ST}$ (O7-H2)

Table AII.5: Calculated Infrared Spectrum of structure with Mg^{2+} (Fig. V.5) and Assignments

Studi Computazionali e Sperimentali delle interazioni soluto-membrana in sistemi per desalinizzazione tramite membrane a scambio ionico.

Ricerche precedenti hanno dimostrato che il trasferimento di soluti neutri attraverso membrane è influenzato dalla presenza di ioni in soluzione. Nel contesto dell'intesificazione dei processi, la conoscenza dei meccanismi molecolari coninvolti è di fondamentale importanza per migliorare e predire le prestazioni dei processi. Lo scopo di questa Tesi di Dottorato è l'utilizzo combinato di approcci computazionali, quantistici e molecolari, e metodologie sperimentali per migliorare la comprensione dell'influenza degli ioni sui flussi dei soluti. Nella prima parte del lavoro, alcune proprietà degli ioni in soluzione sono stati calcolati e comparati con i flussi di zuccheri in membrane per NanoFiltrazione ed ElettroDialisi. Successivamente, sistemi composti da Membrane a scambio Cationico equilibrati da più contro-ioni e glucosio idratato sono stati esaminati tramite Meccanica Quantistica/Meccanica Molecolare per poter studiare la solubilità dello zucchero nella matrice polimerica e le interazioni relative alla diffusione come l'energia di coesione tra catene polimeriche. Nell'ultima parte della tesi, angolo di contatto, calorimetria a scansione differenziale e gli spettri vibrazionali sono stati misurati per caratterizzare le proprietà fisiche della membrana e la possibile influenza del contro-ione sulle membrane a scambio cationico.

Questo lavoro, dimostra che la natura del contro-ione modifica l'energia di coesione tra i frammenti di polimero della membrana. A sua volta, l'energia di coesione influenza la diffusione di composti organici neutrali attraverso le membrane.

Computationele en experimentele studies aan membraan-opgeloste stof interacties in ontzoutingssystemen met ion-uitwisselingsmembranen.

Eerder werk heeft aangetoond dat de overdracht van neutrale opgeloste stoffen door membranen wordt beïnvloed door de aanwezigheid van ionen in oplossing. In het kader van procesintensificatie is de kennis van de betrokken moleculaire van fundamenteel belang om de procesprestaties te verhogen en te voorspellen. Het doel van dit proefschrift is om een gecombineerde quantum/moleculaire computationele benadering en experimentele methoden te gebruiken om zodoende beter te begrijpen hoe ionen de flux van opgeloste stoffen beïnvloeden. In het eerste deel van het werk worden enkele eigenschappen van ionen in oplossing berekend en vergeleken met suikerfluxen in nanofiltratie en elektrodialyse membranen. Hierna worden systemen van kation-uitwisselingsmembraanmateriaal, in evenwicht met verschillende tegen-ionen en gehydrateerd glucose, met behulp van Quantum Mechanica/Moleculaire mechanica onderzocht. Hierbij wordt voornamelijk gekeken naar de oplosbaarheid van suiker in de polymere matrix en diffusie gerelateerde interacties als cohesie-energie tussen polymeerketens. In het laatste gedeelte worden contacthoek, differentiële scanning calorimetrie en infrarode spectra gemeten om de fysische eigenschappen van het membraan en de mogelijke invloed van het tegenion op kation-uitwisselingsmembraanmateriaal te karakteriseren.

Dit werk toont aan dat de aard van de tegenionen de cohesie-energie tussen membraanpolymeerfragmenten wijzigt. Op zijn beurt beïnvloedt de cohesie-energie de diffusie van neutrale organische verbindingen door de membranen.

Étude théorique et expérimentale des interactions membrane-soluté dans les systèmes de dessalement utilisant des membranes échangeuses d'ions.

Des études antérieures ont mis en évidence que le transfert de solutés neutres à travers des membranes est influencé par la présence d'ions en solutionAinsi, la connaissance des interactions multiples à l'échelle nanométrique, entre le polymère, l'eau et les solutés (ions, espèces organiques) constituent un verrou pour l'amélioration des performances des procédés membranaires. Dans cette étude une approche multi-échelle fondamentale est proposée, combinant des outils théoriques et expérimentaux, afin d'obtenir les paramètres microscopiques et macroscopiques caractérisant les interactions étudiées pour différentes compositions ioniques. Plus précisément, il s'agit de comprendre comment les ions affectent le transfert d'un soluté organique. Dans un premier temps, certaines propriétés caractérisant l'hydratation des ions sont calculées et comparées aux flux de diffusions de sucres à travers des membranes de Nanofiltration et échangeuses d'ions obtenus pour différentes compositions ioniques. Dans un deuxième temps, des systèmes constitués d'une membrane échangeuse de cations (CMX) équilibrée avec différents cations ainsi que le glucose hydraté sont modélisés en utilisant une approche combinée Mécanique Quantique/ Mécanique Moléculaire. Cette approche a permis d'étudier la solubilité du sucre dans la matrice polymère ainsi que les interactions polymère-polymère comme l'énergie de cohésion. Enfin, l'influence des ions sur les caractéristiques physiques de la membrane CMX est étudiée en utilisant diverses méthodes expérimentales comme la détermination des angles de contacts et des spectres IR ou la mesure de la température de solidification par DSC. Les propriétés vibrationnelles sont également calculées dans le cadre de la théorie de la fonctionnelle de la densité (DFT). L'ensemble de ces données sont comparées avec les grandeurs de transport afin de valider les mécanismes moléculaires proposés.

Ce travail montre que la nature des contre-ions de la membrane modifie l'énergie de cohésion entre les fragments de la membrane. Ainsi, l'énergie de cohésion influe sur la diffusion des composés organiques neutres à travers les membranes.

Computational and experimental studies on membrane-solute interactions in desalination systems using ion-exchange membranes

Previous works have shown that the transfer of neutral solutes through membranes is influenced by the presence of ions in solution. In the framework of process intensification, the knowledge of the molecular mechanisms involved is of fundamental importance to increase and predict the process performances. The aim of this Thesis is to use a combined quantum/molecular computational approach and experimental methodologies to better understand how ions can affect the solute flux. In the first part of the work, some properties of ions in solution are computed and compared with sugar fluxes through membranes for nanofiltration and electrodialysis. In the following, systems composed of Cation-exchange membrane equilibrated by different counter-ion and hydrated glucose are examined by Quantum Mechanics/Molecular Mechanics. This is done mainly to investigate the sugar solubility in the polymer matrix and diffusion related interactions like polymer chain-chain cohesion energy. In the last part, contact angle, differential scanning calorimetry and Infra-Red spectra are measured to characterize the physical properties of the membrane and possible influence of the counter-ion on cation exchange membrane.

This work shows that the nature of the counter-ions modifies the cohesion energy between the membrane polymer fragments. In its turn, the cohesion energy affects the diffusion of neutral organic compounds through the membranes.

Étude théorique et expérimentale des interactions membrane-soluté dans les systèmes de dessalement utilisant des membranes échangeuses d'ions.

Des études antérieures ont mis en évidence que le transfert de solutés neutres à travers des membranes est influencé par la présence d'ions en solutionAinsi, la connaissance des interactions multiples à l'échelle nanométrique, entre le polymère, l'eau et les solutés (ions, espèces organiques) constituent un verrou pour l'amélioration des performances des procédés membranaires. Dans cette étude une approche multi-échelle fondamentale est proposée, combinant des outils théoriques et expérimentaux, afin d'obtenir les paramètres microscopiques et macroscopiques caractérisant les interactions étudiées pour différentes compositions ioniques. Plus précisément, il s'agit de comprendre comment les ions affectent le transfert d'un soluté organique. Dans un premier temps, certaines propriétés caractérisant l'hydratation des ions sont calculées et comparées aux flux de diffusions de sucres à travers des membranes de Nanofiltration et échangeuses d'ions obtenus pour différentes compositions ioniques. Dans un deuxième temps, des systèmes constitués d'une membrane échangeuse de cations (CMX) équilibrée avec différents cations ainsi que le glucose hydraté sont modélisés en utilisant une approche combinée Mécanique Quantique/ Mécanique Moléculaire. Cette approche a permis d'étudier la solubilité du sucre dans la matrice polymère ainsi que les interactions polymère-polymère comme l'énergie de cohésion. Enfin, l'influence des ions sur les caractéristiques physiques de la membrane CMX est étudiée en utilisant diverses méthodes expérimentales comme la détermination des angles de contacts et des spectres IR ou la mesure de la température de solidification par DSC. Les propriétés vibrationnelles sont également calculées dans le cadre de la théorie de la fonctionnelle de la densité (DFT). L'ensemble de ces données sont comparées avec les grandeurs de transport afin de valider les mécanismes moléculaires proposés.

Ce travail montre que la nature des contre-ions de la membrane modifie l'énergie de cohésion entre les fragments de la membrane. Ainsi, l'énergie de cohésion influe sur la diffusion des composés organiques neutres à travers les membranes.

Computational and experimental studies on membrane-solute interactions in desalination systems using ion-exchange membranes

Previous works have shown that the transfer of neutral solutes through membranes is influenced by the presence of ions in solution. In the framework of process intensification, the knowledge of the molecular mechanisms involved is of fundamental importance to increase and predict the process performances. The aim of this Thesis is to use a combined quantum/molecular computational approach and experimental methodologies to better understand how ions can affect the solute flux. In the first part of the work, some properties of ions in solution are computed and compared with sugar fluxes through membranes for nanofiltration and electrodialysis. In the following, systems composed of Cation-exchange membrane equilibrated by different counter-ion and hydrated glucose are examined by Quantum Mechanics/Molecular Mechanics. This is done mainly to investigate the sugar solubility in the polymer matrix and diffusion related interactions like polymer chain-chain cohesion energy. In the last part, contact angle, differential scanning calorimetry and Infra-Red spectra are measured to characterize the physical properties of the membrane and possible influence of the counter-ion on cation exchange membrane.

This work shows that the nature of the counter-ions modifies the cohesion energy between the membrane polymer fragments. In its turn, the cohesion energy affects the diffusion of neutral organic compounds through the membranes.